RICE UNIVERSITY

# Low electrical resistivity carbon nanotube and polyethylene nanocomposites for aerospace and energy exploration applications

by

**Pádraig G. Moloney**

A THESIS SUBMITTED
IN PARTIAL FULFILLMENT OF THE
REQUIREMENTS FOR THE DEGREE

**Doctor of Philosophy**

APPROVED, THESIS COMMITTEE

Enrique V. Barrera, Chair,
Professor, Mechanical Engineering & Materials Science

Pulickel M. Ajayan, Benjamin M. and Mary Greenwood Anderson Professor in Engineering, Mechanical Engineering & Materials Science

Neal F. Lane, Malcolm Gillis University Professor, Physics & Astronomy, Senior Fellow, Baker Institute

HOUSTON, TEXAS
DECEMBER 2011

# ABSTRACT

**Low electrical resistivity carbon nanotube and polyethylene nanocomposites for aerospace and energy exploration applications**

by

Pádraig G. Moloney

An investigation was conducted towards the development and optimization of low electrical resistivity carbon nanotube (CNT) and thermoplastic composites as potential materials for future wire and cable applications in aerospace and energy exploration. Fundamental properties of the polymer, medium density polyethylene (MDPE), such as crystallinity were studied and improved for composite use. A parallel effort was undertaken on a broad selection of CNT, including single wall, double wall and multi wall carbon nanotubes, and included research of material aspects relevant to composite application and low resistivity such as purity, diameter and chirality.

With an emphasis on scalability, manufacturing and purification methods were developed, and a solvent-based composite fabrication method was optimized. CNT MDPE composites were characterized via thermogravimetric analysis (TGA),

differential scanning calorimetry (DSC), Raman spectroscopy, and multiple routes of electron microscopy. Techniques including annealing and pressure treatments were used to further improve the composites' resulting electrical performance. Enhancement of conductivity was explored via exposure to a focused microwave beam. A novel doping method was developed using antimony pentafluoride ($SbF_5$) to reduce the resistivity of the bulk CNT. Flexible composites, malleable under heat and pressure, were produced with exceptional electrical resistivities reaching as low as $2*10^{-6}\ \Omega\bullet m$ ($5*10^5$ S/m).

A unique gas sensor application utilizing the unique electrical resistivities of the produced CNT-MDPE composites was developed. The materials proved suitable as a low weight and low energy sensing material for dimethyl methylphosphonate (DMMP), a nerve gas simulant.

# ACKNOWLEDGEMENTS

I thank my wife, Dr. Anne van de Ven, for her unwavering love, support, patience and positive outlook during this doctoral experience. I also thank my father and mother, Dr. Paddy Moloney and Rita O'Reilly, for raising me and giving me the privilege of something that was not available to them, a formal secondary and college education. A very special thanks to my young son Fionn, whose birth, first year and infectious smile sustained me during the final year of this project.

I am very much indebted to my advisor Dr. Enrique Barrera, for his mentorship and support. I thank my committee member, Dr. Pulickel Ajayan for his counsel and creativity. I am very grateful to Dr. Neal Lane, for the years of advice and guidance he has given me, including through this thesis committee.

I thank the members of the Barrera research group, in particular Andres Rodela, for their friendship and camaraderie. I appreciate very much the support of my collaborators at NanoRidge Inc. I also acknowledge my friends and former colleagues at NASA Johnson Space Center, and across the agency, for providing me with a strong practical foundation in nanoscale science and its application. I am very grateful to both Dr. Jing Li and Dr. Yijiang Lu of NASA Ames Research Center for their assistance in microscale nanotube measurements, and to Dr. Saunab Ghosh of the Weisman Group at Rice University for training me to collect and use nanotube chirality data. I am indebted to many across the Rice University community, too

numerous to list here, from custodian to professor, for their advice and input throughout this doctoral experience and in the content of this research.

# TABLE OF CONTENTS

# LIST OF TABLES

# LIST OF FIGURES

# CHAPTER 1: INTRODUCTION

The increasing use of electrical systems to replace hydraulics in aerospace, combined with the rigors seen by undersea umbilicals for energy exploration, creates a real need for lightweight conductors to replace copper wire. The creation of such a conductor is the central goal of this thesis.

In Chapter 2, the rationale for research is presented, both the need and a brief on the proposed solution to meet that need, a polymer nanocomposite. A background on polyethylene (PE), the polymer designated as the matrix material for this work, is included with special attention paid to material aspects relevant to composite processing. A similar background on carbon nanotubes (CNT), whose unique properties include the promise of low electrical resistivity, is also put forward. Consideration of what factors affect electrical resistivity, which include nanotube chirality, are presented. Finally, a review of the most promising CNT-PE composite research is discussed.

Chapter 3 lays out the steps taken to prepare, characterize and optimize the CNT for use in a low resistivity composite. An improved and scalable purification procedure, suitable for large amounts of CNT, was developed and compared to more established methods. In an effort to bridge this materials-engineering goal with the latest fundamental nanotube research, a chirality and diameter assessment was

carried out and presented. A multi-scale analysis of nanotube resistivities was attempted and the data gathered included in the chapter.

Combining the CNT with polyethylene, with a focus on medium density polyethylene (MDPE), and extracting the best electrical performance possible from the produced composites, is central to Chapter 4. A scaled-up and improved solvent blending procedure was created and its products analyzed. The electrical resistivities are noted and detailed microscopy, spectroscopy and other analysis is employed to understand the nuances of different composites' resistivity performance.

Chapter 4 continues with an emphasis on techniques explored to improve the electrical resistivity of the as-produced composites. Annealing and pressure is investigated, with success, while more inventive research using focused microwave beams is less promising that originally envisioned but proves itself worthy of future research. A novel doping route, using antimony pentafluoride ($SbF_5$), was developed in order to improve the fundamental electrical performance of the CNT, and is included in this chapter.

An innovative, flexible and low energy gas sensor, made from the low-resistivity composites developed in Chapter 4, is presented in Chapter 5. This chapter begins with a broad investigation of the relevant literature, the identification of the most suitable analyte, and then lays out the development and discussion on the sensor invented.

# CHAPTER 2: BACKGROUND AND RATIONALE

## 2.1 RATIONALE FOR RESEARCH – INDUSTRIAL APPLICATIONS OF ELECTRICALLY CONDUCTIVE POLYMER CABLES

### 2.1.1 Oil and Gas Undersea Umbilicals

Offshore exploration for fossil fuels continues to push into deeper water (>3000m) and with longer exploration or "step-out" distances (>50km)[1]. These subsea networks require power cables or "umbilicals" of increasing length, which must deliver significant amounts of power for a design life up to 20 years or more. As depths and distances increase, conventional copper wire will fail under its own mass, which produces the need for new conductors.

This need for a new conducting cable material was the basis for the Research Partnership to Secure Energy for America (RPSEA)-sponsored program involving Rice University, NanoRidge Inc. and its partners, entitled "Ultra-High Conductivity Umbilicals: A paradigm Change in Conductors Using Carbon Nanotubes" whose aim was to produce an engineering prototype of a "polymeric conductor". Figure 1(d) below shows the CNT-based cable, while Figure 1(e) shows the cross-section of the nanotube filled polymer wire.

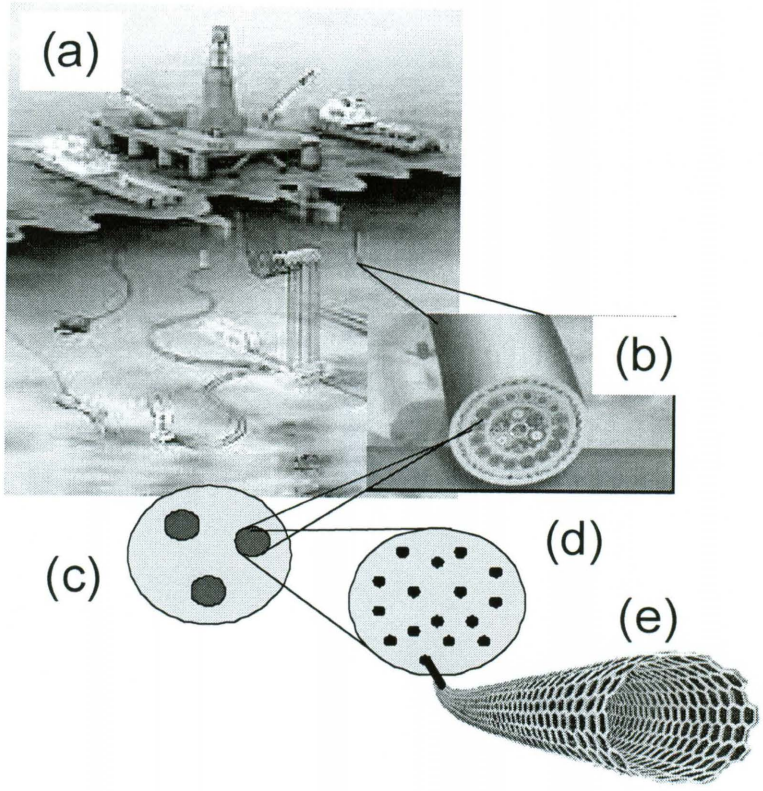


Figure 1: Schematic showing predicted schematic of PNU in use in undersea umbilical [1]

Much of the research in this thesis was funded by this study, and most importantly, it played a central role in dictating some of the technical approaches taken, namely using carbon nanotubes as a filler to produce a conducting polymer, and the choice of matrix or polymer, polyethylene. The program proposed a "polymer nanotube umbilical" or PNU whose material capabilities could reduce the diameter and weight of current materials such as aluminum (Al) and copper (Cu) (Figure 2). The polymer was proposed as a binder allowing the manufacture of a strong, yet flexible cable. Current umbilicals typically contain a thermoplastic extruded layer, which

surrounds bundles of functional components. These sub sections are then assembled into a compact tubular structure [1]. This use of a thermoplastic and the subsequent recommendations on polyethylene (PE) from umbilical manufacturers as part of the RPSEA program, was the primary reason PE was used in this thesis.

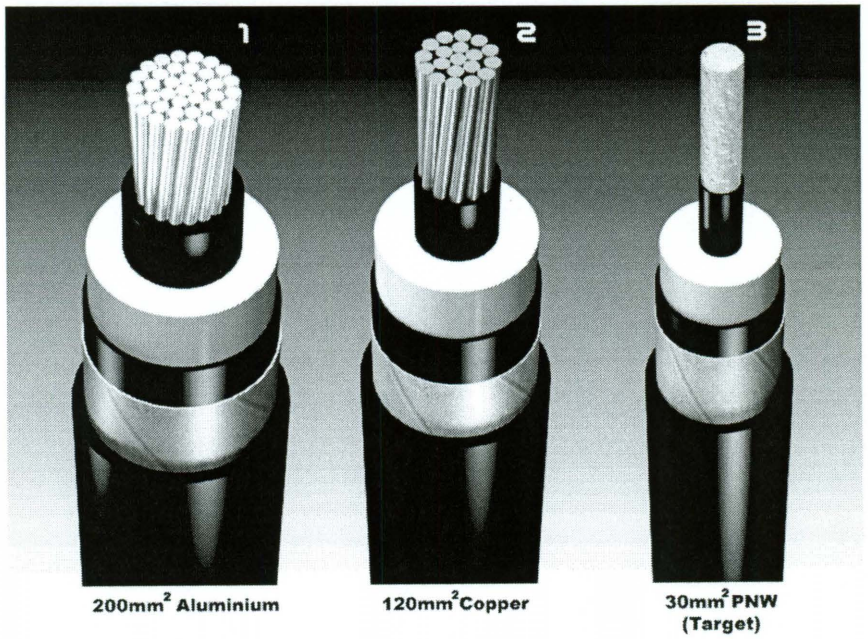


Figure 2: Comparison of Al and Cu to proposed PNU cable [1]

Studies were carried out showing the potential weight loss from using CNT-enhanced polymers, predicting a significant reduction in mass and an increase in buoyancy (Table 1).

| | Cable 1 | Cable 2 | Cable 3 |
|---|---|---|---|
| Cable area (mm2) | 200 (Al) | 120 (Cu) | 30 (PNU) |
| Mass in air (kg/m) | 1.45 | 1.82 | 0.54 |
| Diameter (m) | 0.038 | 0.0327 | 0.0253 |
| Mass of displaced water (kg/m) | 1.16 | 0.86 | 0.52 |
| Weight in water (N/m) | 2.820 | 9.406 | 0.242 |
| Or (kg/m) | 0.288 | 0.959 | 0.025 |

Table 1: Current and proposed cable weights [1]

CNTs were proposed due to their high current density capacity [2], and conductivities that are possibly one order of magnitude in excess of Cu [3] and weights that are 1/6$^{th}$ [3].

### 2.1.2 Aircraft Electrical Cables

The previous Space Exploration initiative at the National Aeronautics and Space Administration (NASA) had set out an ambitious plan of manned and unmanned missions to explore both the Moon and Mars. Solutions to reduce mass and increase energy are always relevant to space systems, and will continue to be whatever future NASA missions beyond earth's orbit replace the cancelled Exploration architecture. The wiring mass estimate for the Crew Exploration Vehicle (CEV), or Orion, was approximately 940 lbs. for the Control Module and 720 lbs. for the Service Module. It was expected this number would have grown as the design matured and the actual wire routing in the vehicle was determined. An additional historical reference to wiring mass growth as a system evolves, is the Space Shuttle. It contained 228 miles of metallic wire, which, including relevant connectors, was

originally in excess of 4,500lbs. That number now had grown to well in excess of 5,000lbs as the shuttle faced retirement. The increased use of electrical systems in aircraft to replace hydraulics has only hastened the need for lightweight conductors in aerospace.

In addition to the reduction of wiring mass, enhancements are sought by the aerospace industry for lightning strike, static electricity build-up mitigation and protection for composite structures of aircraft and spacecraft. An active area of research to provide solutions to these challenges is the use of nanoscale materials to improve the conductivity of polymers as a replacement for traditional metal wiring.

In support of this goal of higher conductivity cables for aircraft use, the National Institute of Standards and Technology (NIST) Advanced Technology Program (ATP) supported a multi year effort involving Rice University, Nanoridge Inc. and Boeing (NIST). This program was also key in funding this thesis, and in influencing the technical approaches taken, especially one of its key requirements being the production of a cable composed of electrically conductive carbon nanotubes embedded in a polymer [4]. One supporting element of this program worth noting was a key foundational requirement, not part of this thesis research; that of the supply or sourcing, and use of highly metallic carbon nanotubes.

## 2.2 POLYETHYLENE – POLYMER MATRIX

Polyethylene (PE) is one of the most widely used polymers or plastics. PE has a linear chemical formula of $H(CH_2CH_2)_nH$ [5]. As mentioned, its choice as the polymer matrix for this thesis stems originally from the recommendations of umbilical manufacturers. Through these requirements or recommendations, it was decided medium density polyethylene (MDPE) would be the primary polymer matrix of this thesis. MDPE has a density range of 0.926–0.940 g $cm^{-3}$, and good shock and drop resistance properties [1,6]. It is also noted as resistant to stress cracking and being less notch-sensitive than high density polyethylene (HDPE).

### 2.2.1 Electrical Properties

PE is considered chemically inert due to the small dipole moments associated with the carbon-hydrogen and carbon-carbon covalent bonds, which limit reactions between the polymer and potential reactants [7]. In fact, with its lack of free electrons, PE is widely used as an *insulating material* for cables. Although it has a relatively simple chemical composition, PE's electrical properties are complex. Peacock lists resistivity, permittivity, dissipation factor, dielectric strength and arc resistance as key quantities studied in polyethylene engineering. The first three are relevant at low electrical "stress", while the final two come into play at high stresses.

PE has a bulk resistivity on the order or greater than $10^{16}$ Ω•cm, and a dielectric constant of 2.25 – 2.35 at 1MHz [7]. It is noted in the literature that bulk resistivity of PE is not just dependent on chemical composition, but can be modified through contaminants and additives[7]. The chemical composition also affects morphology, which affects melting temperature and in turn resistivity. This does provide some optimism that the addition of a highly conductive filler material, such as metallic carbon nanotubes, may provide the *twenty two* order of magnitude change in resistivity to match that of copper. Changes in bulk resistivity were a key focus of this thesis.

The dielectric constant or relative permittivity is a measure of the materials inertness to an electric field. PE has a low dielectric constant because of its aforementioned lack of polar characteristics. It also has a low dissipation factor (D) which is a ratio of the lost to stored energy in an alternating electrical field. Increases in temperature decreases the dielectric strength of PE, most notably with melting of crystalline structures. For this reason, high density and linear polyethylene are used for high voltage insulator applications. Polyethylene has both crystalline and amorphous regions, and it is thought that the boundary between these creates trap sites for electrons, affecting its dielectric properties [8].

It has been shown that the mean free path in low-density polyethylene films can be increased by increasing crystallinity, making electron transport more efficient [9]. Tanaka et al. increased the mean free path length from under 5nm to greater than

15nm by annealing. However, the mean free path is only one component that electrical resistivity depends upon, and the resultant improvement in resistivity was negligible considering the target resistivity of copper. However, the use of annealing will be put to consideration during the thesis research.

High electrical fields will cause PE's insulting abilities to breakdown in both a chemical and mechanical manner, as the electrical "stresses" utilize impurities, catalyst residues, absorbed water and polarizable bonds in carbonyl and vinyl groups to find a path for current to flow through [10]. Lower molecular weight PE's are more susceptible to failure from high voltage electrical fields, principally through formation of conductive paths, also known as "trees" or "treeing" [7,10]. These microscopic paths can also be formed at electrical or sulfide-based paths of cavities and contaminants.

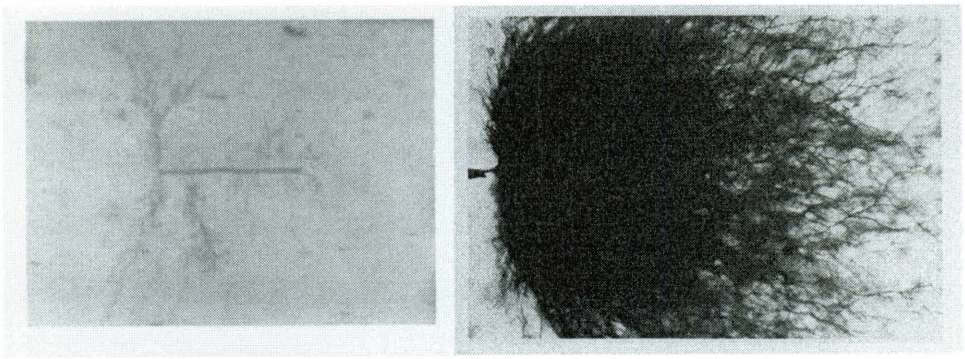

Figure 3: *Left*: Tree growth from fiber in polyethylene (30X mag)[10], *Right*: Treeing from inserted needle in cross-linked polyethylene [11]

The addition of CNT to PE may provide a number of possible routes for treeing to begin from the mechanical stresses, thermal stresses and possible increase in oxidation of the polymer. This may alter bulk resistivity in a controlled manner. There is little attention paid in the literature to these phenomena with regards to the electrical resistivity of nanotube polymer composites, and none with regards to polyethylene and SWNT. Past research has even shown the possible benefits of carbon and other inorganic fillers in cross-linked polyethylene as *prevention* to this dielectric breakdown or treeing [11], a situation that does not assist in this study's cause to reduce bulk electrical resistivity. In general, understanding of "nanodielectrics", especially in nanocomposites, is still considered relatively immature [12,13].

A distinct decrease in resistivity is noted in many composite mixtures of insulators and conductors once a critical volume fraction of the conductive filler is attained. An accepted explanation for this is that a percolating network of conductive fillers has been achieved, and that any additional reduction in resistivity is due to the increased connectivity and conductivity of the network [14,15]. Dielectric composites consist of well-dispersed conducting non-touching particles whose electrical connectivity in an insulating matrix is via tunneling [16,17]. Polyethylene is an uncommon choice of matrix for either approach. Vionnet-Menot et al. suggest there is little relationship between the critical volume fraction and the change in conductivity, while Bauhofer's extensive review suggests shape of the particle may have little to play either [18,19]. Relatively recent research has attempted to address

the tunneling-percolation problem in the intermediate regime between the "percolation-like" and the "hopping-like" regimes [16,20]. The former is a distinct and noticeable change in conductivity while the later is a continuous relationship with inter-particle distance. Through what was originally proposed in the RPSEA project, a hopping-like solution in polyethylene was put forward.

### 2.2.2 Solvents and Conditions for Polyethylene Processing

Dissolving the polymer matrix for manipulation with nano fillers has often played a useful role in the author's prior research in carbon nanocomposites [21-23]. The preferred solvents for PE are refluxing xylene, decalin or dichlorobenzene (DCB) at a temperature in excess of the melting point [7]. Complete dissolution in solvent is sometimes used as a first step to reducing polymer entanglement on route to creating high modulus, highly orientated, samples through wet spinning, solid state extrusion or drawing, or fiber growth from sheared solutions [7]. This is notable given the research of this thesis is in support of the creation of conducting PE cables. Preparation for wet spinning typically requires ~6% w/v concentrations [7]. Unfortunately, other than gel-spun fibers, PE products processed from solution are of little commercial interest.

In addition to being in excess of the melting point (140-170°C), using an excess of solvent reduces overlap between adjacent coils of polymer, which decreases the amount of intermolecular entanglement along the polymer chains [7]. If cooled

rapidly, the result will be a PE with relatively few entanglements compared to melt-crystallized PE. This is an important point to consider when contemplating dispersing carbon nanotubes, and their large aspect ratios, effectively in a polymer. It has been shown that PE chains configure themselves as random coils when allowed to equilibrate from a molten state or when dissolved in solvent.

PE crystallization from solution is dependent on the control of some key issues such the interactions between the solvent and the polymer, the concentration of the polymer in the solvent, the temperature and the molecular elongation [7]. A general guide that has been suggested is that the lower the concentration and the higher the temperature, combined with the lower the molecular weight of the polymer, will enhance the regularity of crystal formation [7].

## 2.3 CARBON NANOTUBES

### 2.3.1 Manufacturing Methods and Sources

In this thesis, nanotube types produced via different methods were explored. CNTs can be produced via a number of ways. These methods include arc discharge, chemical vapor deposition (CVD), laser ablation and high-pressure disproportionation of carbon monoxide (HiPco). These techniques are based on nanotube formation from carbon feedstock in the presence of a metal catalyst(s). The main differences are with the type and form of carbon feedstock and metal catalysts used.

In the CVD and HiPco processes, the CNTs are formed from the decomposition of carbon-containing gases [24]. With the arc and laser ablation processes, the CNTs are formed by the vaporization of solid carbon. High temperatures, often >800°C, are used in the active regions of the reactors to produce single carbon atoms or carbon atom clusters which eventually form CNTs. Each method produces tubes with unique properties, and the material can even vary depending on the area of the reactor it is harvested from.

The arc process was used by Iijima to produce the first SWNT [25]. It is still considered a batch process for SWNT production that often produces a large variation in diameters (1.0-1.8 nm). With laser ablation CNT, a laser is used to vaporize a solid

carbon target containing approximately 1 atomic weight percent of metal catalyst [26]. It has been shown to produce 1g per day of larger diameter SWNT (~1.4 nm).

### 2.3.2 Nanotube to Nanotube Junctions

It has been suggested that the resistivity of a network of CNT is far more dependent on the network or interconnectivity between the tubes, rather than the distance from the electrode [27]. Further research has supported this claim [19,28].

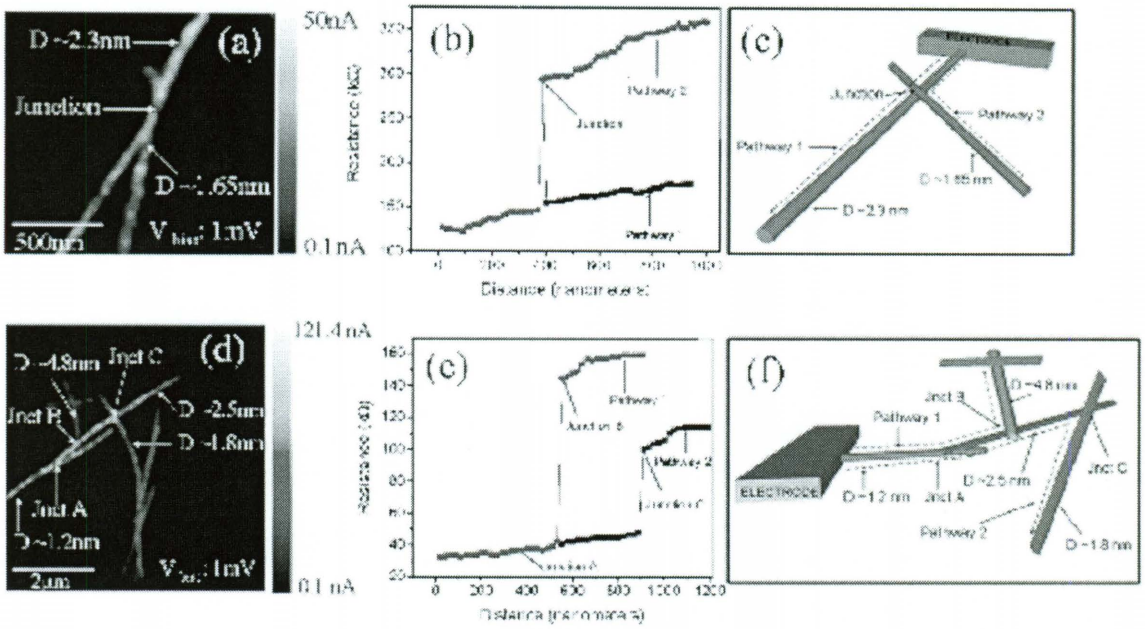


Figure 4: Local resistance analysis via atomic force microscopy (AFM) of pathways through bundle and individual tubes [29]

Recent studies have also shown that resistivity of nanotube networks can be lowered by reducing the bundle size of tubes, ideally to single tubes (Figure 4)[29]. A qualitative summary of nanotube to nanotube junctions was recently formulated for the RPSEA project [1], and is presented in Table 2 below

| Junction Type | CNT Rope - CNT Rope | SWNT - CNT Rope | Semiconductor-Semiconductor | Semiconductor-Metallic | DWNT-DWNT | m-SWNT -m-SWNT |
|---|---|---|---|---|---|---|
| Relative Contact Resistance | 5 (5 is High) | 4 | 3 | 3 | 2 | 1 (1 is Low) |

Table 2: CNT-CNT junctions and their relative contact resistances [1,6]

### 2.3.3 Nanotube Type and Chirality

Armchair quantum wires (AQW) are metallic-SWNT (m-SWNT) wires, which rely on ballistic electron transport and resonance quantum tunneling [1,30,31]. As already noted, obtaining metallic CNT in quantity was a key deliverable of the ATP project, with dependent research such as success of the nanotube-polymer composite in this thesis. Different forms of the same nanotube type can be described by their chiral vector (n,m), where n and m are the integers of the vector equation (Figure 5).

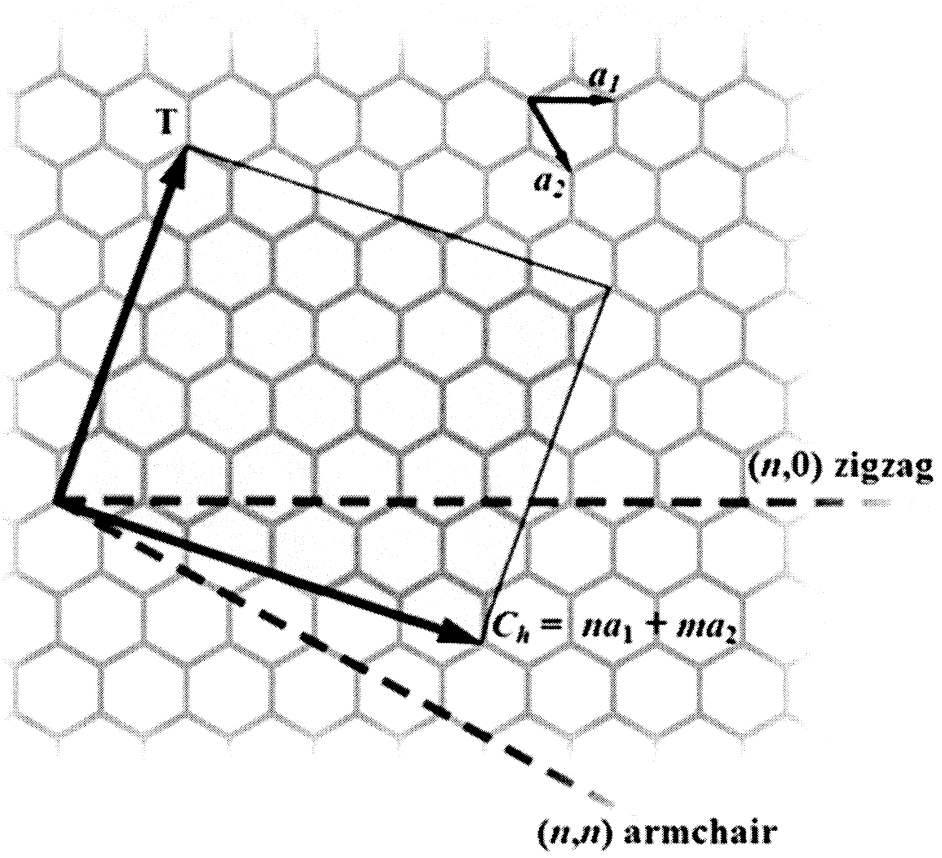


Figure 5: Chiral vector map of graphite [32]

The chirality or twist is described by (n,m), which in turn describes the lattice structure and conductivity of the tube. SWNT material is metallic if n and m can be divided by three. While not AQW CNT, nanotubes of various chiralities were explored as part of this study.

## 2.4 CARBON NANOTUBE AND POLYETHYLENE COMPOSITES

### 2.4.1 Carbon nanotube and polymer composites

In their thorough review of CNT-polymer composites, Bauhofer summarized the highest performing composites in terms of electrical conductivity or resistivity (Figure 6)[19]. Summarizing this further, one can see that composites with the lowest resistivities had less than a stellar performance in comparison to the target set for this study, that of copper (Table 3). It is noted that these "best of the best" composites utilized polymers more suitable to the task than the one designated for this thesis, polyethylene. The amount, or wt%, of CNT used in these examples was also not insignificant.

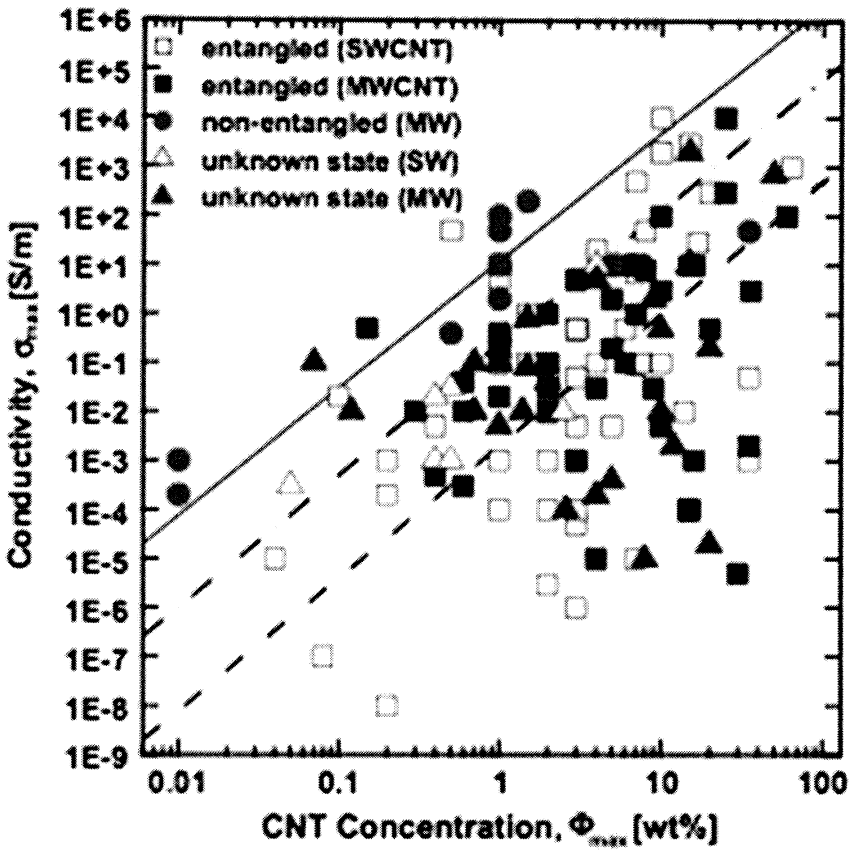


Figure 6: Review of electrical conductivity of CNT-polymer composites [19]

Skakalova et al. achieved a low resistivity of $1*10^{-2}$ Ω•cm with their composite of SWNT and PMMA [33]. Using a simple doping method of thionyl chloride ($SOCl_2$), they reduced the resistivity of the SWNT from $2e^{-3}$ Ω•cm to $4e^{-4}$ Ω•cm, and the SWNT-polymer composite from $6*10^{-2}$ Ω•cm to $1*10^{-2}$ Ω•cm. Combined with the choice of polymer, the composites took the form of thin layers created by evaporation of solution, a low scale manufacturing method which reduces the relevancy of this research towards this thesis.

| Composite Type | Resistivity | wt% CNT |
|---|---|---|
| $SOCl_2$ SWNT PMMA [33] | $1*10^{-2}$ Ω•cm | 10 |
| SWNT PANI [34] | $3*10^{-1}$ Ω•cm | 15 |
| MWNT PU [35] | $2*10^{-1}$ Ω•cm | 15 |

Table 4: Summary of lowest resistivity composites in the literature

Blanchet et al. also took the approach of creating thin films, of SWNT and polyaniline (PANI), for their study. The only note of relevance of their work towards this thesis, was that neither nanotube type (HiPco and Laser), nor purity (leftover metal catalyst), affected their results. It was only the dispersion of the nanotubes that was considered significant.

### 2.4.2 Carbon nanotube and polyethylene composites

There is a limited amount of research and data within in the literature pertaining to composites of polyethylene and CNT, especially when compared to the body of work dedicated to combining CNT with thermosets and other thermoplastics. Within pre-existing efforts on polyethylene and CNT, there is an even more limited subset that concentrates on, or even touches upon, the study of electrical resistivity or conductivity of the CNT-PE composites. Given the aforementioned starting high resistivity of polyethylene, this is not surprising.

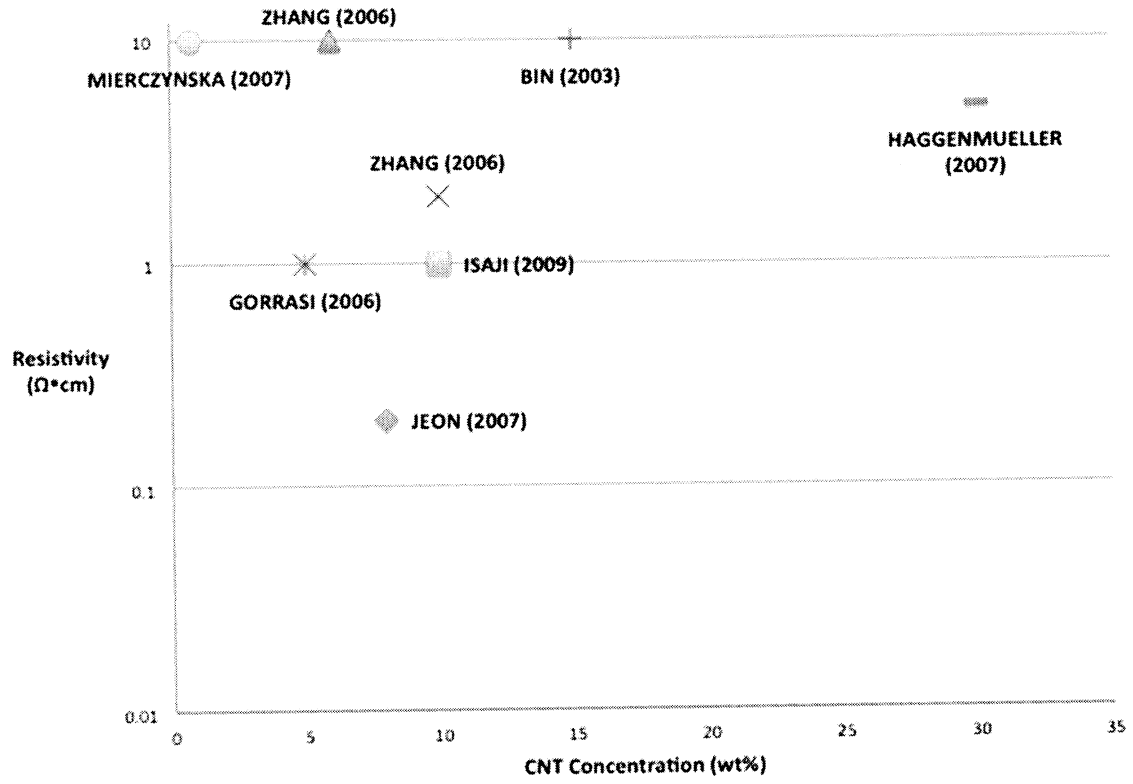


Figure 7: Summary of lowest resistivity carbon nanotube and polyethylene composites

In 2003, Bin et al. combined MWNT of 10-20 nm diameter with ultrahigh weight molecular weight polyethylene (UHMWPE) via gelation/crystallization from solution in decalin, or decahydronaphthalene, a saturated analog of naphthalene [36]. They found that resistivity was at its lowest of 10 Ω•cm at a 15wt% loading and then saw an increase with resistivity with higher loading, thought to be due to worsening dispersion in solution due to higher shear stress and hence, larger amount of tube entanglement. The percolation threshold was found at approximately 10wt%. They discovered that mechanical stretching up to a draw ratio of 100 actually increased resistivity to 100 Ω•cm. In 2006, Chen and Bin repeated this work to make MWNT-UHMWPE composites, also including other polymers at varying ratios, but did not improve upon their previous electrical performance. Isaji et al. continued this group's research by fabricating UHMWPE/LMWPE and 10wt% MWNT composite films via a solvent blend in decalin. Through thermal cycling they reduced the resistivity further to 1 Ω•cm

Xi et al. utilized paraffin as a solvent and reduced the percolation threshold of MWNT-UHMWPE composites to 3wt% and achieved a lowest resistivity of 10-100 Ω•cm [37]. Zhao et al. utilized similar first steps, using solution casting method in dimethylbenzene to prepare MWNT-LDPE film composites up to 30wt% [38]. The films were mechanically mixed in a Banbury mixer as a final processing step. A

percolation threshold was noted at 15wt% and a minimum resistivity of approximately 1 * $10^7$ Ω•cm at 30wt%.

Using a "hot coagulation" method, or solvent blend, of dichlorobenzene (DCB), Haggenmueller et al. produced composites of SWNT (produced via laser ablation) and LDPE and MDPE respectively [39,40]. This work achieved a resistivity between 1 and 10 Ω•cm at a 30wt% loading. Jeon et al. used similar methods and solvent to produce SWNT-HDPE composites up to 8wt% with a 0.2 Ω•cm, a lowest resistivity observed in the literature reviewed. A percolation threshold at 0.13wt% was noted [41].

With regards to mechanical approaches to creating CNT polyethylene composites, McNally et al. used a melt blending method using a Haake mini-twin screw extruder to produce MWNT-MDPE composites in various ratios up to 10 wt%[42]. Increasing MWNT loading past this amount was probably not possible due to the increasing viscosity of the MWNT-MDPE mixtures and the torque needed to mix such pre-composites. They noted a percolation threshold of approximately 7.5 wt% and a lowest resistivity point of 1000 Ω•cm. Using hot pressing of mechanically mixed powders of MWNT-UHMWPE has shown a resistivity limit of 100 Ω•cm [43]. A similar hot press approach was utilized by Gorrasi et al., but was preceded by high energy ball milling (HEBM) of linear low density polyethylene and MWNT powders up to 10wt% [44]. They achieved a percolation threshold at 2wt% and a plateauing reduction of resistivity to approximately 1 Ω•cm at 5wt%.

Mierczynska et al. prepared composites using UHMWPE granules covered in both SWNT and MWNT [45]. The composites were processed via the mixing of polymer "microgranules" with CNT, followed by sintering. They noted that effective dispersion in solvent prior to the addition of polymer granules and drying, reduced the percolation threshold by approximately one order of magnitude for SWNT composites. The processing time of mixing was studied showing that increased dispersion of CNT and breaking up of bundles is achieved, and hence a reduction in resistivity of up to one order of magnitude is possible, but that further mixing appears to retract some of that improvement, possibly by reducing CNT interconnectivity and pushing the material to polymer voids. Best results of 10 Ω•cm for 0.75wt% MWNT-UHMWPE and 100 Ω•cm for 3wt% SWNT-UHMWPE were noted.

Zhang et al. also took an unusual mechanical mixing approach to their composites of SWNT with HDPE [46]. They *sprayed* SWNT aqueous solutions onto HDPE powders before mechanical mixing. While they claim that this process had benefits towards dispersion and rheological properties, there was no direct conclusion the process reduced resistivity. A percolation threshold was noted at 4wt% while the reduction in resistivity began to plateau at 10 Ω•cm with 6 wt%. Of note, was that the rheological percolation threshold was lower than the electrical one (1.5wt% vs. 4wt%). This was explained as a higher effect on resistivity by absorbed polymer layers around tube and tube bundles than on rheology. In further work, Zhang et al.

reduced the resistivity to 2 Ω•cm at a loading of 10wt% and improved percolation threshold to 0.6. They achieved these improvements by processing the powders in solvent and producing films, rather than melt mixing.

Overall, one can see from the literature, there are numerous challenges involved in achieving low electrical resistivity in nanocomposites of polyethylene and carbon nanotubes, while a wide variety of technical approaches and methods have yet to provide a clear route to matching the low resistivity of copper.

# CHAPTER 3: LAYING THE FOUNDATION: NANOTUBE TYPE, PROCESSING & CHARACTERIZATION FOR COMPOSITES

## 3.1 CARBON NANOTUBE TYPE AND PURIFICATION

Over the span of research conducted for this thesis, a number of nanotube types from various sources were utilized. These included SWNT produced via HiPco (Rice University), laser ablation (NASA Johnson Space Center) and CoMoCAT (Southwest Nanotechnologies Inc.) methods, in addition to two sources of MWNT (Mitsui and Bayer). Double wall carbon nanotubes or DWNT (CCNI) were also explored in the later stages of research. A diverse selection of CNT was used in seeking the best mix of properties for a conductive polymer composite cable. These include electrical conductivity, dispersability and compatibility with the composite matrix, availability and cost.

### 3.1.1 As-Received Nanotube Material Quality Assessment: Protocol

The challenges of a wide variation in initial quality of nanotubes produced via different manufacturing methods, and successful characterization of these deviations, have already been introduced in Chapter 2. The initial qualities of CNT used in this study were no exception. Using the most useful elements of established protocols, the starting quality of CNT was explored [47].

Non-tubular carbon content was evaluated using SEM and TEM. CNT were prepared as-received for SEM, mounted on aluminum SEM pucks using double-sided adhesive carbon tape. A variety of SEM instruments were used by the author during the course of this research including FEI Quanta 200 ESEM and Hitachi S-5500.

TEM samples were prepared by probe sonicating (Cole Parmer 750W) at 20kHz for 3 minutes in 20-30mL of dimethylformamide (DMF – Sigma Aldrich). One drop of this suspension is placed on 200 mesh lacey carbon grids on filtration paper. The majority of TEM work was completed using a JEOL 2100F, with some additional scanning transmission electron microscopy (STEM) characterization (Hitachi S-5500).

A quantitative assessment of nanotube purity was performed by TGA in air at 5°C/min to 800°C. Flow was set at 100sccm unless otherwise indicated. Three instruments were used interchangeably during the course of this research: TA Instruments SDT Q600 TGA/DSC (NASA Johnson Space Center and Rice University) and Q500 TGA (NanoRidge Inc.). Ceramic crucibles were used in the former instrument type and platinum in the latter.

### 3.1.2 As-received Nanotube Quality Assessment: Results

The as-received materials from Mitsui and Bayer had similar low residual catalyst amounts. In Figure 8 below, TEM images A1 and A2 highlight the slight amount of catalyst found in the Mitsui MWNT, and the good integrity of the tube sidewalls. It also confirmed the tube diameters centered in the 40-60nm range. Residual catalyst amounts of less than 8wt% were confirmed by TGA (Figure 9). As a result, these materials did not warrant any further purification.

The SWNT from Southwest Nanotechnologies (also known as "SWeNT") was the commercial grade CG100 type, and had a residual catalyst content of less than 5% (Figure 10). SEM and TEM, as seen in Figure 8, qualitatively confirmed this. Images B1 and B2, high resolution SEM and TEM respectively, show the low amount of residual metals. However, TEM analysis brought to light an issue with these tubes that would later be thought to play a role in composite conductivity; an amorphous carbon layer often found on the tube or bundle surfaces. As CG100 is both produced and purified via proprietary means, it is not clear what caused this. Spectroscopic analysis via the TEM and SEM did confirm the presence of fluorine, which the author suspects is present due to a purification procedure using hydrofluoric acid. SWeNT did supply a very limited amount of what was described as higher conductivity SWNT, grade "CG200", which was analyzed via TEM and TGA, and also faced chiral analysis. It proved to have an enormous amount of residual catalyst (>20wt%) and was not any more conductive in composite use.

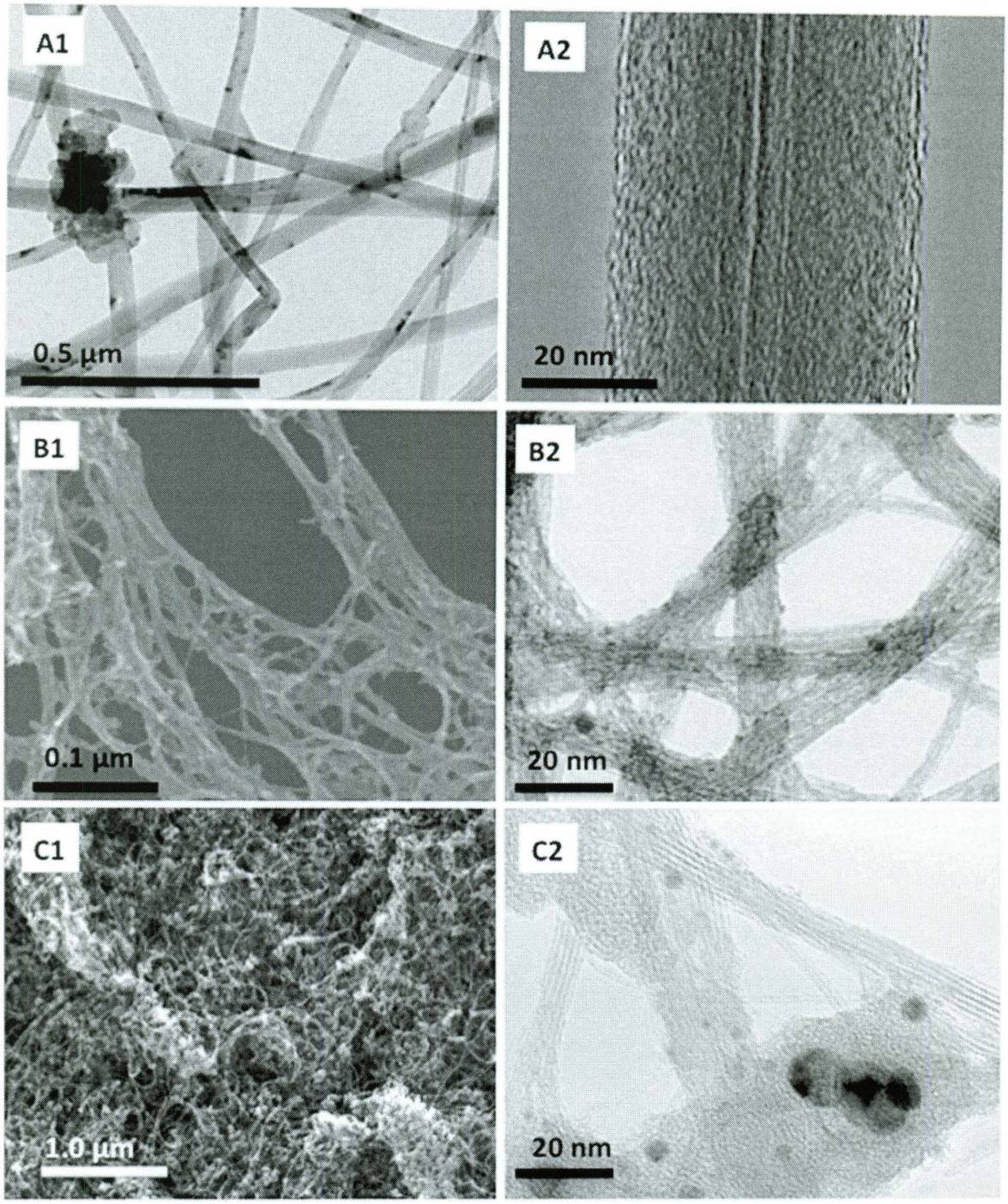


Figure 8: (A1 & A2) TEM of as received Mitsui MWNT, (B1 & B2) SEM and TEM images of as-received SWeNT CG100 CoMoCAT SWNT, (C1 & C2) SEM and TEM of as-produced laser SWNT.

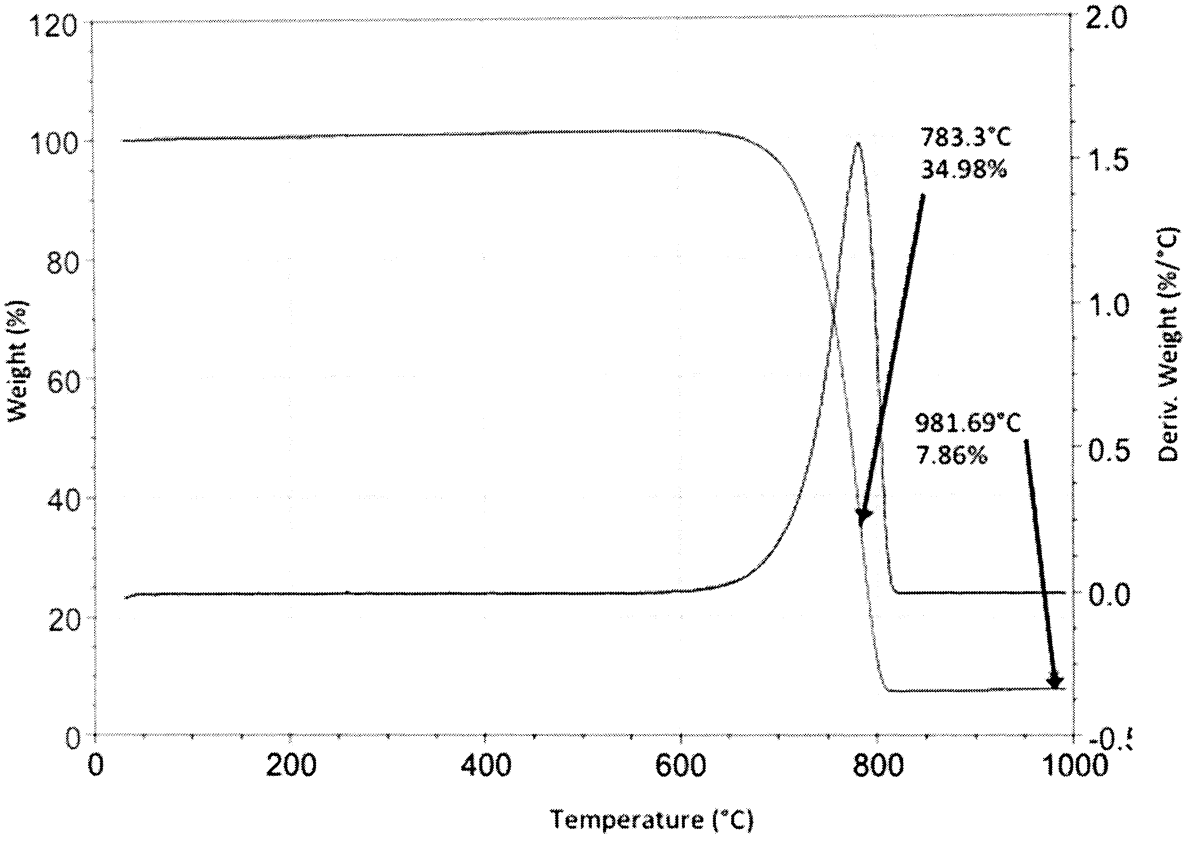


Figure 9: TGA analysis of as-received Mitsui Corp. MWNT showing low residual catalyst

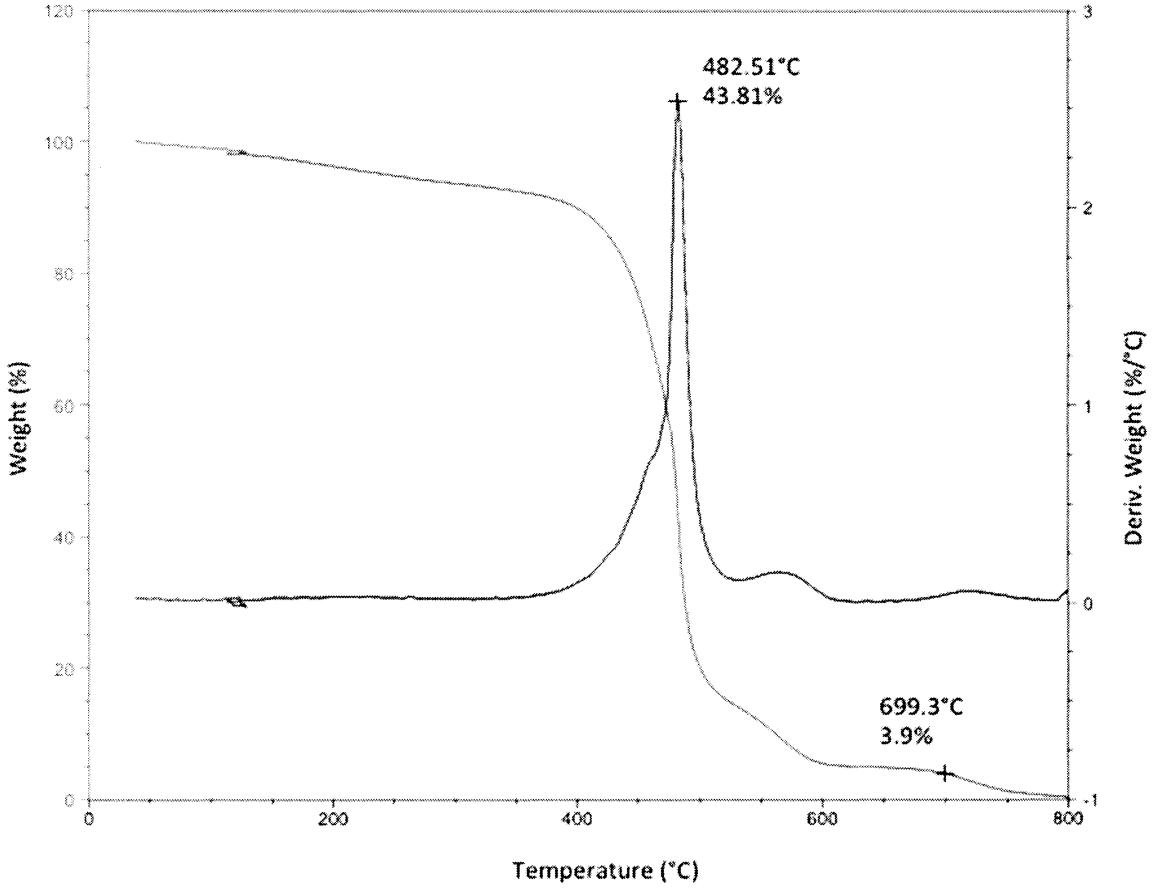


Figure 10: TGA analysis of as-received SWeNT Inc. CG100 SWNT

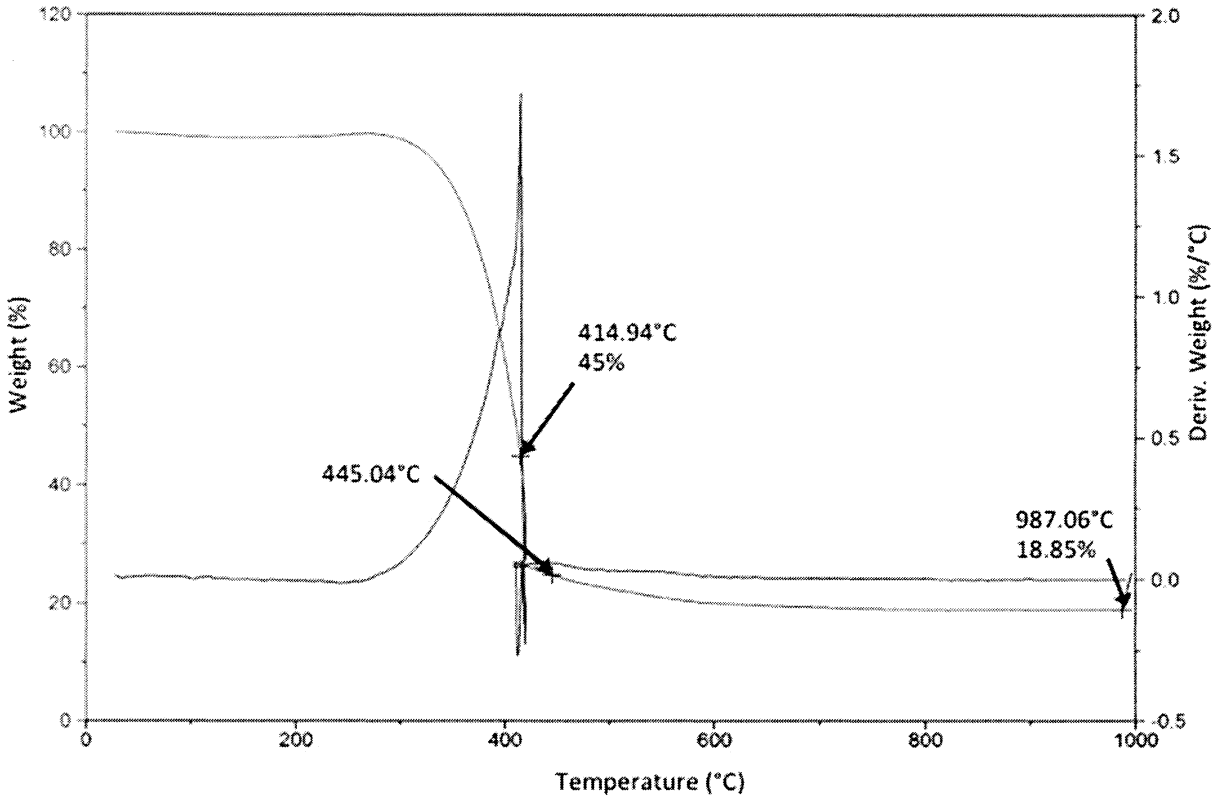


Figure 11: TGA analysis of as-produced laser SWNT

Figure 8 C1 and C2 show representative SEM and TEM of the laser-produced material. It highlights a material known for producing larger diameter tubes, with less residual catalyst. However, as confirmed by TEM in C2, the catalyst is typically wrapped in onion-like layers of carbon, which presents an issue with purification. The laser material contained between ~19wt% catalyst, as confirmed via TGA (Figure 11). It was decided given both the limited amount of material on hand, and knowing the inefficiency of purification procedures, that this SWNT would be used as received. It was also noted that this unique material is no longer produced by NASA Johnson Space Center.

The SWNT produced via both laser ablation and HiPco methods were received with significant residual catalysts. The HiPco material contained approximately 35% residual catalyst. Given this high number, and the important role HiPco material would play in producing composites with polyethylene, purification of the material was pursued.

### 3.1.3 Purification of Nanotubes

Figure 12 highlights the typically high residual metals content in HiPco material, this example was ~33wt%. This material, often iron coated in oxide and carbonaceous species, would have to be removed before use. The as-received HiPco SWNT material was purified using two different methods. The first method was via a previously-developed multistage procedure, which encompasses slow oxidation in humid air at 250-325°C for 24 hours, stirring in concentrated hydrochloric acid (HCL), washing to neutral pH with DI water and methanol and annealed at 800°C in argon (Ar) for one hour[48]. The relatively low temperature wet air oxidation step exposes metal particles from within carbon shells. Also, the water has been shown to enhance the low-temperature catalytic oxidation of carbon, which assists in the removal of non-tubular carbon content. The HCL step then extracts the iron or residual catalyst. The author has utilized this protocol extensively in the past, in addition to its modified form [49], and found it consistently able to reduce leftover catalyst impurities to 2.5-5wt% (Figure 13) and have a yield of ~20-40wt%.

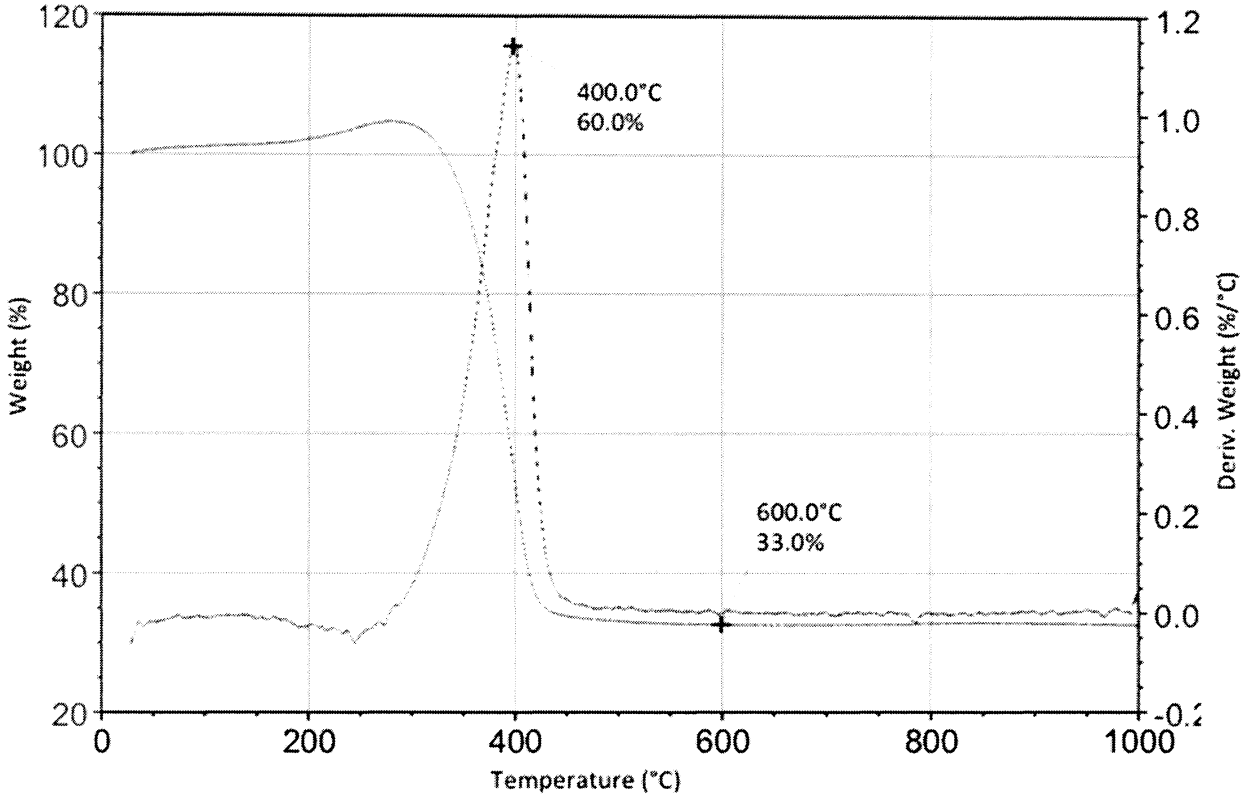


Figure 12: TGA analysis of as-received HiPco SWNT showing residual catalyst content

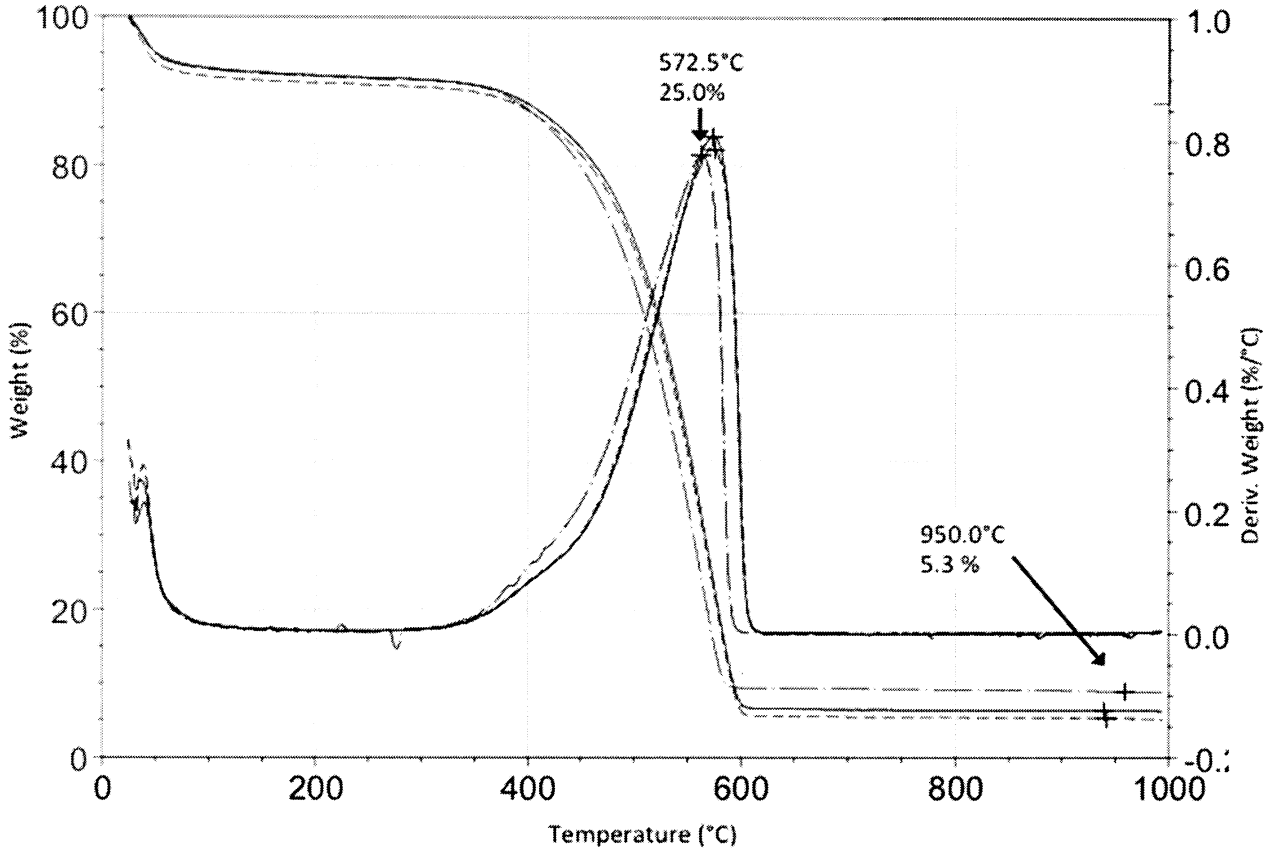


Figure 13: TGA analysis of HiPco SWNT purified via the slow oxidation method

In an effort to find a process more suitable for easy purification of larger amounts than 500mg of CNT, and one with a greater yield, a second process was also explored. The carbon coated leftover catalysts were dissolved by reaction with a "one-pot purification method" of hydrogen peroxide ($H_2O_2$) and HCL at 40-70°C for 4-8 hours [50]. This process combines the oxidation of raw carbon materials by $H_2O_2$ with the removal of metals by HCL. Maintaining the pH to 1-3 reduces the consummation of SWNT by $H_2O_2$. It is thought the $H_2O_2$ penetrates graphitic shells though imperfections and combines with the iron to assist in the oxidation of the carbon coatings (Figure 14). The metal particles act as a catalyst to effect the

purification via Fenton's chemistry to produce hydroxyl radicals. Wang et al. noted that the reactivity of the SWNT with $H_2O_2$ rests sharply on temperature. It was observed that below 60°C the reaction is scarcely observable, while at 90°C the semiconducting SWNT are more reactive than metallic because of faster oxidation caused by hole-doping by $H_2O_2$[51]. This protocol also offers the advantage that the purifying materials are relatively affordable and benign. $H_2O_2$ is an oxidant common in wastewater treatment while HCL is a common industrial chemical than can easily be turned into a common salt (NaCl).

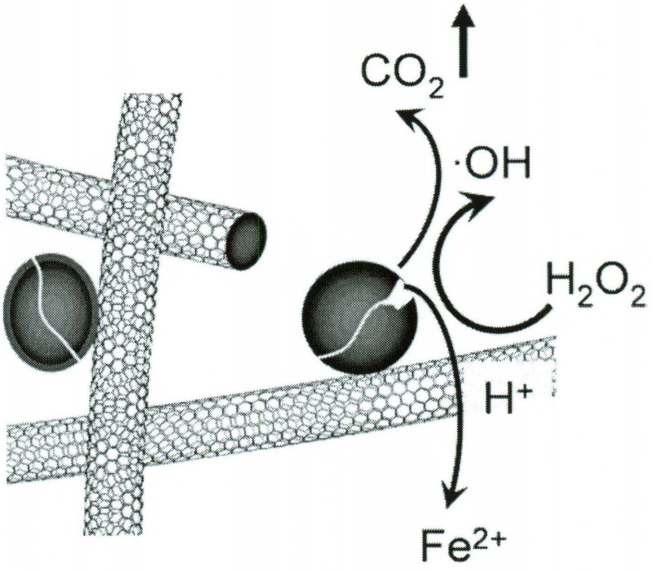


Figure 14: Schematic of localized catalytic reaction of $H_2O_2$ with iron particles in carbon shells [50]

The original protocol calls for a 20-50mg portion of raw HiPco to be mixed with 20mL of 1N HCL and 20mL of 30% $H_2O_2$ in a 250mL open flask and stirred with a Teflon coated magnetic stirrer to form a slurry. The slurry is then heated on a hot plate at 60±5°C for 4 hours. 20mL of HCL and 20mL of $H_2O_2$ are then added at the end of each hour. The SWNT are filtered and washed with 500mL of purified water ($H_2O$).

After some initial experimentation, this process proved relatively easy to scale up. 2.8g of HiPco SWNT was down packed using isopropyl alcohol (IPA – Sigma Aldrich) in its container from the as-received "fluffy" form into a safer-to-handle compacted state. 2.5g of SWNT were mixed with 500mL of 1.0N standardized HCL (Alfa Aesar) in a triple-neck round bottom flask, and actively stirred with a Teflon stir bar throughout the reaction. Using a variac and a heating mantle, the temperature of the mixture was heated to 60°C and monitored via thermometer. 200mL of $H_2O_2$ and 200mL of HCL is then added. Smaller volumes of $H_2O_2$ and HCL were initially used, but were found via TGA and TEM to be less effective than originally hoped. 200mL represents a volume that matches effectivity of reaction with practicality of experimental setup for this scaled-up protocol.

A vigorous bubbling and boiling was observed as the exothermic reaction took place. The excess HCL was found to serve a number of purposes including maintaining the pH at a low enough level to prevent the $H_2O_2$ attacking the SWNT [50] and effectively dispersing the large amount of tubes being processed. The heating

mantle is lowered to match the heat of reaction produced so that the temperature does not exceed ~75°C. As with the original protocol, the solution turned a green or yellow color, which is indicative of iron dissolution.

After one hour, it was observed that the reaction had abated and the temperature was actively maintained above 60°C. At this point 200mL of $H_2O_2$ and 200mL of HCL was added once more. These steps were enacted a total of four times as found in the original protocol. Given the acidity of the HCL, the strong oxidizing nature of the $H_2O_2$ and the propensity for large amounts of heat to be produced, the author found that temperature management to be critical and the incremental increase in experimental volumes tested, to be a useful preparation. At the end of the fourth hour the external heat is turned off and the stirring reduced to a slow rate.

The slurry was then filtered using a glass filter. The material was washed and filtered with deionized water until a neutral pH is achieved. It was found that 3-5L of water is necessary and that filtration will take ~8hours.

Prior experience of both the author and his collaborators at NanoRidge Inc. has shown that SWNT filtered with deionized water becomes highly compacted with large bundle sizes which is less than ideal as a working material facing dispersion via either mechanical or chemical means. A higher packing density is probably to blame from the SWNT being drawn together by the action of surface tension during drying[52]. Additional research has been conducted to formalize these observations,

and it is thought that the relatively slow evaporation of water, migrating through the sample via capillary action and of variable concentration, is causing disproportionate contraction [53](Figure 15).

**Table 1 – The properties of buckypaper collated from casting MWCNTs in solvents of differing surface tension**

| Solvent | Film diameter (mm) | Apparent density (g $cm^{-3}$) | Porosity (%) |
|---|---|---|---|
| Dichloromethane | 15.4 ± 0.1 | 0.28 | 85.8 ± 0.2 |
| Hexane | 14.7 ± 0.2 | 0.26 | 86.9 ± 0.4 |
| Methanol | 14.8 ± 0.2 | 0.28 | 86.2 ± 0.9 |
| Toluene | 14.8 ± 0.3 | 0.30 | 84.8 ± 0.9 |
| Water | 13.0 ± 0.7 | 0.32 | 83.9 ± 0.4 |
| Triton-X100 | n/a | 0.42 | 79.2 ± 1.1 |

Each figure was derived from an average of three samples per solvent and includes the standard deviation.

Figure 15: Data from the literature showing density and porosity of CNT papers formed via evaporation [53]

Although this explanation simplifies the obvious solvent-solvent and SWNT-solvent interaction differences between solvents, it formalizes results that solvents such as alcohols and benzenes create less dense and more porous agglomerations of SWNT under evaporation (Figure 15). To abate this issue, the still wet filtered material was then washed with IPA and filtered. The material was then slowly dried using a Pyrex dish on a hotplate, while continuingly cutting and dicing the material with a razor blade. This produces a fine powder, which disperses more effectively in solvent.

TGA analysis of the as-purified material showed success in terms of residual catalyst, with amounts less than 4wt% (Figure 16). However, the nature of the second derivative peak, or oxidation peak, is broader in nature than the TGA in data for the previous purification method, and has a lower peak temperature.

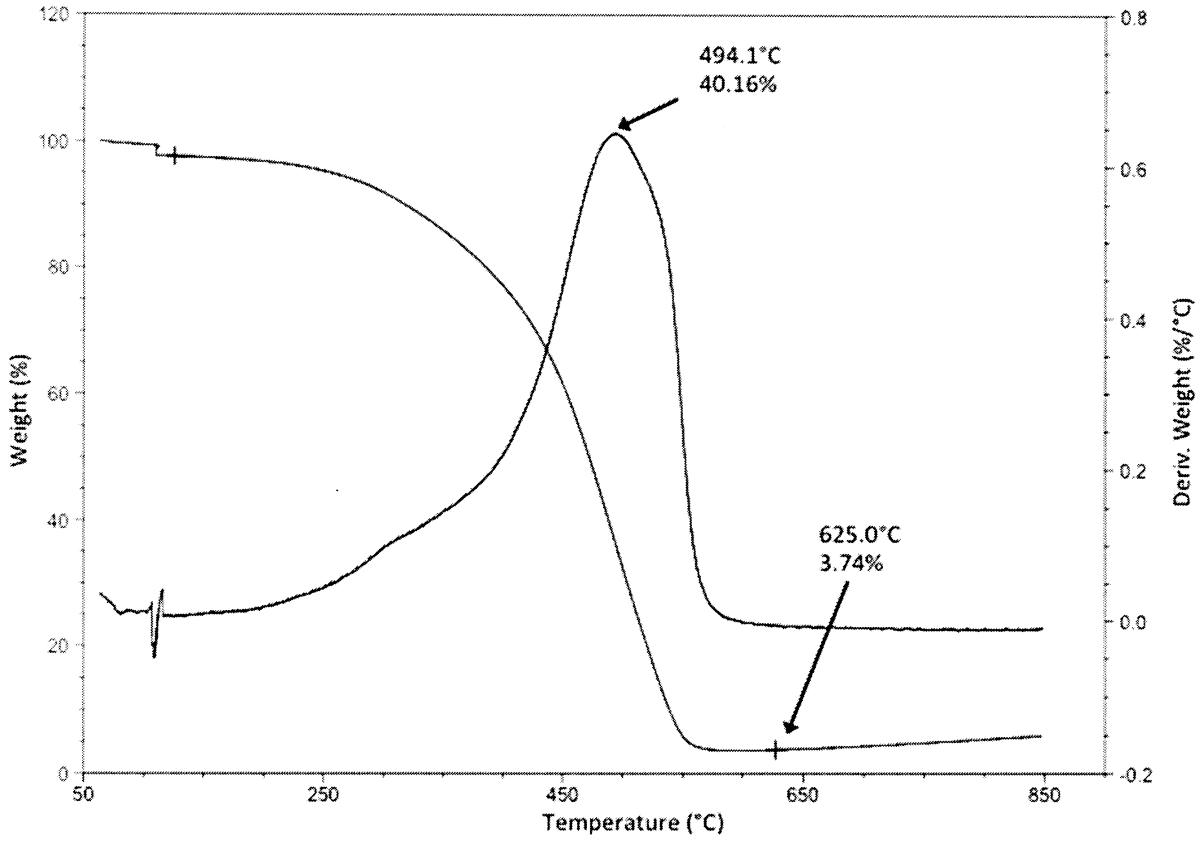


Figure 16: TGA analysis of HiPco SWNT purified by scaled up "one-pot" method showing low residual catalyst mass

This suggests a less homogeneous product has been produced by this purification procedure, and there is a higher amount of residual amorphous carbon. To confirm that the purification procedure did not damage the SWNT sidewalls, Raman

spectroscopy was carried out (Figure 17). The ratio between the G band (the graphite related optical mode) at 1550-1605 $cm^{-1,}$ and the D band (defect or disorder induced) at ~1350 $cm^{-1}$ is accepted as an accurate measure of nanotube damage or modification [54].

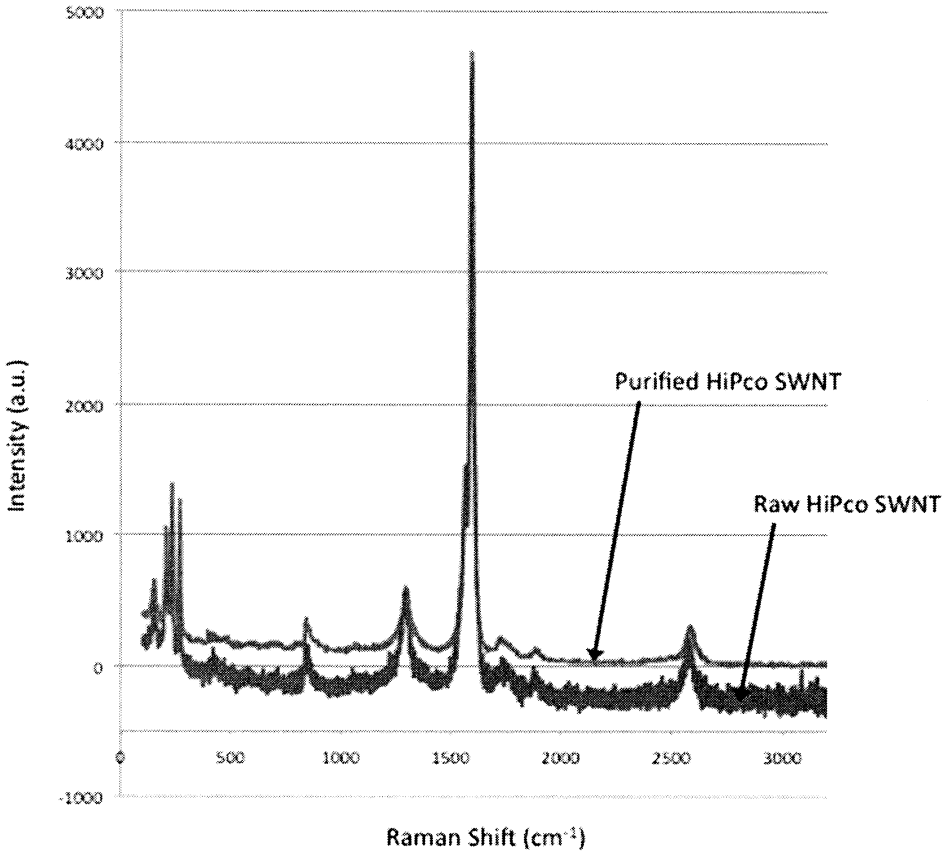


Figure 17: Raman spectra comparing HiPco SWNT before and after modified "one-pot" purification protocol

Figure 17 shows no significant changes in this D-G ratio between as-received material and the purified SWNT. This is comparable in performance with the lower-scale slow oxidation method already explored.

SEM and TEM were also carried out on the "before" and "after" SWNT. Figure 18 A1 and A2 show the fluffy nature of the as-received tubes and the significant amount of residual catalyst respectively. Figure 18 B1 does highlight the compacting nature of this purification procedure, which is no worse nor better than the slow oxidation process, while the TEM in B2 shows the process ability to reduce residual catalyst.

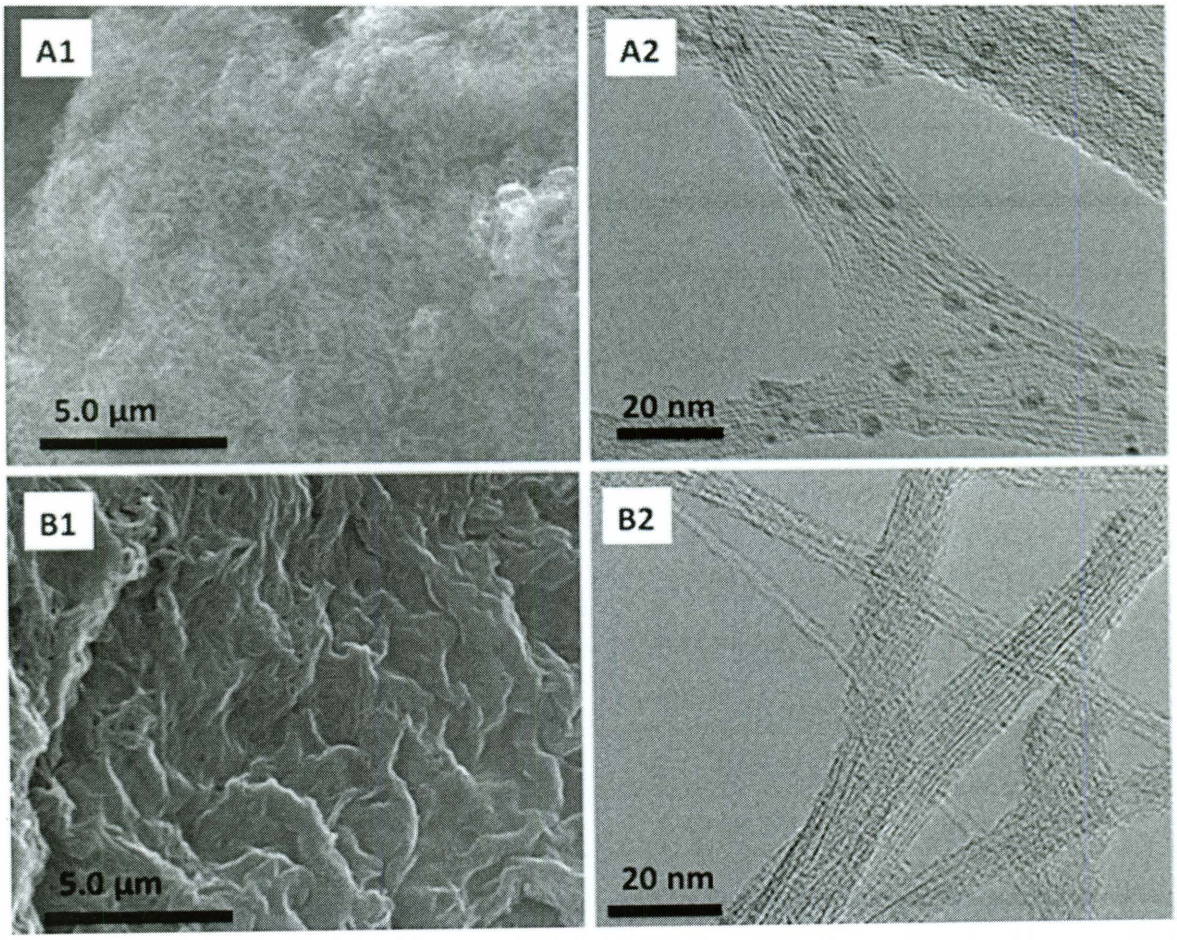


Figure 18: SEM and TEM image (A1 & A2) of as-received HiPco SWNT, SEM and TEM image (B1 & B2) of HiPco SWNT purified via scaled up "one-pot" protocol

Overall, the modified and scaled-up "one-pot" process proved a success in a number of aspects including scalability (>1g can be processed easily), effectivity (residual catalyst reduced) and efficiency (yield of 60-80%). The differences in homogeneity of tubes between the two purification methods were put to consideration when the materials were used for composite fabrication.

## 3.2 NANOTUBE CHIRALITY AND DIAMETER ASSESSMENT

As already discussed, carbon nanotubes may differ in diameter and chirality. Previous work in the literature is clear that due to differences and distributions in CNT properties such as these, CNT polymer composites are far from ideal systems [19]. In this thesis, an attempt was made to get a handle on this issue, via characterization. Even though the emphasis of this study is on the production of macro scale polymer composites with improvements in electrical resistivity, the role of nanoscale properties such as chirality were explored. There appears to be little or no examples in the literature of previous attempts to bridge the gap between research of chirality and effects at the macroscale.

There are a number of approaches for characterizing SWNT (n,m) distributions, including microscopic tools such as TEM, scanning tunneling microscopy (STM) and AFM. These methods are tedious at best, and difficult to build statistically relevant result sets. Analysis methods for bulk amounts of SWNT include Raman [55,56], ultraviolet visible near infrared (UV-vis-NIR) absorption [57] and near infrared (NIR) fluorescence [58].

The author was familiar with the work of the Weisman Group at Rice University, through previous funding and collaboration efforts at NASA Johnson Space Center (Alliance for NanoHealth NASA JSC-NNJ06HC25G). Using the latest emission and absorption spectrometer designed by this group [59], data was collected and used to

identify and quantify numerous SWNT structural species in the relevant bulk samples used in this research. The system employs fixed wavelength diode lasers to excite emission, a broadband lamp to probe absorption spectra and NIR and visible spectrometers for absorption and fluorescence measurement. It also disentangles the spectral contributions of (n,m) species that may overlap by fitting the emission spectra under constraints based on the large prior spectroscopic database collected by the Weisman lab. Using NIR fluorescence is considered the most up to date bulk SWNT spectroscopic technique, and is based on distinct band gap photoluminescence from individualized SWNT [59]. It is claimed this technique is more sensitive than Raman or absorption. However, it is relevant only for semiconducting species of SWNT (~2/3 of most as-produced) because metallic tubes are non-emissive. Also, this technique is not relevant to MWNT materials.

### 3.2.1 Sample Preparation

Solutions of SWNT were suspended by 1wt% 4-Dodecylbenzenesulfonic acid (SDBS) surfactant in deuterium oxide ($D_2O$) at a concentration of 1.5mg/5mL ($D_2O$, unlike $H_2O$, will not overlap or interfere with the bands of interest for spectrometry). These solutions were bath sonicated for 30 minutes (Sharpertek XP), followed by tip sonication for 3-5 minutes in continuous mode at 8W RMS (Microsonic Ultrasonic Cell Disrupter). These steps were then followed by centrifugation for 120 minutes at 50,000RPM (Beckman Coulter Optima Max Ultracentrifuge). The various supernatants were then taken off and found to be (by eye) well dispersed but still too concentrated for reliable measurement. To improve absorbance and dispersion,

a dilution of 2X to 4X with the 1wt% SDBS solution was then used. The samples were then placed in cuvettes for analysis.

### 3.2.2 Results

The complete dataset is presented in Appendix A. For brevity, the data and analysis from NASA JSC Laser Ablation SWNT, Batch JSC 390 AQW is presented, while a summary of results for the rest of the SWNT types is presented. Figure 19 shows

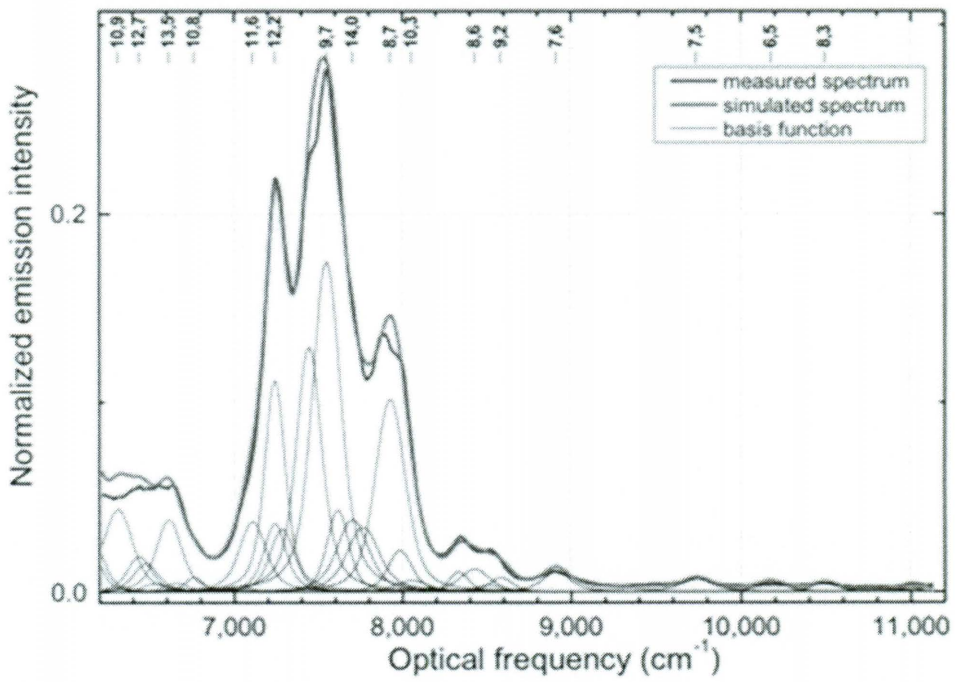


Figure 19: Fluorescence emission from Laser Ablation SWNT excited at 785 nm

the fluorescence emission from the laser nanotubes excited at 785nm. The blue line shows the experimental data, the individual grey/black lines are calculated contributions from indicated (n,m) species and hence diameters, while the red line shows the full simulated spectrum. The signal from each (n,m) species is found by integrating its peak along the emission axis at the excitation frequency giving maximum emission. A lot of fine-tuning, optimization and data fitting takes place in the background [59] to make this an effective method and instrument.

Figure 20 below shows the graphene sheet plot constructed from the full three laser excitation (660, 729, and 785 nm). Density or abundance of these distributions is illustrated by the thickness or weighting of the hexagon lines.

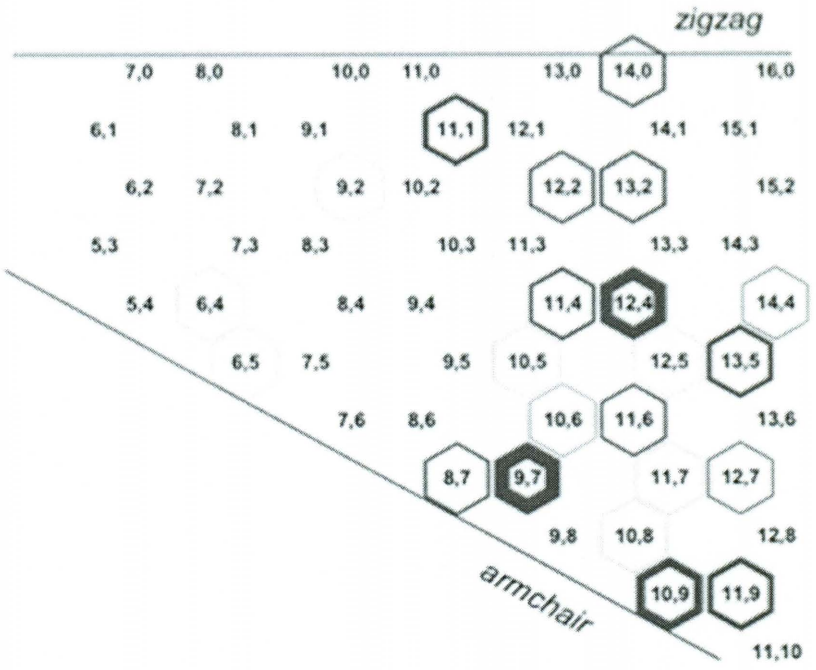


Figure 20: Graphene sheet plot showing the calculated (n,m) species relative abundance in laser ablation SWNT

Diameter distribution is graphically represented in Figure 21. As noted by the author from prior experience, the laser material has a larger diameter distribution in general than HiPco or other SWNT material.

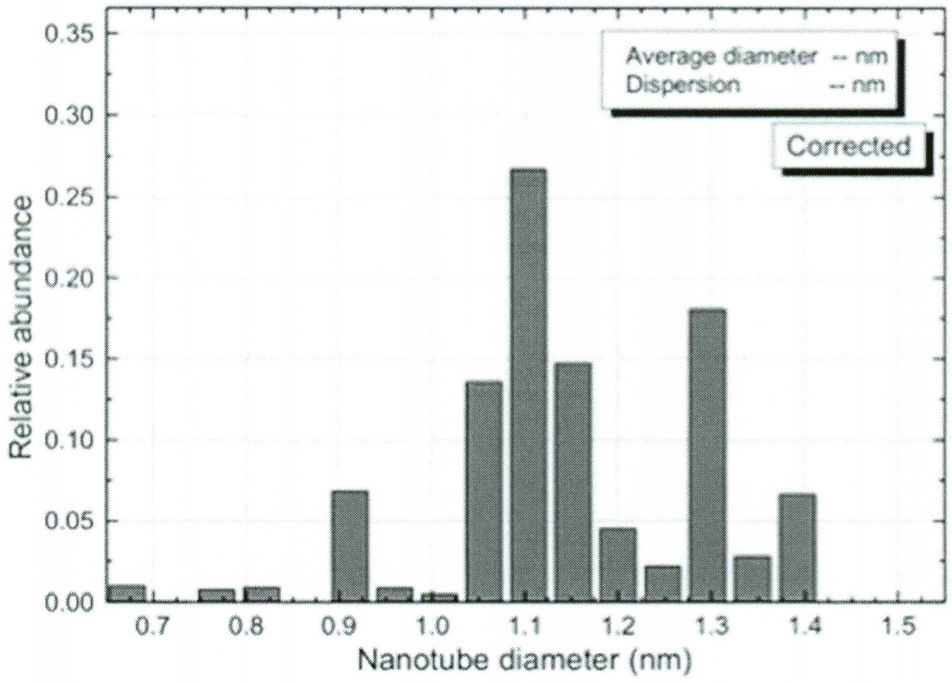


Figure 21: Diameter distribution histogram of laser ablation SWNT

Table 5 summarizes the data found by this analysis. As expected, the laser material provided a larger diameter nanotube, while the commercially available CG100 was the smallest. A challenge with this technique is deducing SWNT composition from what can be described as discrete slices of the full excitation emission [59]. While using the Weismann Lab empirical based models for SWCNT excitation and

emission spectra can solve this issue, approximations in these models can lead to inaccuracies in addition to overlapping emission peaks.

| **SWNT Type** | **Diameter (nm)** | **Comment** |
|---|---|---|
| SWeNT CG100 | 0.75 - 0.95 | Mostly semiconducting |
| SWeNT CG200 Lot 400 | 0.75 – 1.1 | Mostly semiconducting |
| SWeNT CG200 Lot 700 | 0.75 – 1.15 | Mostly semiconducting |
| NASA JSC Laser | 1.05 – 1.4 | Mostly semiconducting |
| Rice University HiPco | 0.8 – 1.4 | Mostly semiconducting |

Table 5: Summary of diameter and general findings on SWNT material

While this analysis was incapable of providing direct statistics on metallic tube species content of the various tube batches, it did provide data useful for matching the tube types in this study, with composition data previously presented by the Weisman group (Table 6). With these positive "fingerprints", metallic content can be reasonably assumed from the literature.

| Nanotube Type | % Metallic | % Semiconducting |
|---|---|---|
| Rice U. HiPco SWNT | 37 | 63 |
| SWeNT CG100 SWNT | 48 | 52 |
| NASA Laser SWNT | 45 | 55 |

Table 6: Metallic and semiconducting compositions (adapted from [60])

## 3.3 RESISTIVITY ASSESSMENT OF CARBON NANOTUBES

Resistivity analysis of nanotubes used in this study, before deployment as fillers for polyethylene composites, was conducted. In a similar vein to the chirality assessment, the author identified the need to bridge engineering data with scientific studies by analyzing the CNT across length scales, from macroscopic bulk resistivity, to microscale and onto nano. This was in an effort to identify CNT conductivity aspects across the length scales and see if any affect bulk properties and why.

### 3.3.1 Resistivity Assessment on the Macroscale

Macroscale resistivity was tested using a simple process of compressing a "buckpaper" of nanotubes in a press, and then testing resistivity using a 4-point probe. 50-150mg of material was weighed, placed in a 1cm diameter stainless steel die and pressed (Carver Press) under 20,000lbs pressure for 5 minutes. The CNT disks were then removed for electrical measurement.

A 4-point probe (Jandel) was used to measure electrical resistance of various CNT types available. The probe was instrumented with a Keithley 6221 DC & AC Current Source paired with a Keithley 2182A Nanovoltmeter. The system was setup in *delta mode,* which is typical for use on low resistance devices where noise from thermal electromotive forces (EMF) maybe an issue. An alternating current source with coordinated voltage measurements is used towards that end. Typically, the current

varied in a square wave fashion from 20*10-6 amps to -20*10-6 amps for a total of 1000 readings per test. A graphical representation of the current swing and measurement is shown in Figure 22.

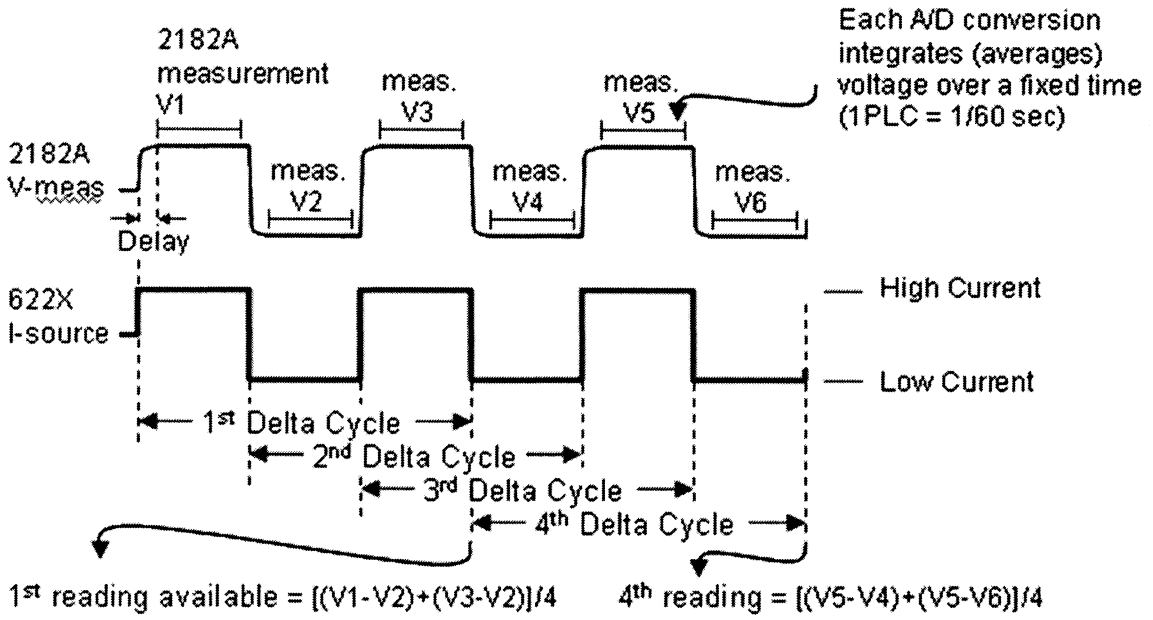


Figure 22: Graphical explanation of *delta mode* used in obtaining 4-point probe data

At least three measurements where taken at different positions on the sample and then averaged. Each measurement file produced 1000 readings for resistance, calculated from voltage divided by current (V/I), which was then converted to resistivity, ρ, in units of ohm•cm (Ω•cm). This conversion begins with the equation:

$$\rho = 2*\pi*s*(V/I)$$

Where **s** is the spacing of the probe in cm and **V/I** is the resistance in ohms [61]. The vast majority of the samples tested during this study did not contain semi-infinite dimensions, in particular thickness, as assumed by this equation. Valdes showed that when the sample thickness **t** is <= 5s, the true resistivity can be calculated from [62]:

$$\rho = 2*a*\pi*s*(V/I)$$

Where **a** is a thickness correction factor plotted by Valdes. For **t/s** <= 0.5, this plot is a straight line providing a value of **a** of:

$$a = 0.72\ (t/s)$$

Plugging this into the basic equation one obtains for samples where **t/s** <= 0.5 one gets:

$$\rho = 4.53*(V/I)*t$$

This equation was utilized throughout the research presented as the vast majority of samples had dimensions of **t/s** <= 0.5, unless otherwise indicated. Resistivity measurements of as-received CNT are presented in Table 7. All resistance measurements were verified by using a second experimental setup comprised of a Cascade C4S-67 4 point probe combined with Agilent 34410A Digital Multimeter.

The resistivity data summarized in Table 7 *appears* to verify a relationship between bulk resistivity and chirality.

| Carbon Nanotube Source & Type | Resistivity (Ω•cm) |
|---|---|
| SWeNT CG100 SWNT | $1.4 * 10^{-2}$ |
| NASA JSC Laser SWNT | $6.4 * 10^{-3}$ |
| Rice University HiPco SWNT | $1.7 * 10^{-2}$ |
| Mitsui MWNT | $6.3 * 10^{-2}$ |

Table 7: Bulk resistivities of the various carbon nanotubes initially considered

The chirality data presented, organized the CNT by metallic content in the following order: SWeNT CG100 > NASA Laser > Rice University HiPco. However, the table above shows that the as-received laser CNT has a lower resistivity ($6.4 * 10^{-3}$ Ω•cm) than the SWeNT CG100 equivalent ($1.4 * 10^{-2}$ Ω•cm) . The author suggests this is due to two factors. Firstly, the CG100 have clearly been coated in amorphous carbon as seen in the TEM and secondly, their diameter is noticeably smaller than the laser CNT. It has been suggested that larger diameter SWNT provide higher conductivities in both buckypaper and composite forms [19].

### 3.3.2 Resistivity Assessment on the Microscale

Microscale resistance measurements were conducted by the author at NASA Ames Research Center (ARC). Using a chip-based platform previously developed by ARC for gas sensing [63], nanotube resistance was measured by microscale platinum interdigitated electrodes integrated as sensor pads on silicon chips. Each chip consisted of multi-layer array of sensor pads fabricated from P-type boron-doped silicon (100) wafers, a 0.5 μm silicon dioxide (SiO2) layer and patterned 200 nm thick lines of platinum to form the interdigitated electrodes or sensor pads. Each pattern had 10 or 20 μm finger widths with finger spacing's of 4, 8, 12 or 50 μm This platform was successfully used by the author in the development of a CNT-based radiation sensor [64], which functioned on the basis of CNT resistance change under radiation stimuli. This measurement method had the advantage of measuring 10-100 nanotube to electrode contact points, an electrical network many orders of magnitude smaller than the billions of CNT present in the bulk samples.

The sensor chips were prepared by washing with methanol, acetone and finally isopropyl alcohol. The chips were then installed into a plastic leaded chip carrier (PLCC), a standard plastic four-sided chip carrier.

CNT samples were prepared by bath sonicating 15mg/mL solutions of CNT and DMF for at least 2 hours. ~7nL of solution was deposited on each sensor pad using pulled micropipettes of glass fabricated by the author, combined with a microinjection system (NanoInject II, Drummond Scientific) starting at the smallest volume of

2.3nL. Each sensor chip had 60 sensor pads of interdigitated electrodes. Three pads were used for each sample. Resistances were measured using a multimeter (Keithley 2002) and multichannel switch (Keithley 7001). Figure 23 shows the result of deposition of SWNT onto a single sensor pad.

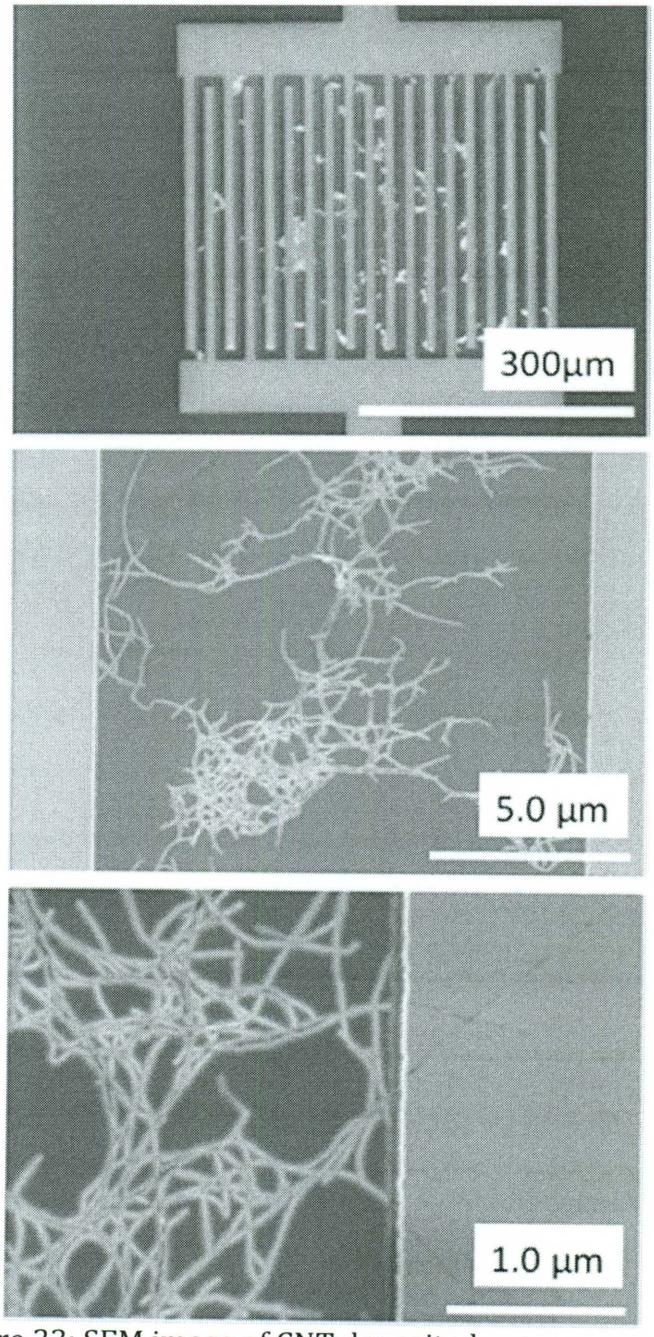


Figure 23: SEM image of CNT deposited onto sensor pad

Image analysis of each sensor pad was carried out by hand, to ensure that both the number of CNT-electrode contacts and relative size of CNT networks were similar between nanotube species tested, and a weighting was applied if there was notable differences. Relative resistance measurements are presented in Figure 24:

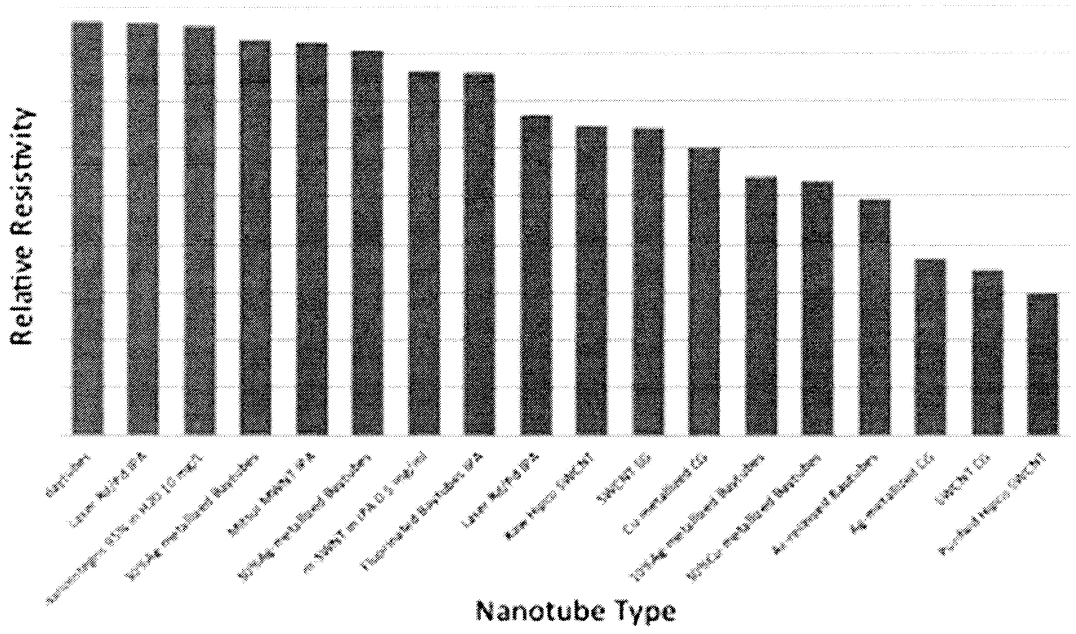


Figure 24: Relative resistance data for various CNT types and species

It should be noted that no accommodation was made for differences in tubes specie contact resistance with the platinum electrodes. The general trend of CNT resistances did not match that found at the macroscale nor did it relate well to chirality measurements. These microscale measurements found that the relative resistances of the CNT followed a pattern of NASA Laser > SWeNT CG100 > Rice University HiPco. The aforementioned chirality data presented organized the CNT

by metallic content in the following order: SWeNT CG100 > NASA Laser > Rice University HiPco, while the bulk resistivity measurements rated as-received laser CNT material having a lower resistivity ($6.4 * 10^{-3}$ Ω•cm) than the SWeNT CG100 equivalent ($1.4 * 10^{-2}$ Ω•cm). The author surmises that perhaps small differences in dispersion and bundle size, unseen using SEM, could have provided these changes. This exercise on the microscale did serve the useful purpose of confirming that MWNT resistivity is larger than SWNT even at this scale, and that much of the touted commercial "enhanced conductivity" nanotube products on the market do not provide added value over purified HiPco.

### 3.3.3 Resistivity Assessment on the Nanoscale

Continuing the journey to bridge the knowledge gap of CNT resistivity across scales, an effort was made to characterize nanotube conductivity on the nanoscale. Multiple avenues of characterization methods were explored. The author trained himself with the use of a Focused Ion Beam (FIB) microscope at the University of Houston, in an effort to replicate early nanotube research [65], and explored methods utilizing AFM. Unfortunately, the complexity involved, the scope of the work (which would warrant a thesis unto itself) and the lack of both facilities and expert technical advice made this task extremely challenging.

Relying on a SEM (FEI) at Rice University, in combination with a 4 probe mechanical nanomanipulator (Zyvex), individual tube measurements were explored. Figure 25 shows the basic configuration of a two point measurement of a Mitsui MWNT.

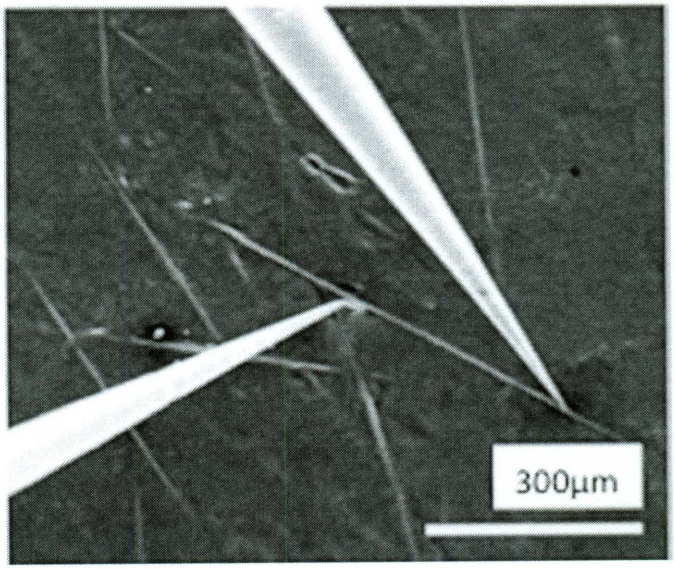


Figure 25: Two-point measurement of MWNT using Zyvex nanomanipulator

Use of this setup had some serious drawbacks. The smallest movement possible with the manipulator was ~50nm which, when combined with the relatively low resolution of an SEM, made manipulation of MWNT extremely challenging and any meaningful interaction with SWNT impossible (Figure 26). The bulk of the equipment itself necessitated a large working distance in the SEM, which reduced image resolution further. The exercise was successful solely in measuring the conductivity of the Mitsui MWNT, which it estimated at $10^{-3}$ Ω•cm, a slight improvement from bulk measurements.

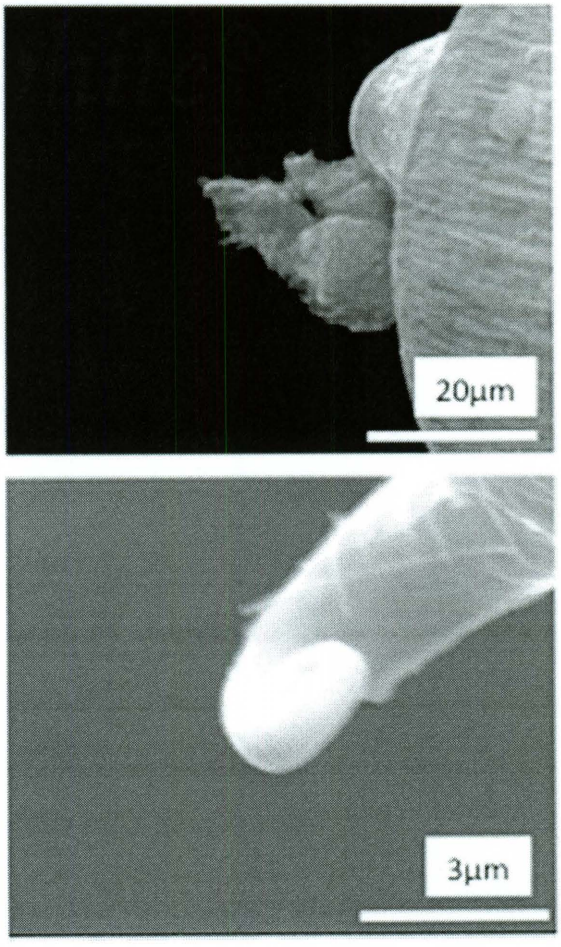


Figure 26: Manipulation of SWNT bundles and tubes

# CHAPTER 4: CONDUCTIVE POLYETHYLENE COMPOSITE

## 4.1 PREPARATION OF CARBON NANOTUBE AND POLYETHYLENE COMPOSITES

### 4.1.1 Solvent Blending

As previously discussed, 1,2-dichlorobenzene (DCB) is an effective solvent for both carbon nanotubes and polyethylene. It has also been shown that solutions of SWNT in DCB do not pass through PTFE membranes (1.2μm), which is critical for successful vacuum filtration [66]. With this in mind, and having prior success combining SWNT with polymer matrices, a simple solvent blending technique using DCB, sonication and vacuum filtration was pursued.

Unfortunately, the obvious conclusion to use DCB for SWNT-polyethylene composite fabrication was not lost on earlier work in the literature. Haggenmueller et al. used what was described as a "hot coagulation method" to disperse SWNT in PE using DCB. HDPE and LDPE were dissolved in DCB at a concentration of 20 mg $mL^{-1}$ at temperatures of 115 and 85°C respectively [39]. SWNT at a concentration of 0.2mg $mL^{-1}$ in DCB were bath sonicated for 48 hours. The bath temperature was increased to 97°C and the PE solution added. Following five minutes of further sonication, the mixture was cooled to below 70°C to allow polymer crystallization. Although not explicitly stated, if following "the previously described coagulation method" [67], this

mixture was then immersed in a large amount (5:1) of room temperature purified water. It is claimed that this step precipitates the polymer immediately due to its insolubility in water. The SWNT are then trapped within the polymer chains and prevented from forming larger bundles. The mixture is then filtered and dried under vacuum at 120°C fro 24 hours. The filtrate was noted as clear.

### 4.1.2 Nanotube and Solvent

Where practical, a concentration of 0.1mg $mL^{-1}$ (or 100mg $L^{-1}$) SWNT in DCB was used in this work for the preparation of composites, which was more in keeping with noted maximum concentrations for successful dispersion [66]. This prevents the presence of large agglomerates seen in similar recent work and deems unnecessary, the decanting steps used in that study [68].

### 4.1.3 Sonication Optimization

With scalability in mind, the protocol presented in this thesis used a *probe* versus *bath* sonicator. Initial experiments used bath sonication, but the multiple days required to disperse the SWNT were found to be inefficient, and the resultant dispersions appeared poor using simple optical microscopy. Bath sonication is limited in the amount of energy it can deliver to a sample. Haggenmueller et al. used a 260W system operating at 48kHz. Sonicators such as this produce a power density at the transducer face of ~1-2 W $cm^{-2}$ using piezoelectric transducers [69].

A 750W ultrasonicator operating at 20kHz (Cole Parmer) with a 13mm probe was utilized for SWNT sonication in DCB. This provides a high intensity cavitational collapse and hence, a large amount of energy on the order of 100's of W $cm^{-2}$, albeit on a smaller area. Given the two order increase in power per area, combined with the approximately one order reduction in possible useful area exposed in comparison to Haggenmueller's protocol, it was estimated that sonication time could be reduced to 2.5 hours. Using simple optical microscopy of SWNT dispersion in DCB, greater than 2.5 hours of sonication offered little improvement.

It has been long recognized in carbon nanotube science that ultrasonication can damage or even cut SWNT [70]. Longer nanotube and nanotube bundle lengths are generally favorable for good electrical conductivity [71]. Hennrich et al. noted a 75% reduction in average length after 30 minutes of ultrasonication during an experiment with similar nanotube-in-solvent concentrations used in this thesis [72]. They provided a relationship of average length L(t) as a function of time t scaling as $t^{-n}$, with n=0.5. However, the overall volumes used for sonication exposure during this work were small, and there was an aspect of nanotube sorting through centrifugation that reduces the relevance of its result to this thesis somewhat. Lucas et al, using MWNT and a large reservoir of circuiting nanotube suspension, came to the conclusion that n=0.2 [73]. This resulted in approximately a 25% reduction in nanotube length during the first 2.5 hours of sonication. While the use of MWNT reduces relevance, the large circuiting volumes and experimental approach is closer

to the protocol of sonication used in this thesis. Given the consideration towards 1. the aforementioned SWNT-PE composite literature, 2. bath versus probe sonication, in combination with 3. the literature on nanotube length reduction from sonication and 4. simple observation of SWNT dispersion on the micron scale, a sonication time of 2.5 hours was settled upon.

### 4.1.4 Polyethylene and Solvent

As noted in the literature, one can improve dissolution and lower polymer chain entanglement by lowering the concentration and increasing the solvent temperature [7]. To that end, this work diverged from prior efforts [68] [39], by increasing the DCB temperature to greater than 120°C (melting temperature) and reducing the concentration to 1mg $mL^{-1}$ where practical.

Differential Scanning Calorimetry (DSC) was carried out on the MDPE both before, and after, solvent processing with DCB. It was found that the crystallinity increased from ~35 to ~45%.

### 4.1.5 Composite Nanotube in Polyethylene Composite

Concentrations, varying from 0.001wt% to 90wt%, of various nanotube types were combined with a number of PE densities, focusing primarily on MDPE. As described, the nanotubes were dispersed using ~2 hours of sonication in DCB. PE was melted and dissolved in solvent at temperatures comfortably in excess of the polymer melting point. The sonicating nanotube and DCB mixture was then heated to match the dissolved polymer. The two mixtures were combined, stirred vigorously using a Teflon-coated stir bar for 30 seconds. The resultant mixture was then placed in a room temperature water bath too cool, while sonication continued for 3-5 minutes. Once the mixture was less than the melting point of the polymer, vacuum filtration would begin using a 0.45μm pore size Teflon filter (Satorius Stedim). The coagulation step described in the literature was not found to improve nanotube dispersion nor reduce electrical resistivity of the composites so was dispensed with early in this research.

The resultant composite samples were then dried in an oven at 65°C to remove excess residual DCB. Unfortunately, no vacuum oven was consistently available for the authors use during this research.

### 4.1.6 Filtrate Observations

It was observed that filtrate from the vacuum process had a yellowish color, independent of nanotube concentration. Concerned that nanotube material had

been lost through the filter, or worse, that the nanotubes had been reduced to amorphous carbon by one or more steps of the process such as sonication, the filtrate material was characterized via TEM. In addition, DCB with no nanotubes was exposed to 2 hours of sonication. It too changed to a yellow color. TEM of this material was also performed as a comparison (Figure 27).

TEM analysis showed what is thought to be DCB sonopolymer as present (there are no TEM examples in the literature). Figure 27-6 through 27-8 shows the evidence seen from the DCB filtrate. This material is clearly different from TEM analysis of polyethylene. One can see examples from the literature in Figure 27-1 through 27-4 are similar in appearance to lamellae structures seen in the filtrate from SWNT-MDPE processing in Figure 27-6, but different in overall dimension. Also, one should note that staining and similar sample preparation was used in these images from the literature. For these images of PE from the literature, the light areas are crystalline while the dark are non-crystalline. Non-crystalline scatter electrons more effectively because of heavy atoms, compared to the crystalline areas which contain only carbon and hydrogen [7]. The structures observed from this research in Figure 27-6 are remarkably similar to nanotube-related graphitic and tubular arrangements seen throughout the authors experience in carbon nanoscience. This similarity was considered throughout this research.

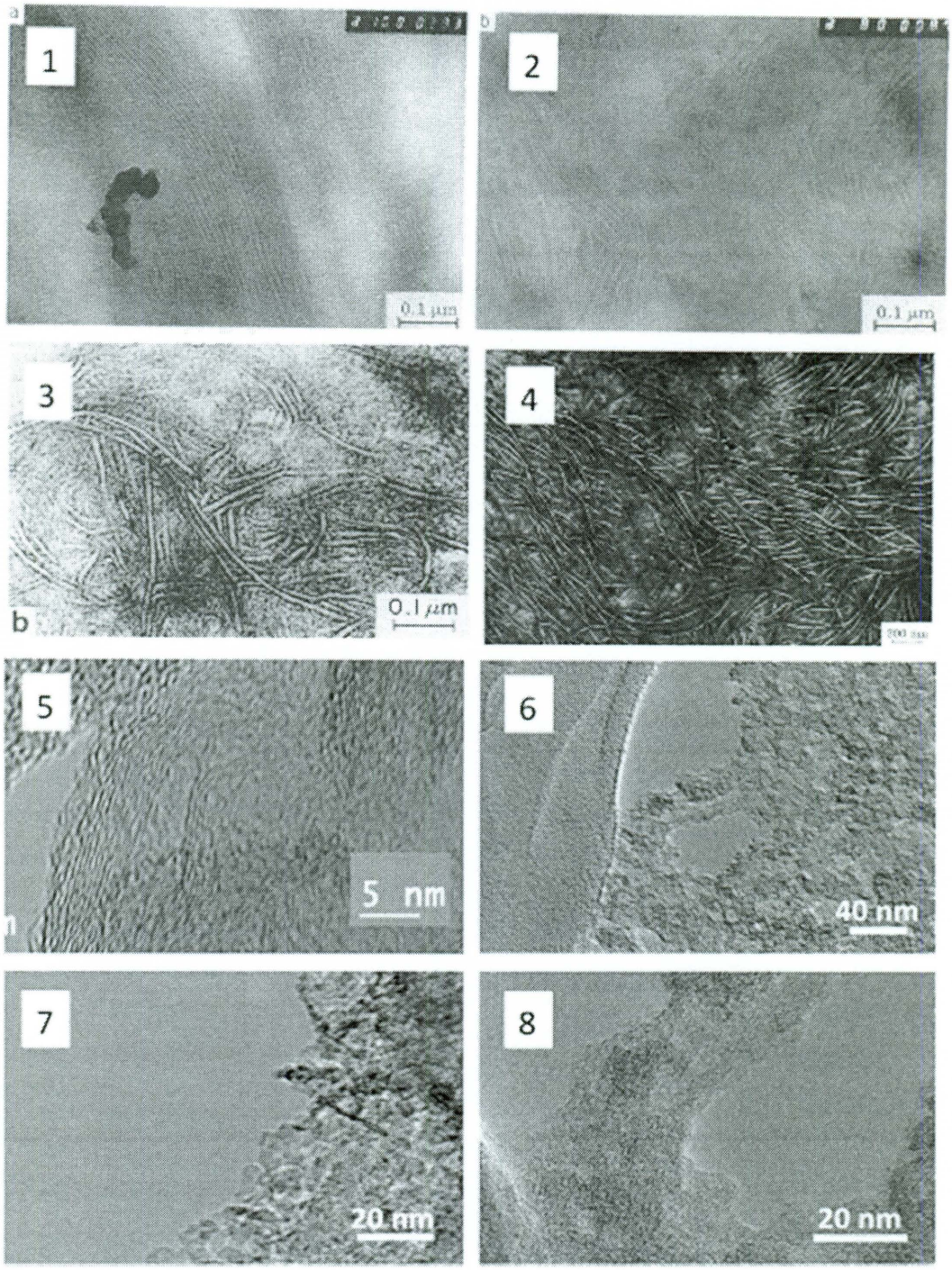


Figure 27: **1 & 2** TEM of low molar mass examples of MDPE showing wide and thin crystal lamellae [74], **3.** HDPE lamellae in central area of spherulite [75], **4.** Lamellae of branched PE [76], **5.** TEM of sonicated DCB filtrate from SWNT-MDPE composite production. **6.- 8.** TEM of sonopolymer material produced by sonication of DCB.

## 4.2 ELECTRICAL RESISTIVITY PERFORMANCE OF CARBON NANOTUBE POLYETHYLENE COMPOSITES

Many hundreds of permutations and combinations of polyethylene and nanotube were explored as part of this study in order to glean the lowest resistivity carbon nanotube polyethylene composite. Some matched the poor performance seen in the literature, understandable given polyethylene's suitability as an insulator, while others were even less desirable. Certain samples and approaches exceeded current results in the literature and it is these that have warranted reporting and discussion.

### 4.2.1 High Density Polyethylene and Electrical Current Conditioning

Composites of 30wt SWNT (SWeNT CG100) and high density polyethylene (HDPE – Sigma Aldrich) were prepared as previously described. These composites proved to have relatively disappointing electrical resistivity performance. In an effort to improve performance, and in collaboration with Nanoridge Inc., electrical current conditioning was explored as a means to improve the bulk resistivity of the composite by passing electrical current through the sample. The composites were crushed and packed into a quartz tube, and electrical contacts applied at each end (Figure 28). Electrical current was passed through using a D.C. (Xantrex XFR 600-2) power supply.

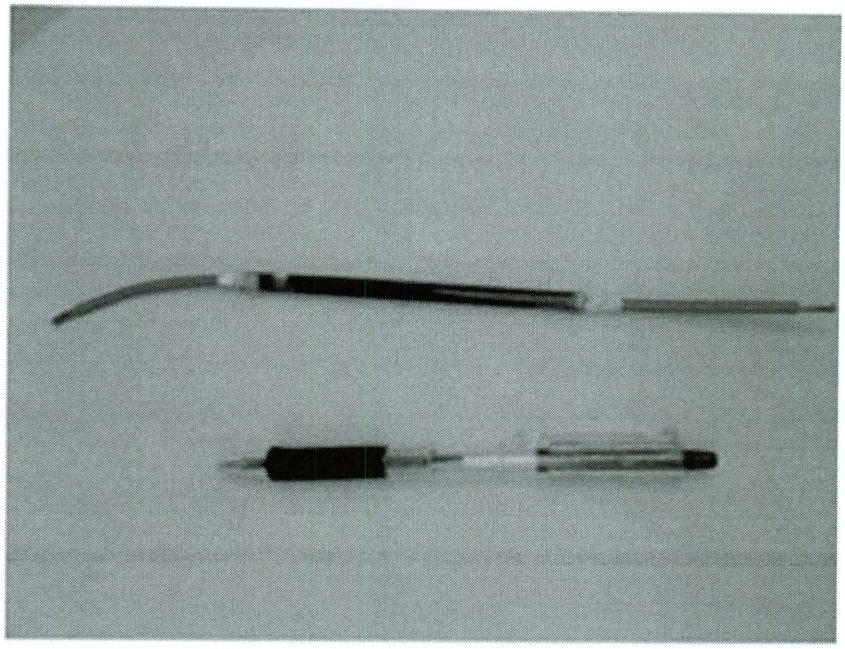

Figure 28: Simple sample setup for electrical and thermal conditioning

Given both evidence in the literature and prior experience, sample tubes were placed in a furnace to melt the sample in order to improve both interconnectivity between the composite pieces and the interface with the copper leads. Initial results did show some promise, with up to a two order of magnitude improvement (Figure 29). This experiment was later advanced and explored in detail by others [68]. This result, and that of the work explored by Chakravarthi, contained a major issue. It was suggested that resistivity improvements were achieved by one or more factors. Firstly, the electrical current was bridging gaps between the nanotubes by burning the polymer or secondly, the CNT were rearranging themselves under the force of electrical field for a more optimized conductive pathway. The second option was never likely in the author's opinion, given the large viscosity of the HDPE and SWNT composite, and the weak electrical fields employed.

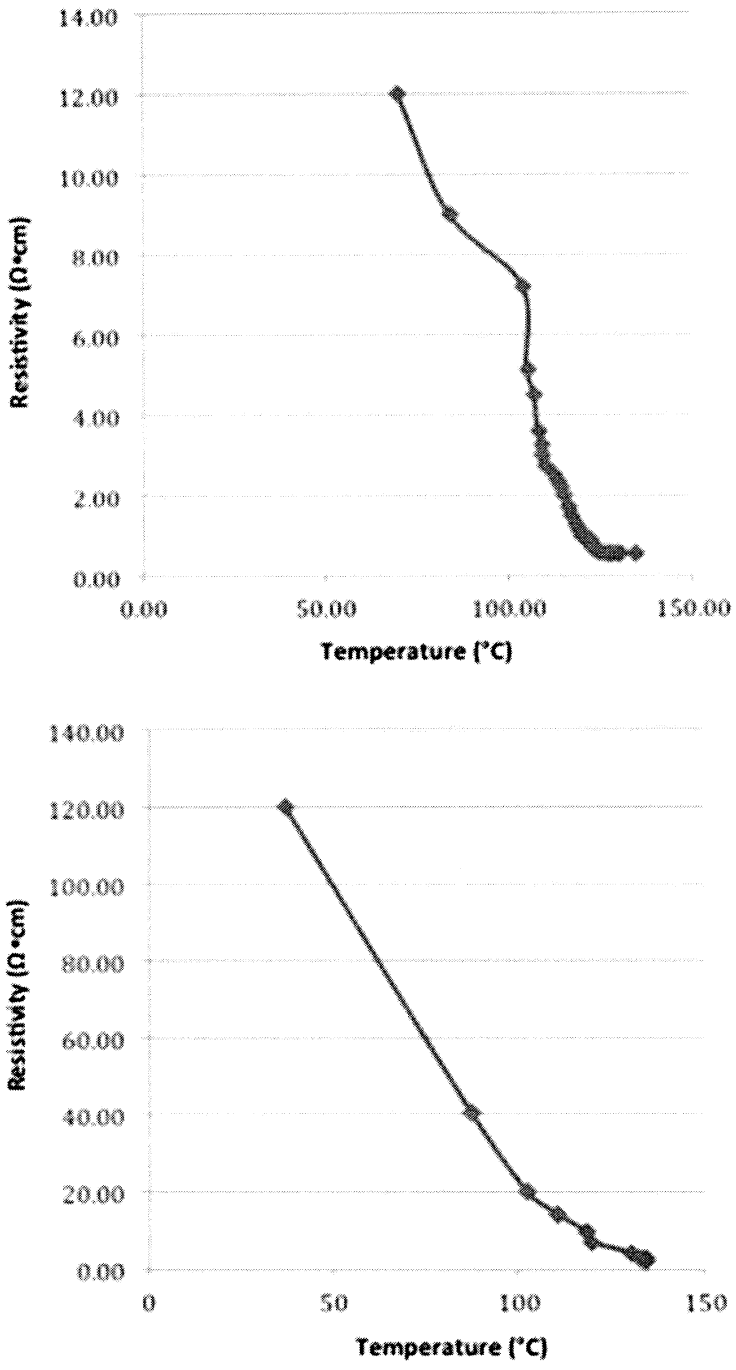


Figure 29: Resistivity improvements through electrical and thermal conditioning

To settle the issue, TGA and Differential Scanning Calorimetry (DSC) were used to characterize the composite both pre, and post, electrical conditioning. Figure 30

shows the 30wt composite, and highlights features typical of polyethylene such as the melting endotherm between 105-135°C and the decomposition peak ~460°C [77] [78].

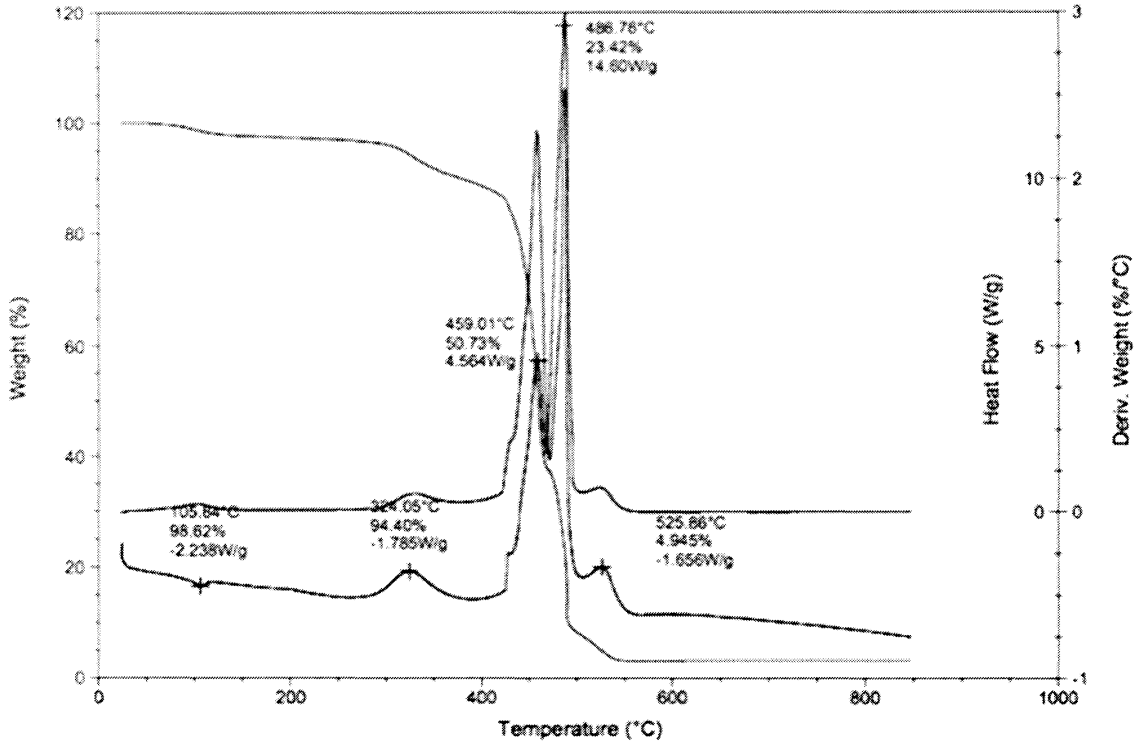


Figure 30: TGA/DSC of 30wt% SWNT HDPE composite *before* electrical and thermal conditioning process

The DSC analysis of the conditioned sample, as seen in Figure 31, is lacking these clear features. With this evidence, and combined with SEM observations, the route of electrical conditioning was deemed unsuitable and left to others to explore further [68].

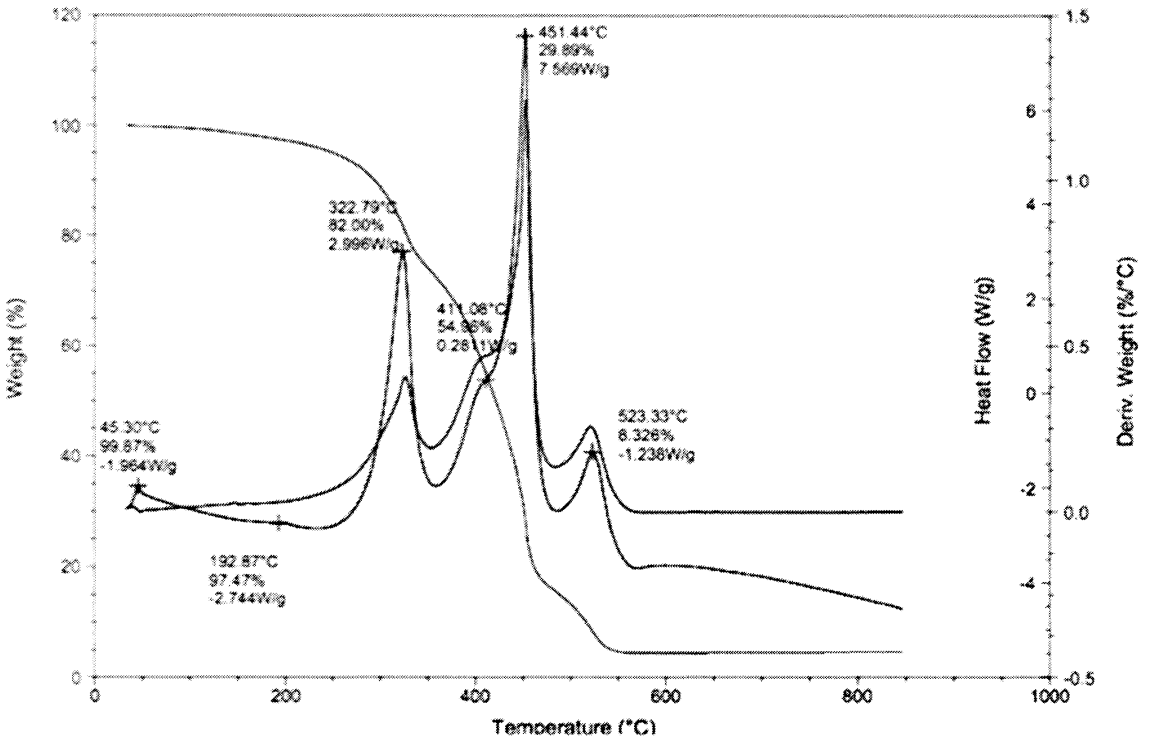


Figure 31: TGA/DSC of 30wt SWNT HDPE post process

### 4.2.2 Carbon Nanotube and Medium Density Polyethylene Composites: High Loading

As previously noted, an effective protocol for distributing CNT into MDPE had been developed as part of this research. However, the results in the literature suggested that even this evolved, more efficient and simplified method might not be effective in meeting the goal of matching copper's resistivity or even bettering prior research. To that end, composites with higher loading of CNT than previously explored in the literature were attempted. The aforementioned tube types, namely SWNT from SWeNT, Rice University and NASA JSC, and MWNT from Mitsui were used. In the later stages of research, DWNT from CCNI were also used. In the literature, issues with processing, viscosity and dispersion were given as reasons that the maximum attempted loading rarely went about 30wt%.

The range of loading explored varied between nanotube types. A critical dependency was the amount of CNT material at hand, which limited the volume of samples that could be produced. For that reason, the broadest range of loadings explored were with HiPco, Mitsui and SWeNT CNT. With the emphasis of this research placed on lowest resistivity, less attention was put on percolation thresholds at low loading than in prior research.

Figure 32 summarizes the resistivities achieved through the plethora of composites produced. Some of the results are unprecedented among composites using MDPE.

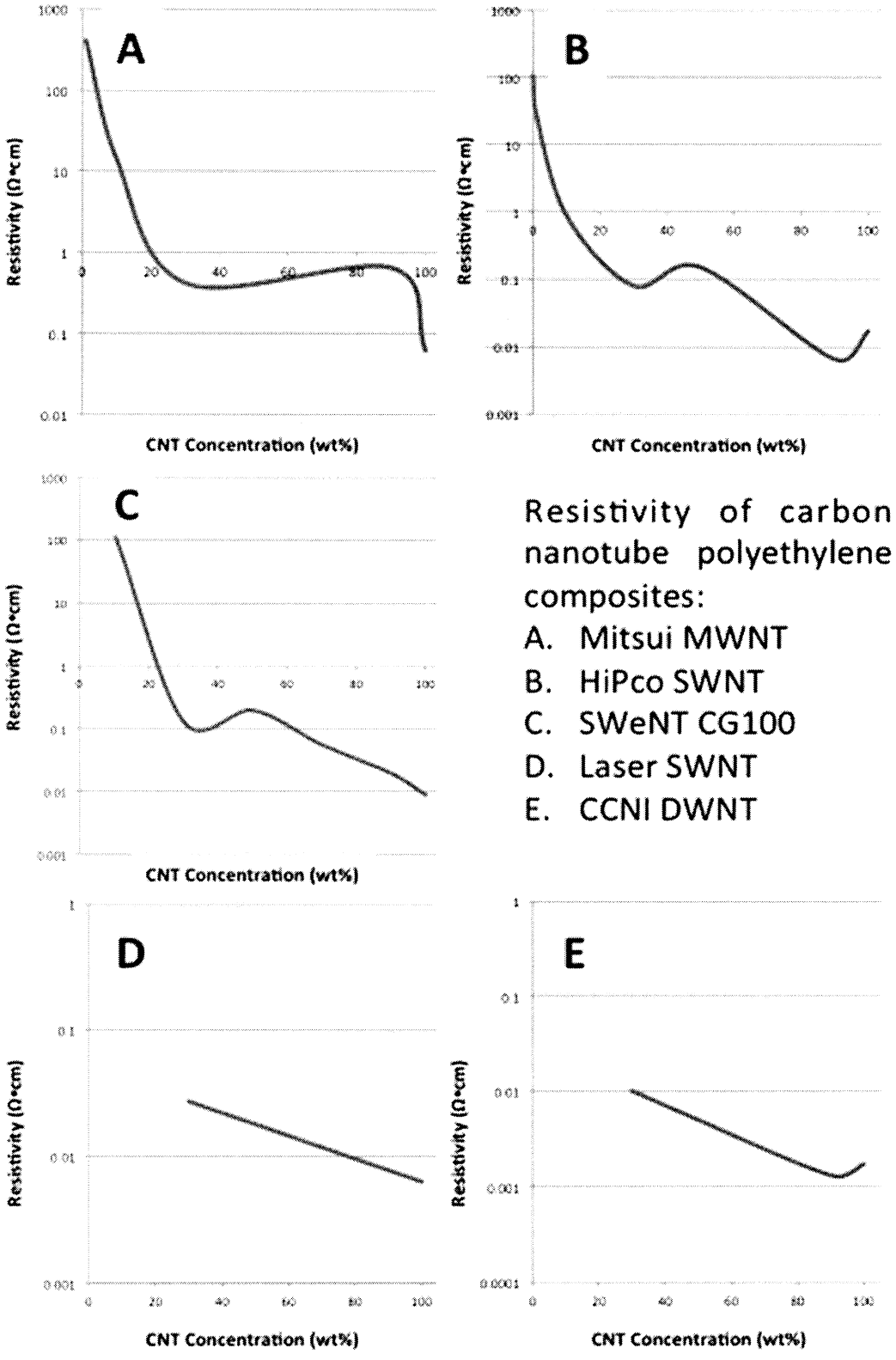


Figure 32: Resistivity vs. Loading for various nanotube types in MDPE

The most impressive of these results are included in Table 8:

| Nanotube Type | Loading (wt%) | Resistivity (Ω•cm) |
|---|---|---|
| HiPco SWNT | 30 | 0.08 |
| HiPco SWNT | 90 | 0.0066 |
| Laser SWNT | 30 | 0.027 |
| DWNT | 30 | 0.01 |
| DWNT | 90 | 0.0013 |

Table 8: Highlights of CNT MDPE composite resistivities

Overall, relatively flexible and conductive composites were produced. Figure 33 shows a 90% DWNT sample that was flexible and resilient to repeated handling and bending, aspects that are not found in 100% nanotube papers.

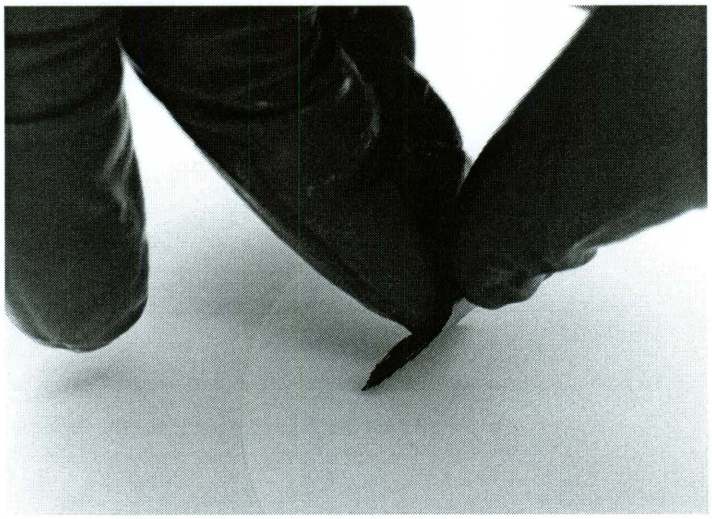

Figure 33: Simple illustration of the flexibility of 90wt% DWNT and MDPE composite

One point of interest that arose from these data was that for HiPco and DWNT MDPE composites, the 90wt% samples were found to be *less resistive* than the earlier bulk resistivity analysis of the *100%* nanotube material. Considering the presence of the highly electrically resistive MDPE, albeit in relatively small amounts, this was surprising.

### 4.2.3 Electron Microscopy and Analysis of High wt% Loading Composites

Extensive electron microscopy was carried out on all the composites to evaluate nanotube dispersion, in addition to composite and polymer morphology. Analysis of SEM imagery of the composite surfaces provided a simple potential answer to the phenomenon of lower resistivity in 90wt% composites versus 100% nanotube samples. As seen in Figure 34, the porosity of the 90wt% HiPco SWNT and MDPE composite suggests that the presence of the MDPE, and the composite fabrication process itself, is actually acting as a forcing function, tightening the bundles of SWNT and reducing the presence of air pockets and small scale porosity in the 100% nanotube sample.

Figure 32 also highlighted the odd trend for resistivity to change tack from decreasing, to rising and back to decreasing, as loading of CNT was increased. The author attributes this to a simple trick of morphology. Strata or layers of polymer and nanotube were formed during fabrication. The size of these layers changed with

adjustment of SWNT loading, which would have a knock-on effect on 4-point probe results.

The author has utilized the porosity and surface area of CNT before, for use in fuel cells [79], and the porosity of these composites were applied to a novel application as seen in Chapter 6.

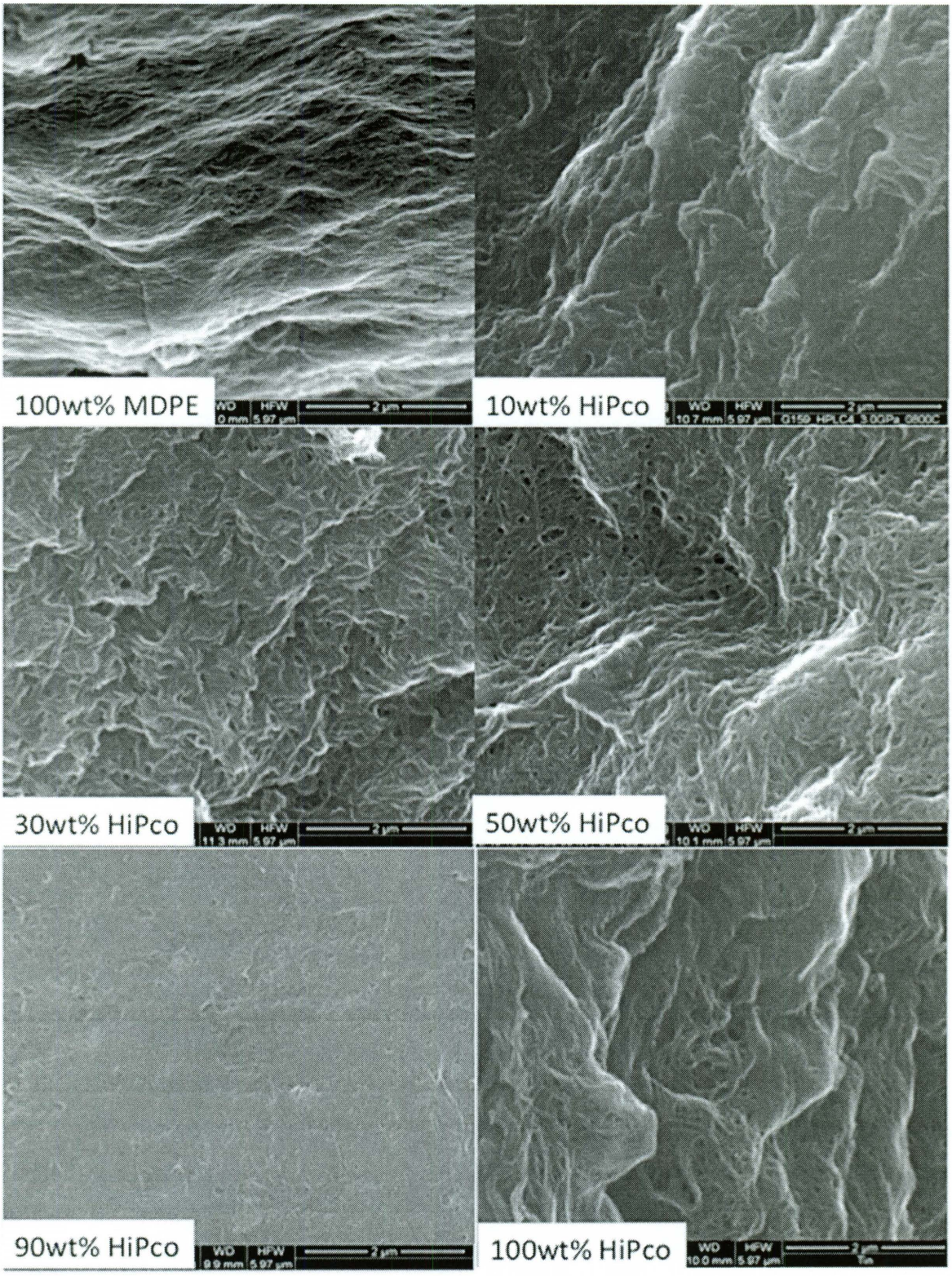


Figure 34: Surface morphology of HiPco and MDPE composites

SEM imagery of *inside* the composites was also enlightening. One aspect discovered was that there was little or no difference seen between SEM samples prepared by simple tearing, and those prepared by the commonly used freeze fracture technique with liquid nitrogen ($N_2$).

Figure 35 is representative of the various loadings of MWNT in MDPE. Throughout the analysis, it was noted that the polymer did not adhere well to the MWNT surfaces, with some exceptions. As the loading increased to 50wt% and beyond, the imagery showed a distinct breakdown in composite morphology, favoring a buckypaper like form with distinct spherical particles of MDPE. Figure 36 shows the equivalent images for the CG100 SWNT MDPE composites. The increase in CNT loading showed less drastic transitions than the MWNT samples. The HiPco composites shown in Figure 37 are representative of a bundle-size transition that varied with changing wt%. Also, a distinct layering or strata was observed in the SWNT composites along the edges. This was probably a result of the vacuum filtration fabrication process.

The porosity, combined with the layers or strata observed, suggests that these composites are far from optimal. The resistivity data collected maybe considered conservative given that it relies on thickness as part of the calculation, and clearly, these materials have a more complex morphology through thickness than expected.

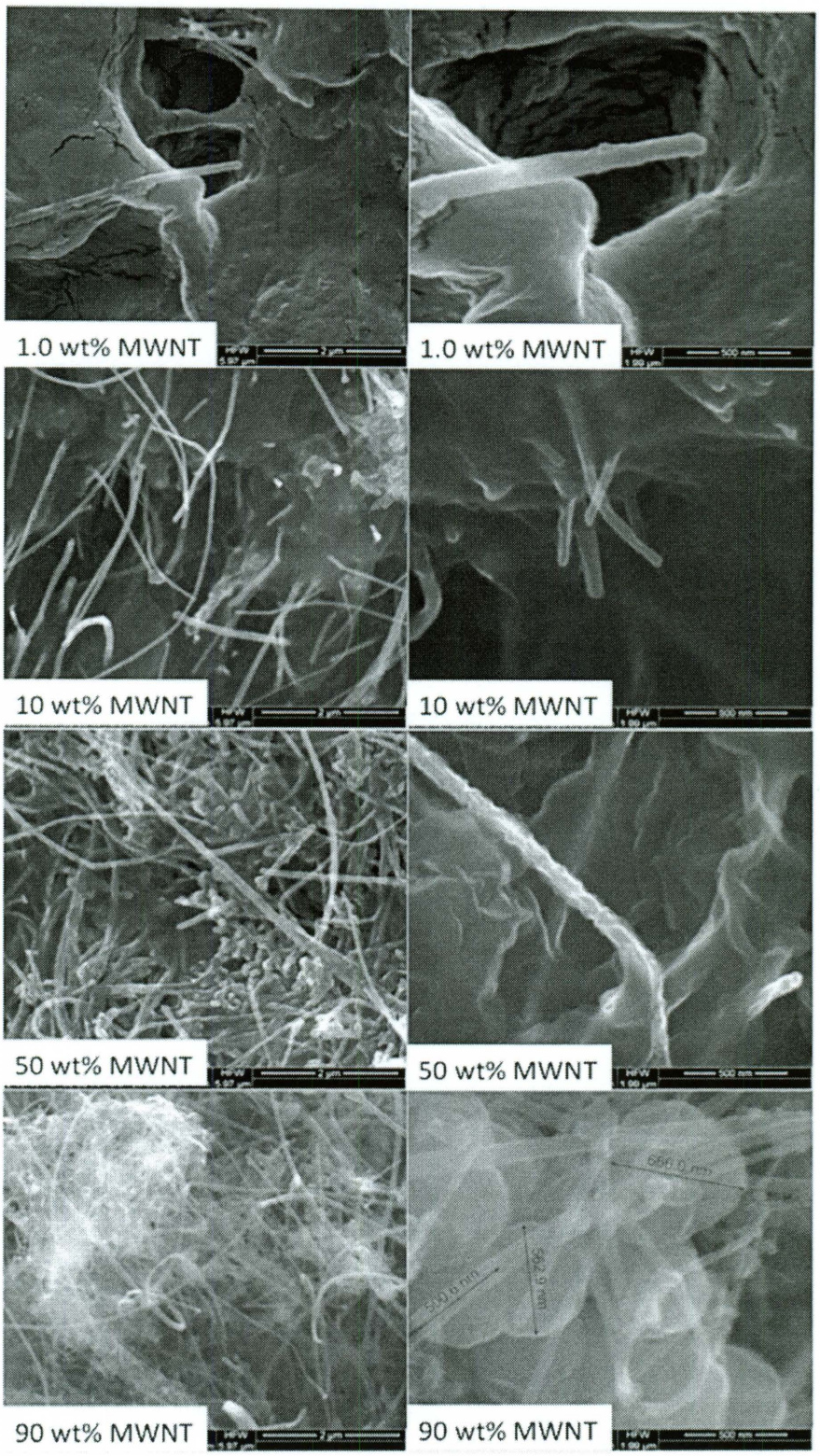


Figure 35: SEM analysis of MWNT MDPE composites

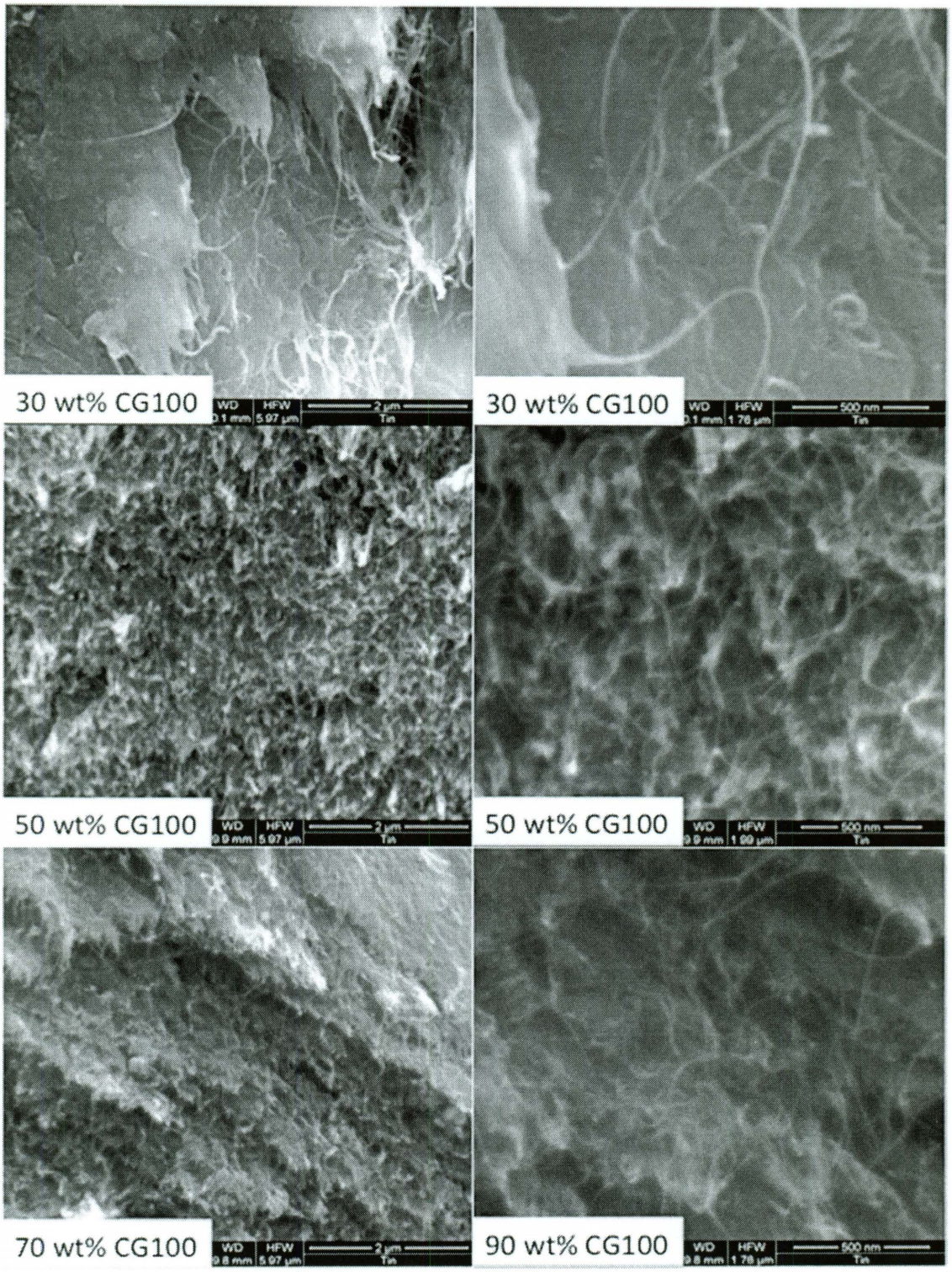


Figure 36: SEM analysis of SWeNT CG100 SWNT MDPE composites

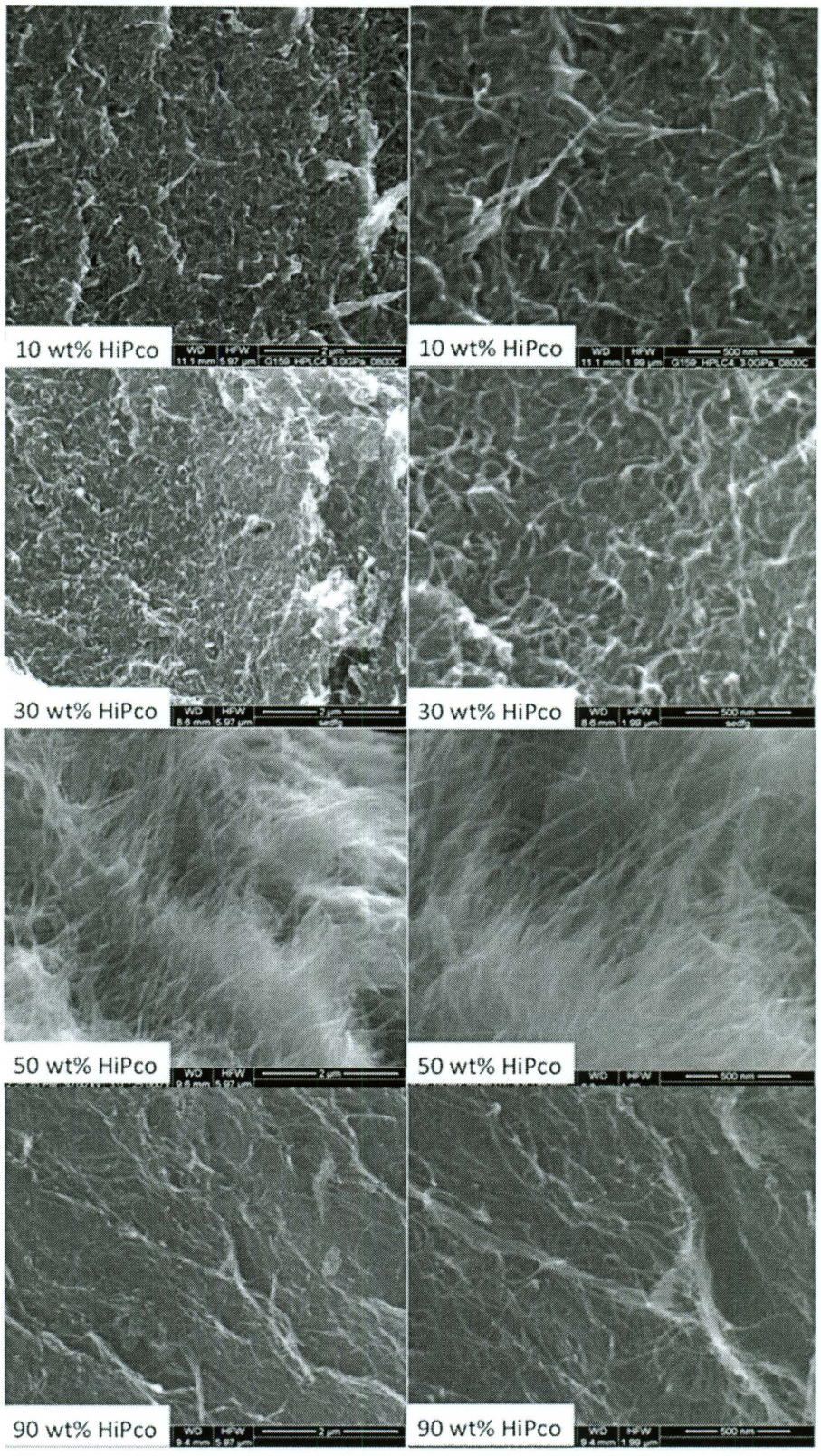


Figure 37: SEM analysis of HiPco SWNT MDPE composites

TEM analysis of the nanotube and MDPE filtrate during solvent processing, sampled just in advance of vacuum filtration, was also carried out in an effort to analyze polymer and nanotube interactions. TEM grids were prepared as described in Chapter 3, with the difference being the solvent used, DCB rather than DMF.

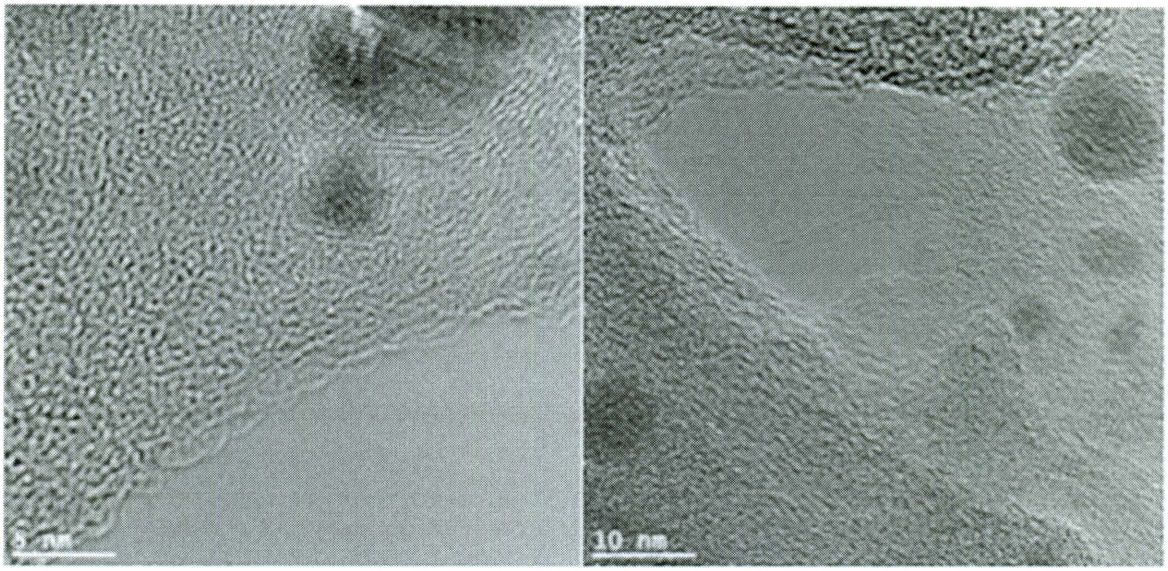


Figure 38: TEM of 30%wt laser SWNT and MDPE pre-filtration

While not providing a plethora of quantitative data, this microscopy did give some insight on how the CNT and MDPE were interacting on the nanoscale. The distinct onion layers of carbon surrounding residual catalyst particles from the laser SWNT were noticeable, and bundles of SWNT could be found throughout the material (Figure 38).

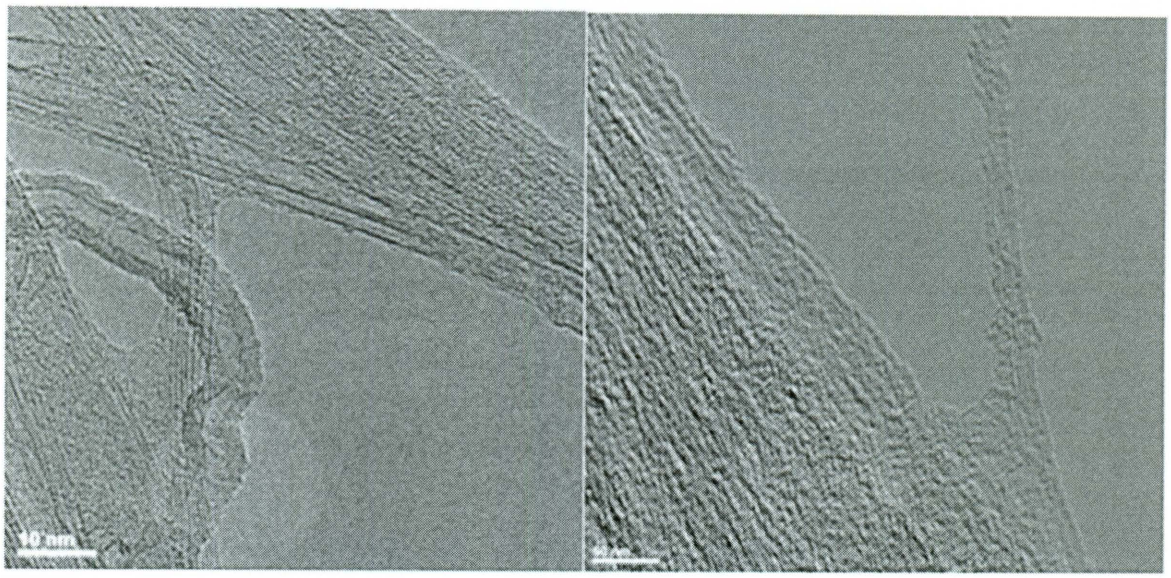


Figure 39: TEM of 30%wt DWNT and MDPE pre-filtration

Similar electron microscopy of the DWNT MDPE composites painted a different picture. The DWNT were found to be better dispersed throughout the polymer, and there was also repeated evidence of polymer wrapping around the nanotube bundles (Figure 39).

No distinct wrapping was found in the CG100 SWNT samples, however, bundles of SWNT and polymer lamellae were found to be present (Figure 40). The HiPco MDPE composite TEM samples were less forthcoming with distinct pronouncements on morphology. Bundles of CNT were found, with little or no lamellae present (Figure 41). The MWNT equivalent was distinct in that there appeared to be little polymer and nanotube interaction. When MWNT were found sticking out of the polymer matrix, their sidewalls appeared as pristine as the TEM images of the as-received material (Figure 42).

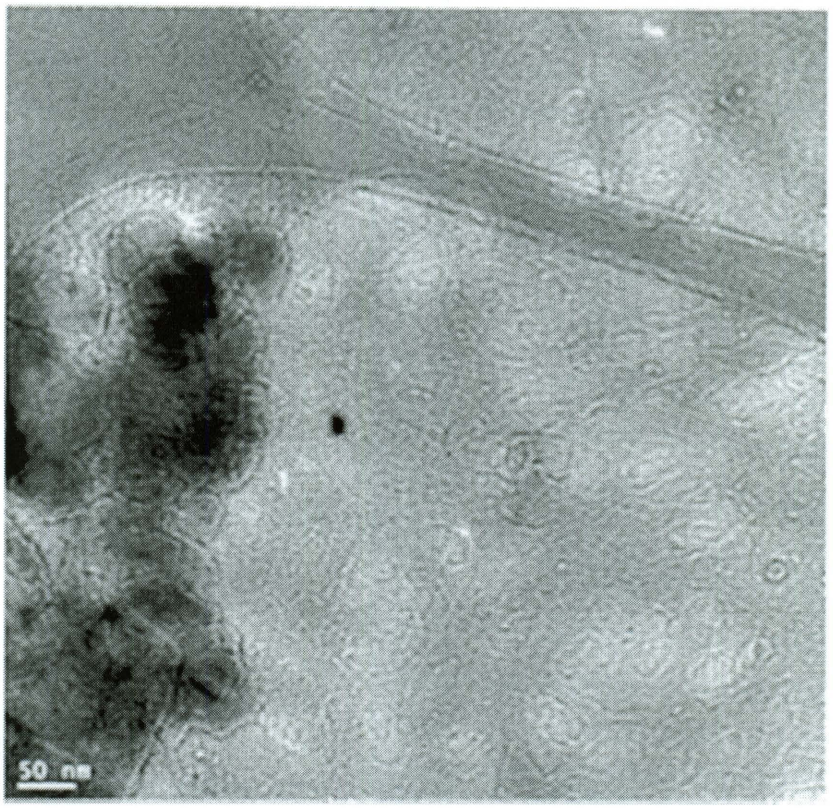


Figure 40: TEM of 30%wt CG100 SWNT and MDPE pre-filtration

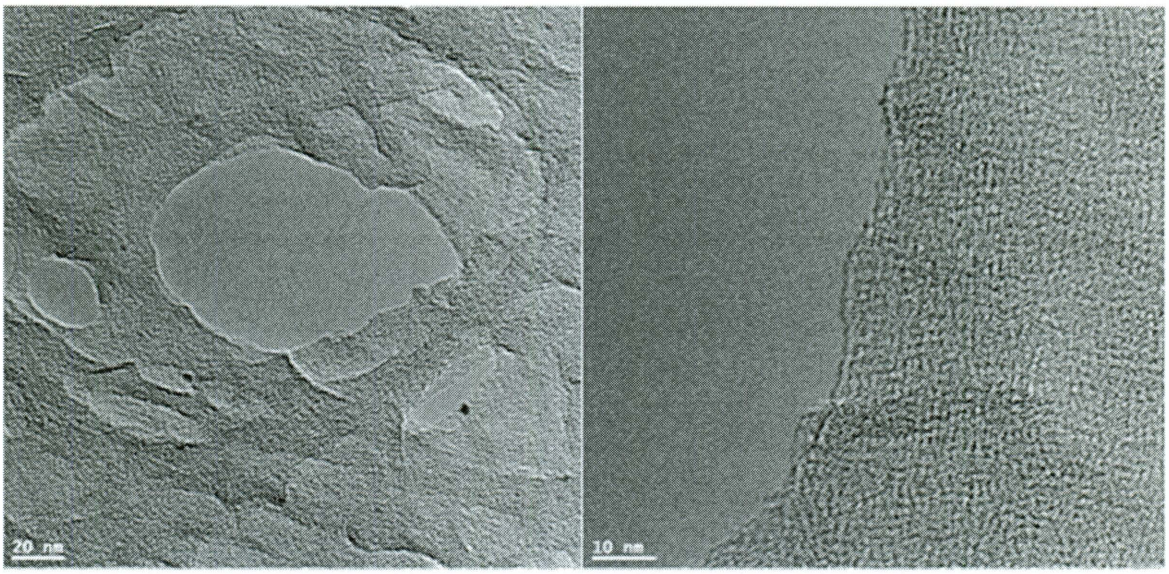


Figure 41: TEM of 30%wt HiPco SWNT and MDPE pre-filtration

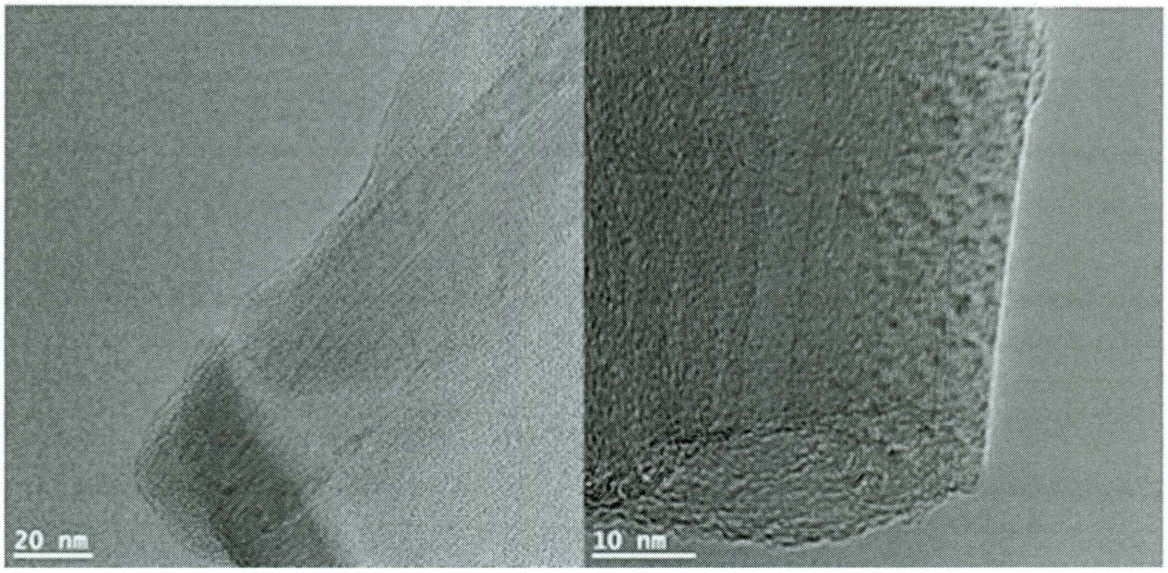


Figure 42: TEM of 30wt% Mitsui MWNT and MDPE pre-filtration

### 4.2.4 Ultramicrotomy of High wt% Loading Composites

In an effort to gather microscopy images that would lend themselves to more quantitative analysis, the author taught himself the art of ultramicrotomy in order to produce samples for TEM. Samples were prepared as described in the literature [80], using a diamond knife and Ultramicrotome (Leica Ultracut). Figure 43 shows prepared samples after placement on Cu Tem grids.

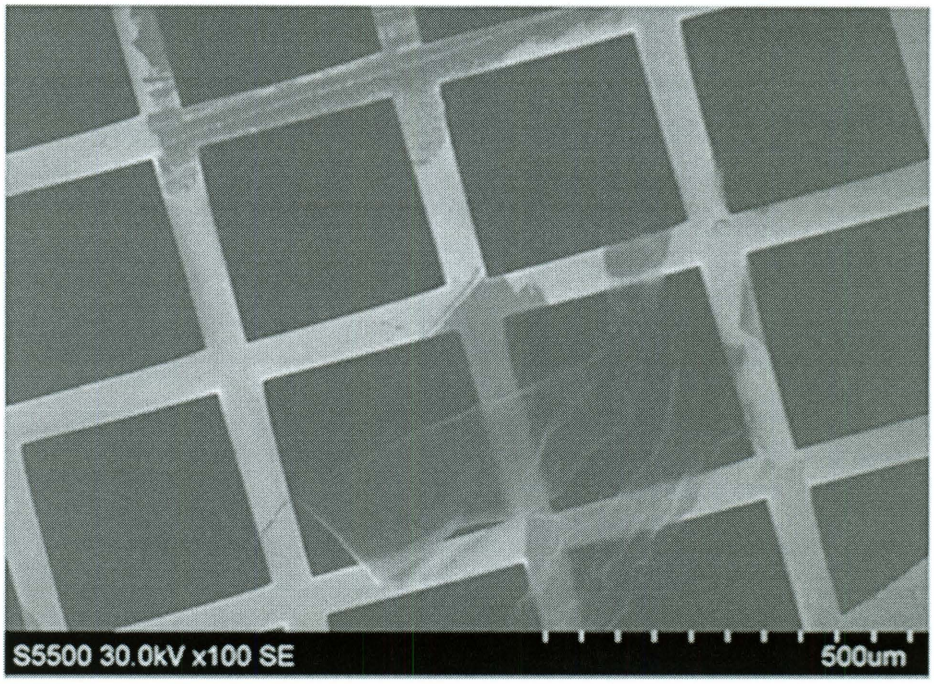


Figure 43: Ultramicrotome sample of CNT MDPE composite on TEM grid

This technique proved laborious and did not yield the deep insight into CNT MDPE interactions on the nanoscale as originally envisioned. Preparing samples of 50nm thickness or less was beyond the abilities of both the author and the equipment.

Compatibility of the sample, a relatively hard composite of SWNT and MDPE, came into play here. Figure 44 and 45 provide some highlights of the images gathered. Overall, they provided no additional insight to the TEM already discussed in the previous section. They were in agreement to the findings from those images however.

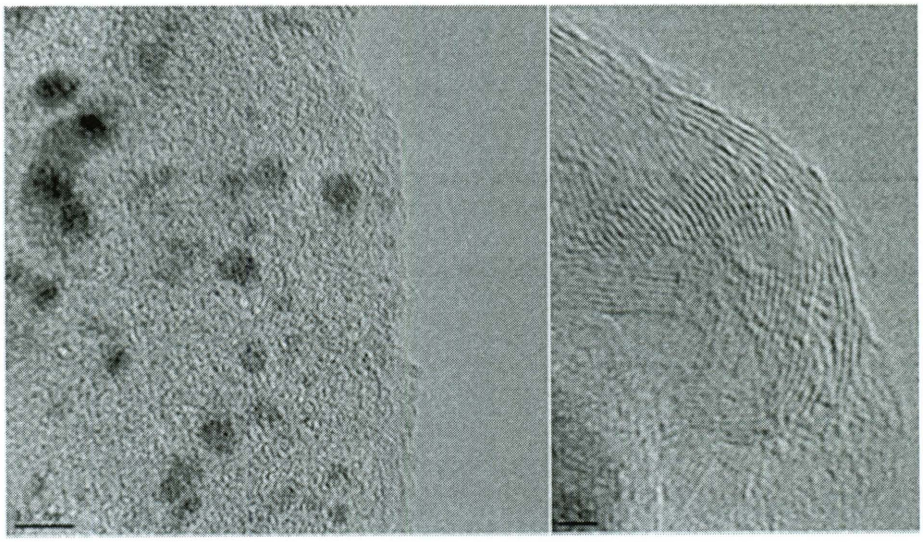

Figure 44: TEM of ultramicrotome sample of 70wt% CG100 SWNT and MDPE

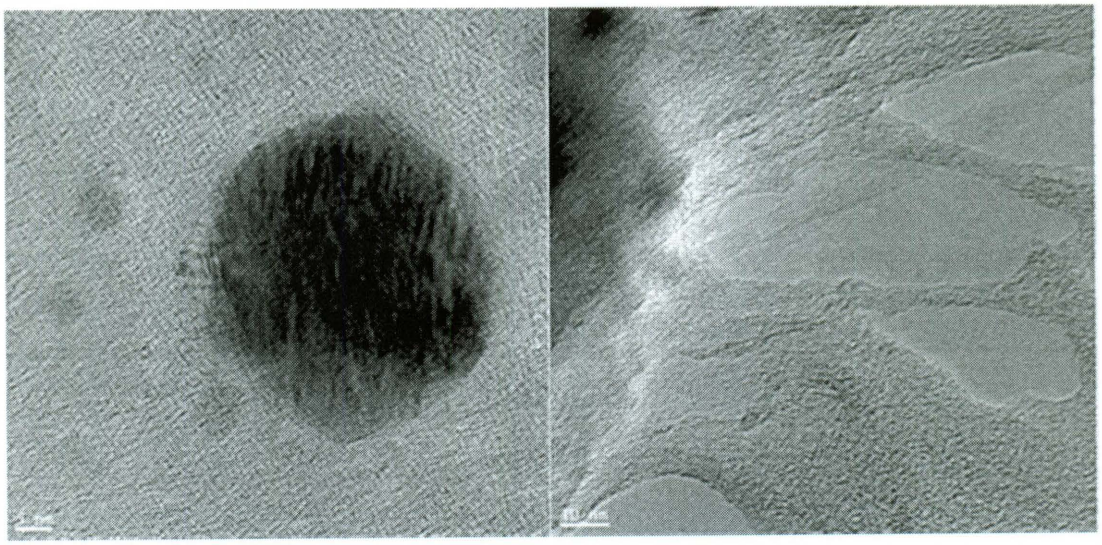

Figure 45: TEM of ultramicrotome sample of 50wt% CG100 SWNT and MDPE

### 4.2.5 Analysis of CNT Bundle Size to Resistivity

Using the aforementioned abundance of microscopy collected, SEM, scanning transmission electron microscopy (STEM) and TEM, a rather laborious study was completed to analyze the average bundle size of the CNT found in 30wt% composites (Figure 46).

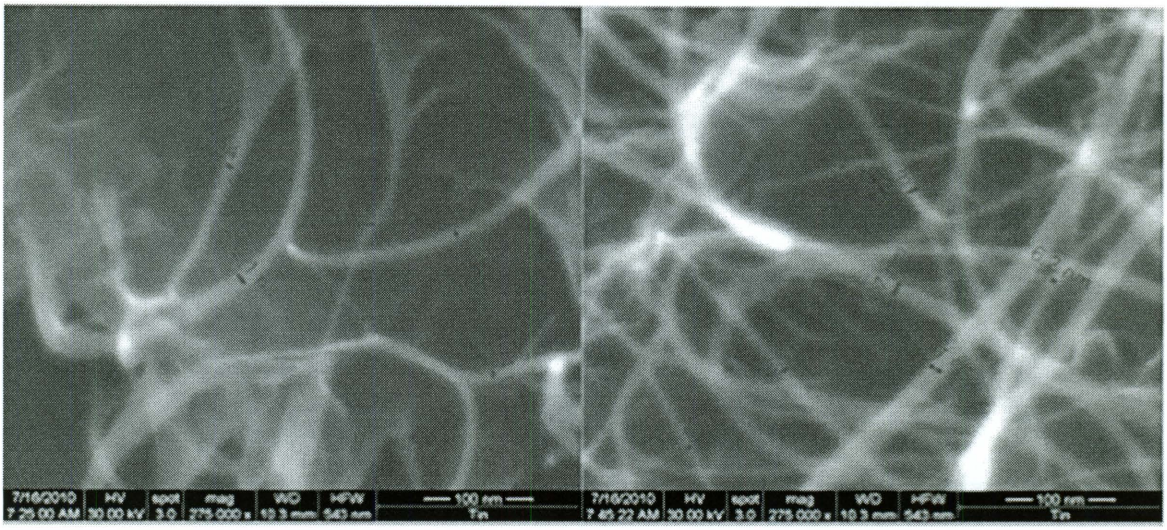

Figure 46: Example of STEM images gathered and analyzed using Hitachi S-5500

These data were then compiled and compared with the relevant resistivity data. While reduction of bundle size does lower resistivity, comparison of bundle size versus resistivity is not relevant across difference nanotube types (Figure 47), instead being outweighed by higher wt % of metallic nanotubes. It can been seen that smaller CNT diameters, and damage or coatings to tube sidewalls, can outweigh the relevance of bundle diameter data.

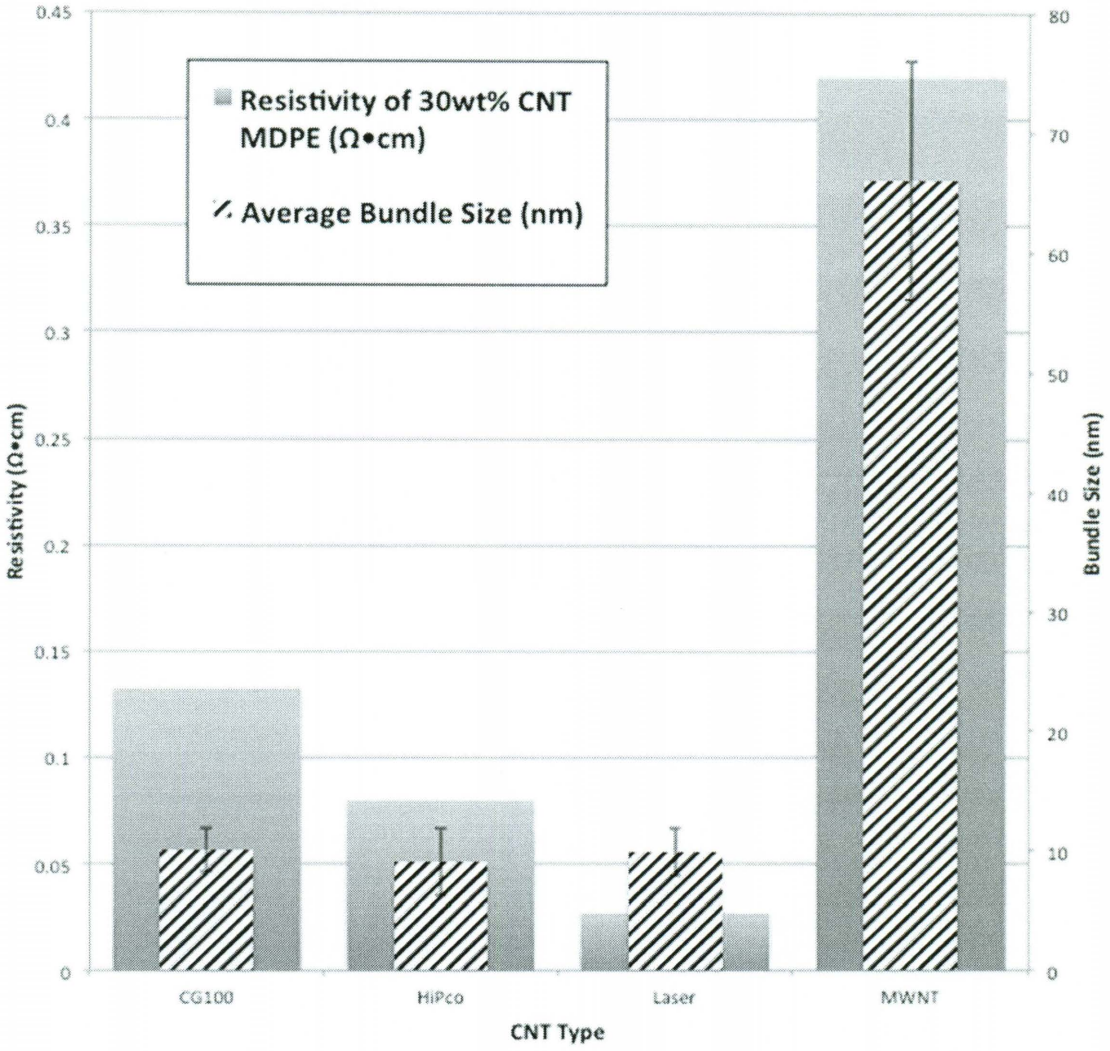


Figure 47: Average bundle size of CNT versus resistivity

The results found for the DWNT were even more marked than the laser tubes, as that composite had more impressive resistivity results (0.01 Ω•cm at 30wt%), and larger bundle size. However, it was not included in Figure 47 due to the scarcity of material and resultant low number of samples to generate relevant statistics.

### 4.2.6 TGA analysis of CNT MDPE Composites – Crystallinity of Polymer

As stated in Chapter 2, the crystallinity of the MDPE may play a role in enhancing (or detracting from) the conductivity of the produced composite. Crystallinity analysis of the CNT MDPE composites was first attempted using TGA/DSC.

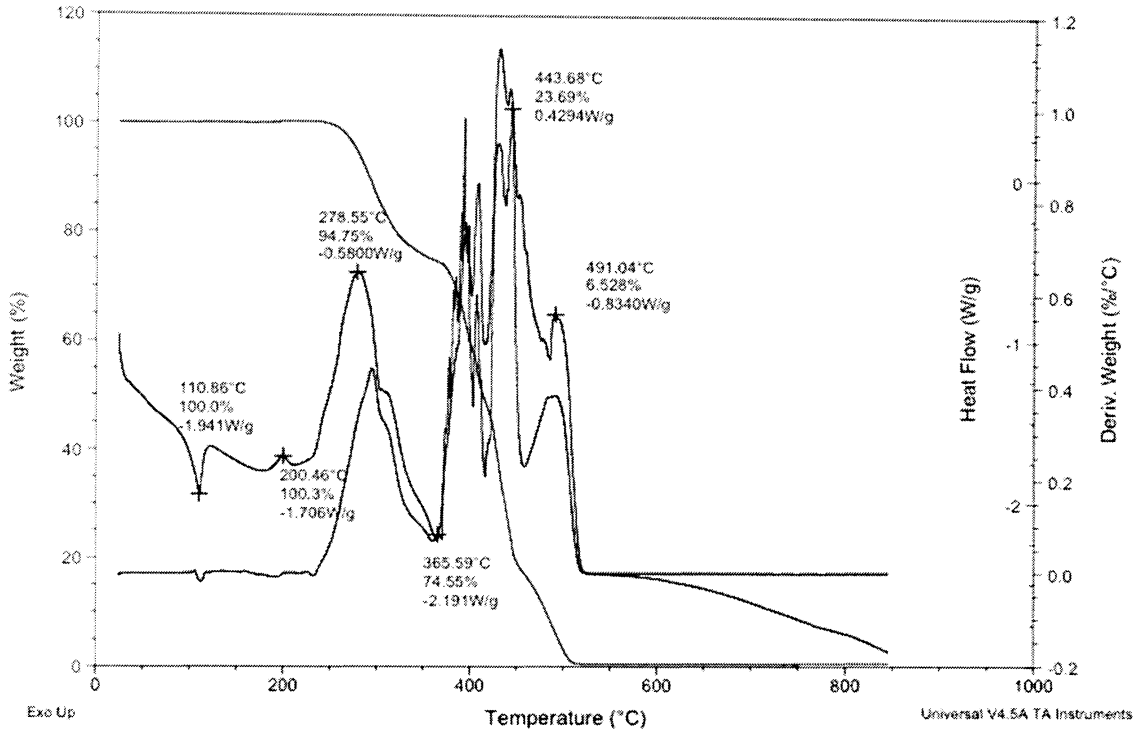


Figure 48: TGA/DSC analysis of raw MDPE

While analysis of the raw MDPE and lower wt% composites did provide the necessary melting endotherms for crystallinity data (Figure 48 and Figure 49), it was found that the samples of most interest to this study, the high wt% composites, did not yield data suitable to gauge crystallinity. The larger amounts of CNT present masked the polymer features in the data. As can be seen in Figure 50, the drop in sample mass due to absorbed water, completely shrouded whatever melting endotherm may have been present due to the polymer.

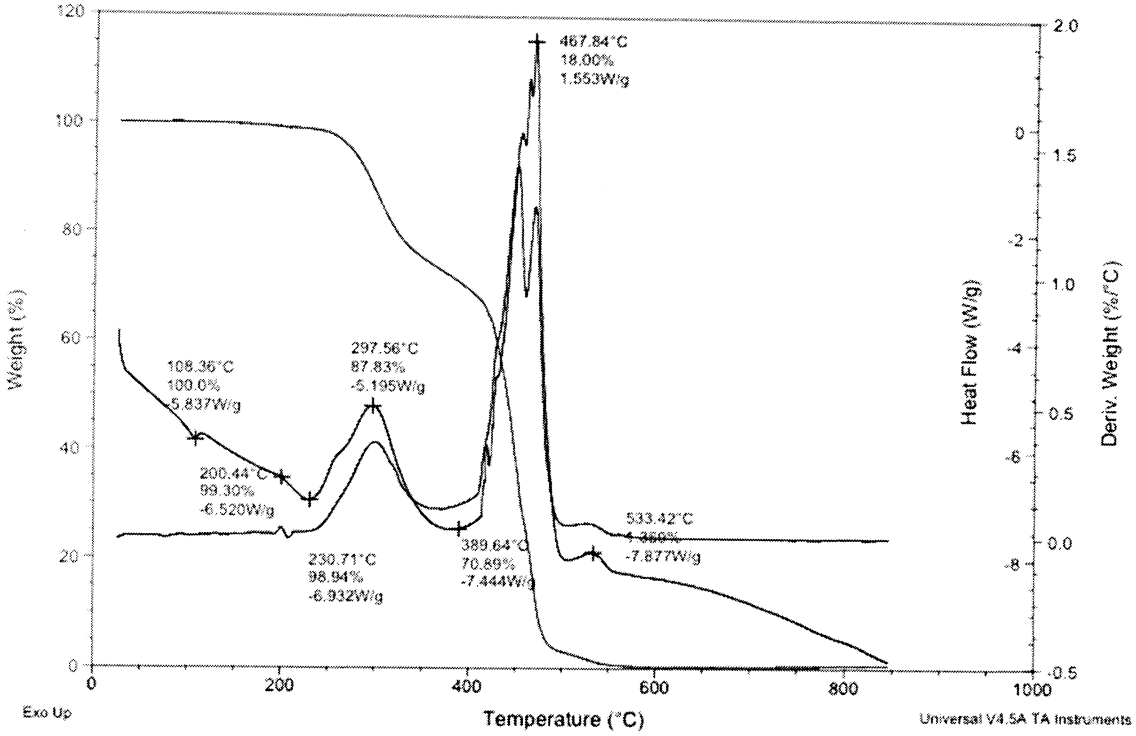


Figure 49: TGA/DSC analysis of 10wt% CG100 SWNT and MDPE

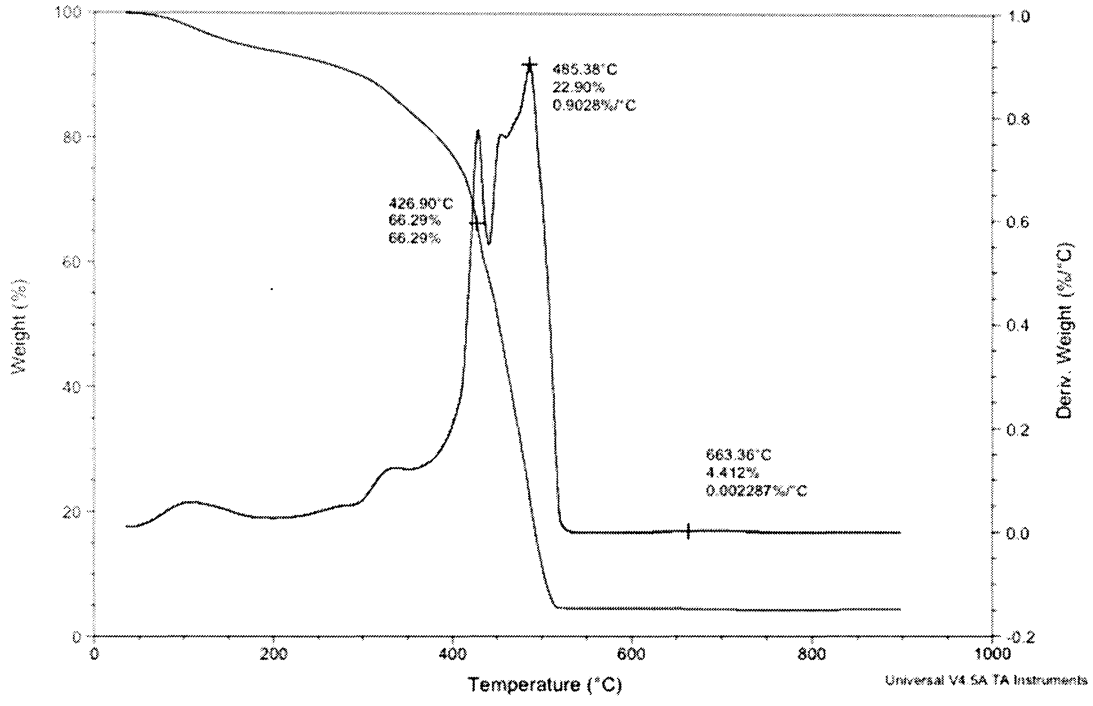


Figure 50: TGA analysis of 70wt% CG100 SWNT and MDPE

### 4.2.7 Raman Spectroscopy analysis of CNT MDPE Composites

As TGA analysis proved inadequate for examining the polymer crystallinity, examples of Raman technique and data from the literature were compared to. Figure 51 highlights the region of most interest for MDPE samples both pre, and post, solvent processing. Stuart et al. showed that $CH_2$ bending in PE is reflected between 1390-1510 $cm^{-1}$ [81]. This bending was related the orthorhombic crystalline material content in the PE, and was more clearly defined at 1416 $cm^{-1}$ by Strobl [82].

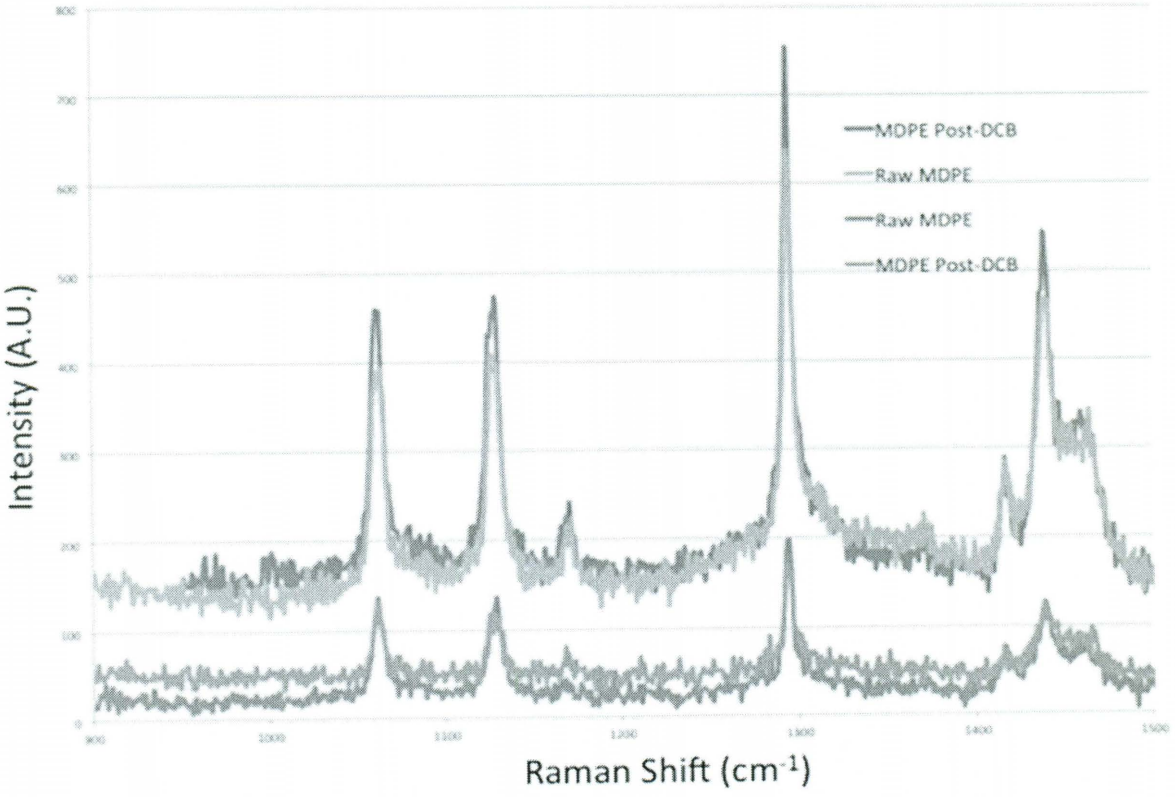


Figure 51: Raman spectra of MDPE

Peaks between 1160-1020 cm-1 have been defined by C-C bond stretching , while those between 1250-1350 are a result of $CH_2$ twisting [81]. Peaks at 1303 and 1080 $cm^{-1}$ can be attributed to amorphous content [82]. Keeping these points in mind, DCB solvent processing appears to have no change on either crystalline or amorphous MDPE content (Figure 51).

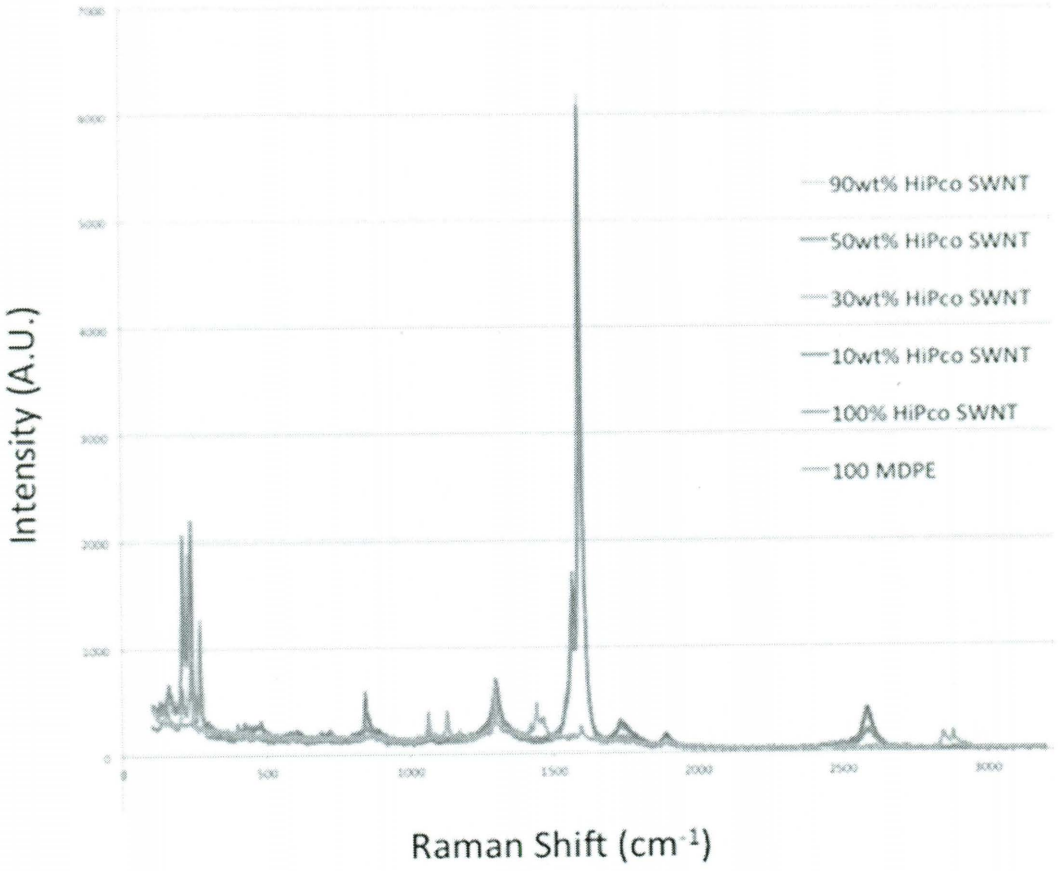


Figure 52: Raman spectra of HiPco MDPE composites

It would appear, looking at the raw data of SWNT composites, that the addition of SWNT in MDPE reduces polymer crystallinity (Figure 52. However, the overall

intensity of the MDPE features are low compared to that of SWNT, and both amorphous and crystalline Raman features were affected. As loading increased beyond 10%, there was little evidence of the unique MDPE signature. One should also note that it overlaps with both the D and G peaks of the SWNT Raman signature.

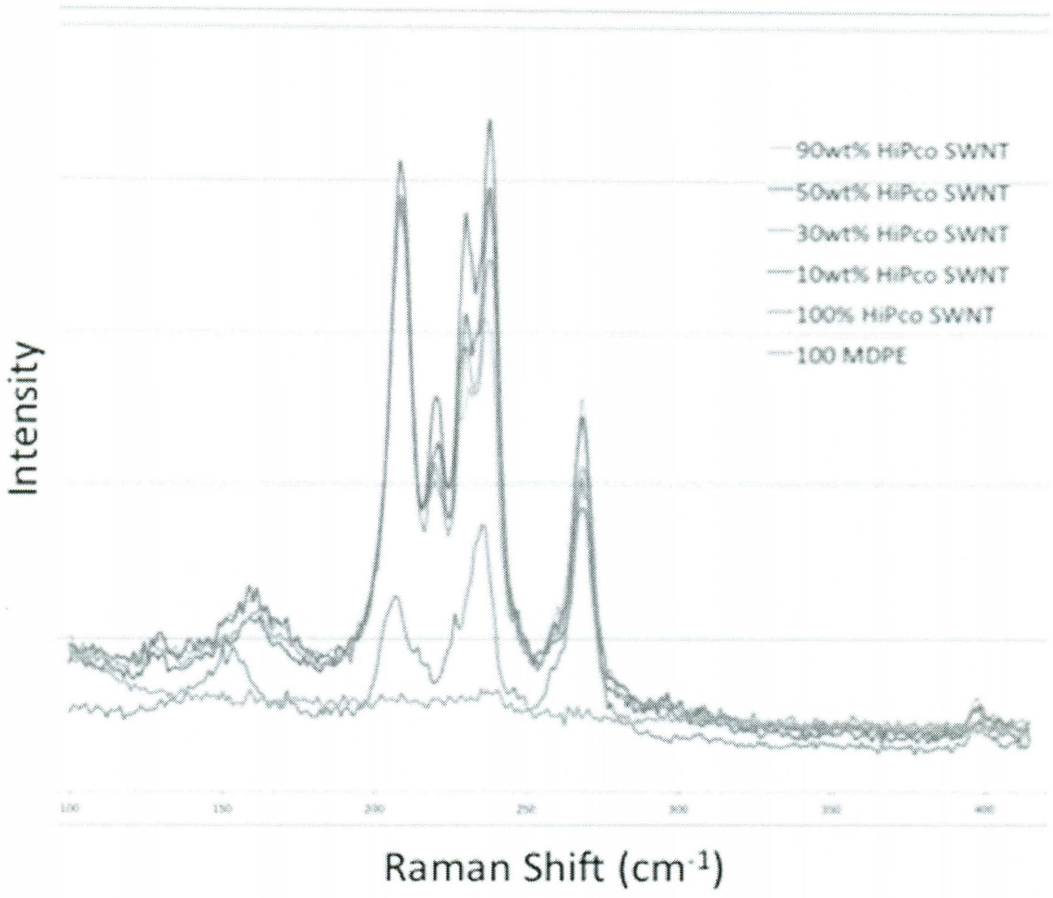


Figure 53: Raman spectra of RBM region of HiPco MDPE composites

Analysis of the D to G peak ratios between 100% HiPco SWNT in Figure 52 and those from the MDPE composites showed no notable difference, suggesting that little or no damage to the SWNT was sustained during composite fabrication, while no shifting in the peaks was observed either. The RBM region also exhibited

negligible shift in peak positions. The increase in strength of the RBMs between 200 and 250 has been attributed to a vibrational mode of the composite being added in this region[83].

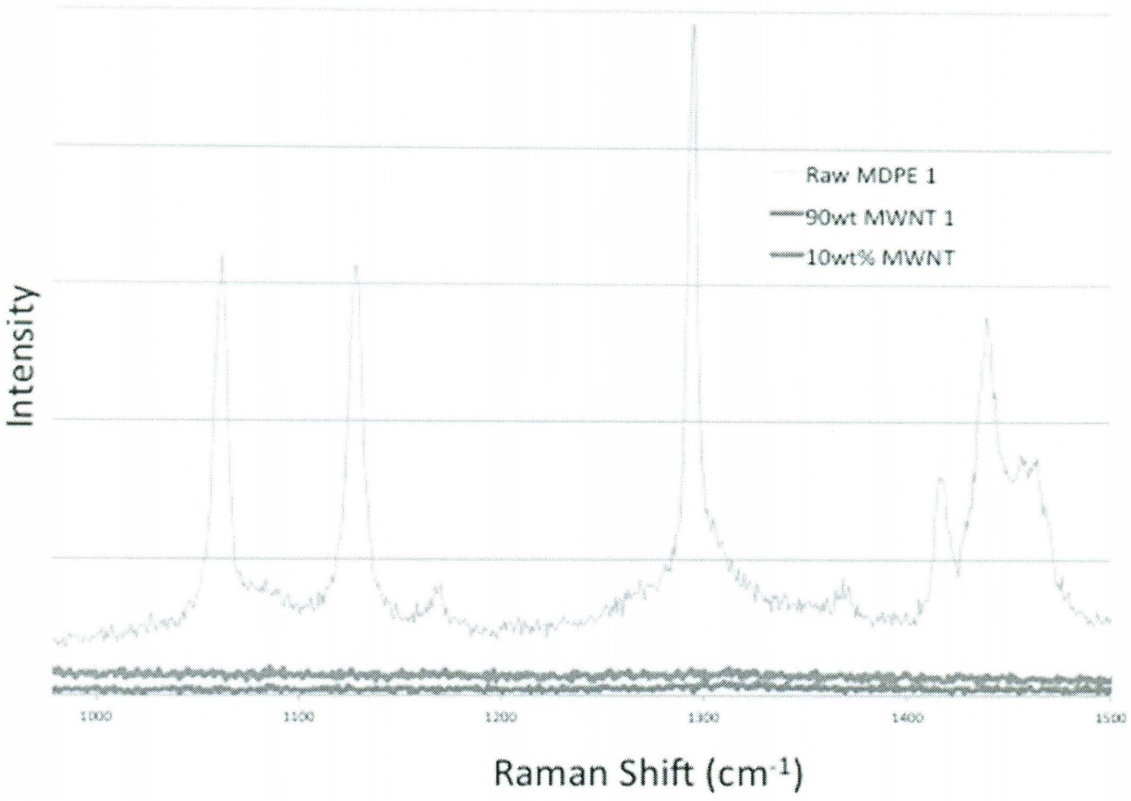


Figure 54: Raman spectra of MWNT MDPE composites

The Raman data focusing on the MWNT MDPE composites was even less exciting. Even at low loadings, features associated with both the amorphous and crystalline content of MDPE were not present (Figure 54).

## 4.3 REDUCING RESISTIVITY

### 4.3.1 Thermal and Pressure Processing

The benefits of annealing and pressure processing for reducing the electrical resistivity in nanocomposites have been espoused in the literature on numerous occasions [40,84]. To that end, a simple process of annealing in a heated press was used to reduce the resistivity of the composites already explored. It proved surprisingly successful.

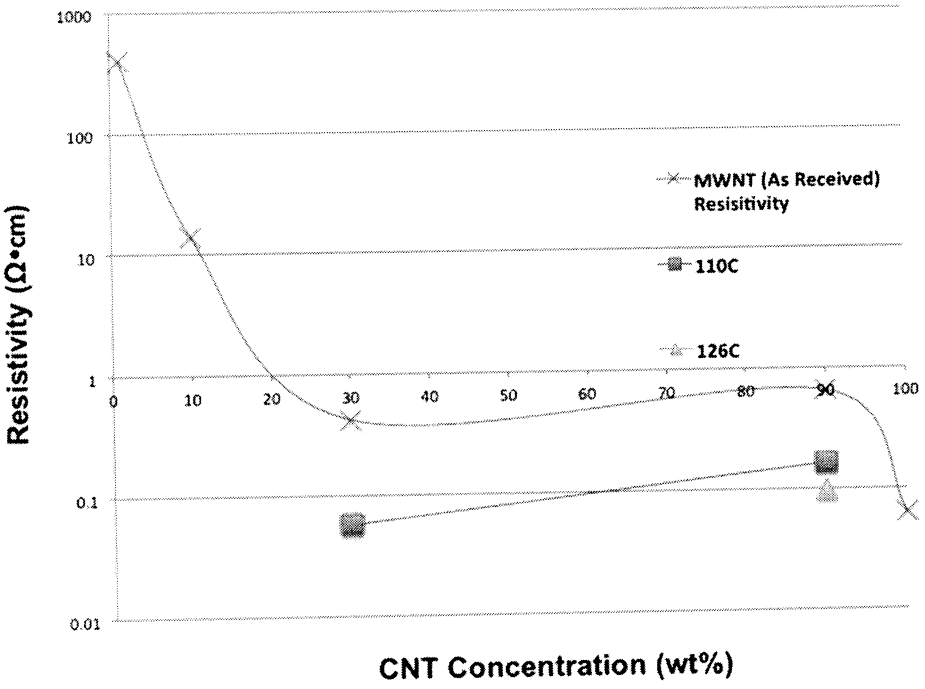


Figure 55: Resistivity vs. loading with pressure & annealing for Mitsui MWNT and MDPE composites

Experiments were conducted using a Carver Press. Samples were placed between two sheets of Teflon, and allowed to reach press temperature before pressure was applied. 20,000 lbs. of pressure was then applied for 15 minutes. An initial temperature of 110°C, the MDPE melting point, was used. Some samples, in particular the high wt% loading examples of CG100 SWNT and Mitsui MWNT, were found to not flow and spread at this temperature. A second round of experiments was conducted at 126°C, which had a more pronounced effect on all the samples tested, especially at high wt%.

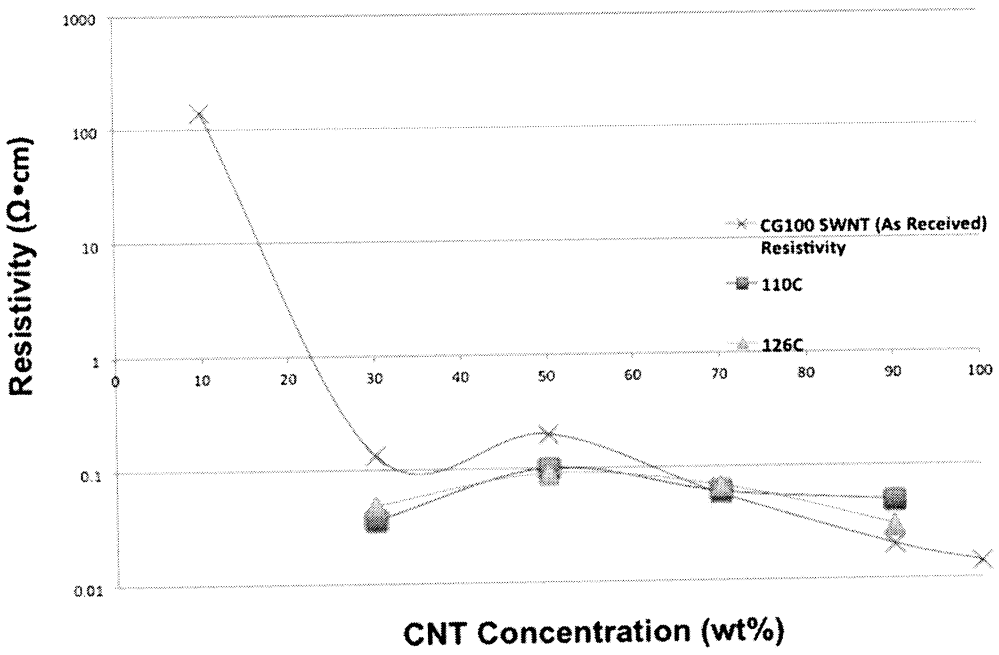


Figure 56: Resistivity vs. loading with pressure & annealing for CG100 SWNT and MDPE composites

Annealing and pressure was found to have little benefit for the CG100 composites at high loading. It was observed these samples did not flow, melt or spread during treatment, and resistivity actually increased (Figure 56). The MWNT samples did benefit from an almost one order magnitude reduction in resistivity, but there was little change in morphology at any scale (Figure 55).

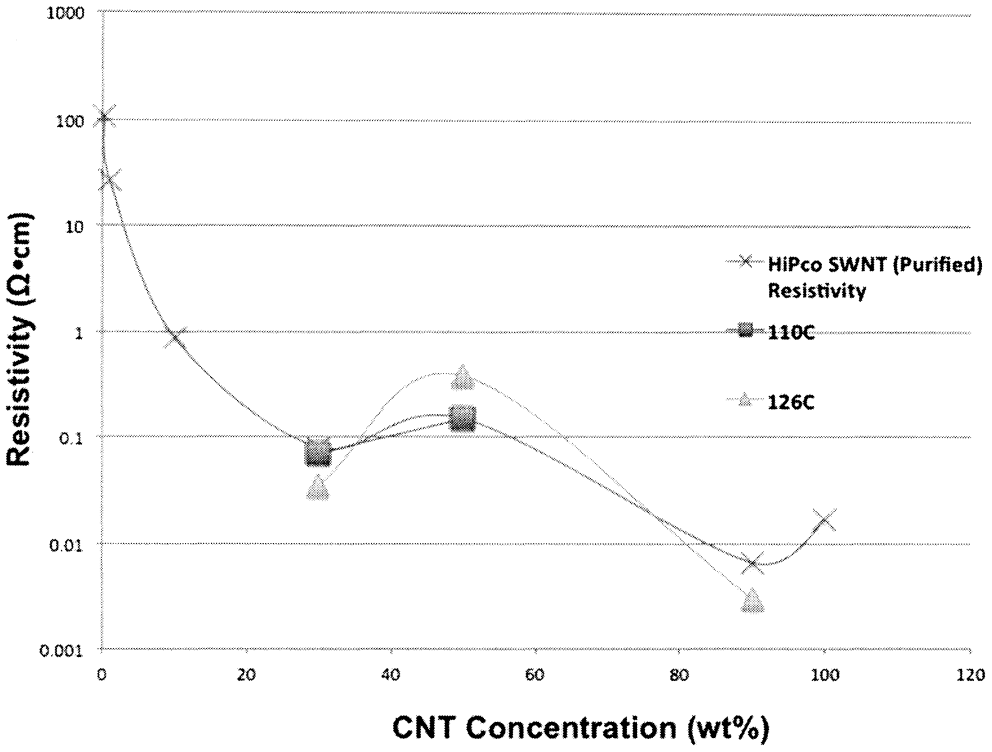


Figure 57: Resistivity vs. loading with pressure & annealing for HiPco SWNT and MDPE composites

The HiPco and DWNT samples showed the most impressive results from annealing and pressure (Table 9). The result of $2 * 10^{-4}$ (Ω•cm) for 90wt% DWNT and MDPE is exceptional considering how flexible, lightweight and formable the material proved in handling.

| **Nanotube & MDPE** | **Loading** | **Resistivity Before (Ω•cm)** | **Resistivity After (Ω•cm)** |
|---|---|---|---|
| HiPco SWNT | 90 | $6.6*10^{-3}$ | $3.0*10^{-3}$ |
| CCNI DWNT | 30 | $1.0*10^{-2}$ | $5.5*10^{-3}$ |
| CCNI DWNT | 90 | $1.3*10^{-3}$ | $2.0*10^{-4}$ |

Table 9: Summary of most promising results from annealing and pressure treatment

### 4.3.2 Microwave Processing

The Tour group at Rice University has shown the heating effect of carbon nanotubes (CNT) with microwaves to be highly efficient, even when included in a polymer to form a composite [85,86]. Higginbotham et al. have shown that even less than 1 wt % of CNT included in a ceramic composite can be heated in excess of 1000°C in minutes using 30-40 watts of microwave energy [21].

Throughout this thesis, an interest or vein has been considered on scalable processes, suitable for industry adoption, to produce and improve electrically conductive nanotube polymer composites. Utilizing a microwave process as a low cost, highly scalable procedure that can improve the electrical conductivity (reduce resistivity) of CNT polymer composites was considered as part of this research.

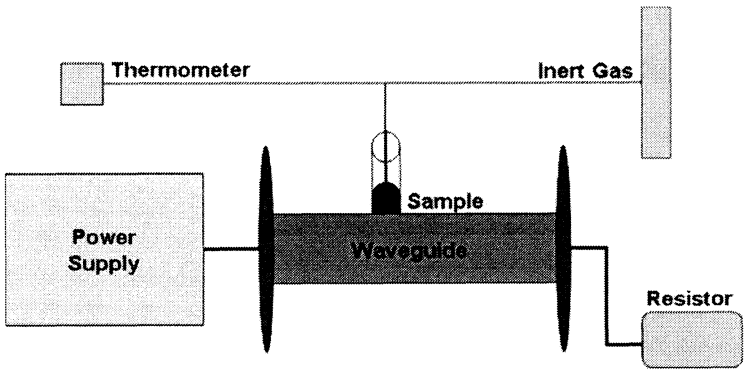


Figure 58: Simple diagram of microwave apparatus setup by the author in collaboration with the Tour Group

A variable power control 2.45 GHz 10–100 W microwave generator (Opthos) was connected via coaxial cable to a waveguide that also acted as sample holder (Figure 58). The CNT MDPE composites were inserted into the waveguide through a 1 cm hole positioned 10 cm away from the microwave source. Power was set to between 35 to 70 W. It was noted that the forward power was greater than the reflected. Therefore, the actual microwave power that reached the samples was considered to be ~30–40 W, defined as the forward minus reflected power. The unabsorbed microwaves were absorbed by a large vessel of water at the open end of the waveguide that acted as a resistor or sink.

As noted in prior sections concerning the literature, the resistivity of CNT polymer composites can be reduced to as low as $1*10^{-2}$ Ω•cm via mechanical, chemical and electrical processing. Often, these steps are costly, time consuming and not scalable from the laboratory to industrial usefulness. Harnessing the heating effect of CNT via microwaves, a novel process for the enhancement of CNT polymer composite conductivity (reduction in resistivity) was observed.

The composite is exposed to microwave energy, thereby causing the CNT to rapidly heat [21]. This thermal energy changes the polymer in the immediate vicinity of the CNT. Electrical resistivity in various composites was reduced. It is thought this reduction in resistivity was due to either:

1. Polymer char between the CNT providing increased electrically conductive pathways (Figure 59) or

2. Polymer char between the CNT providing increased electrically conductive pathways in combination with movement and alignment of the CNT due to the melting of the polymer and electromagnetic forces placed on the CNT by the microwave radiation (Figure 60).

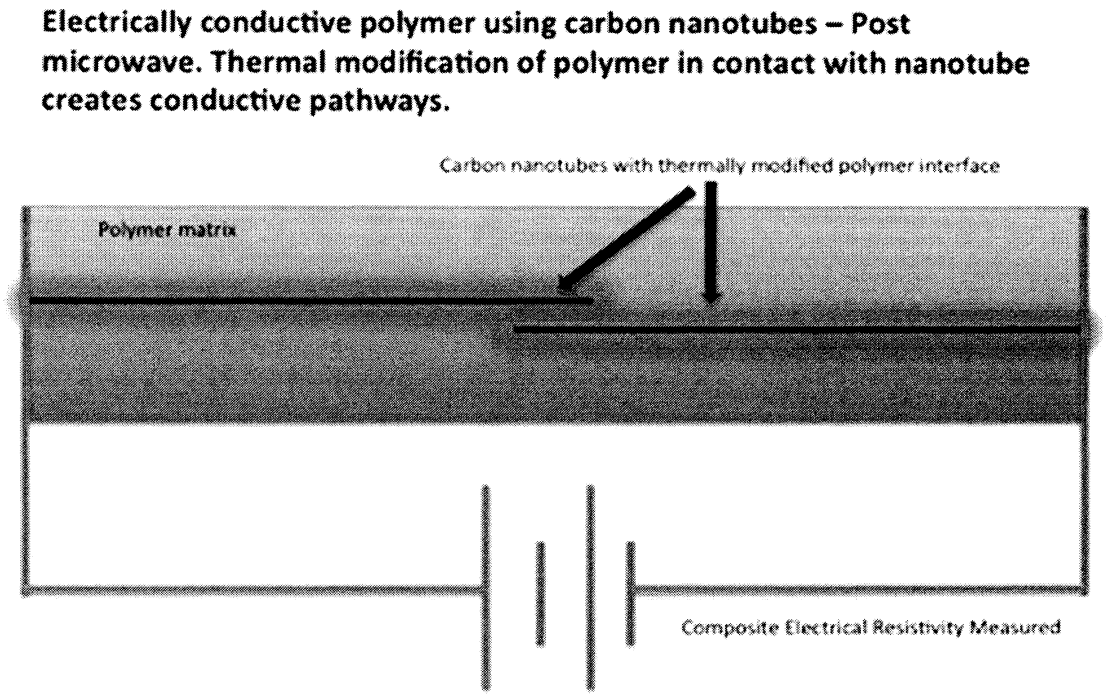


Figure 59: Possible mechanism of resistivity reduction via microwave

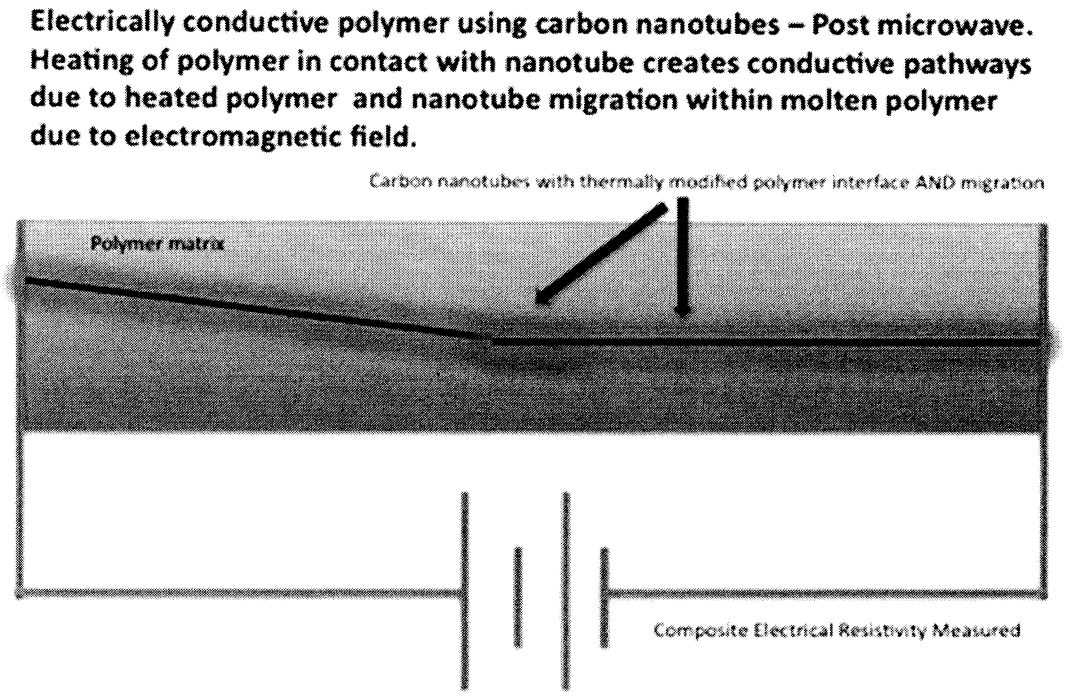


Figure 60: Alternate mechanism of resistivity reduction via microwave

This microwave method did not prove especially effective in reducing the resistivities of CNT MDPE, certainly not to the degree that annealing and pressure achieved. With 30wt% loading SWNT composites, the improvement was one half an order of magnitude of resistivity. TGA analysis confirmed that the method was effective in preventing damage to the polymer; polymer features remained. The method also showed success with thermoset composites produced in collaboration with Nanoridge INC. that are mentioned elsewhere[1,6].

### 4.3.3 Novel Doping Method

In much of the literature, *intercalation* is a term used to describe the reversible incorporation of a foreign molecule between two other molecules, most often in a periodic structure. It is most associated with the incorporation of foreign species between layers of graphite hence the term; graphite intercalation compounds (GICs). The five main subgroups of highly electrically conductive GICs were summarized by Inagaki et al., as shown in Figure 1 [87]. Vogel et al. claimed electrical connectivity of 1 X 10^6 S cm is possible with GICs of arsenic pentafluoride (AsF5) and antimony pentafluoride (SbF5), however this result has never been reproduced [88-90].

Conductivities between 2.1 X 10^4 and 1.0 X 10^5 S cm have been obtained with vapor grown carbon fibers (VGCFs) and AsF5 [91,92]. While using pentafluorides, the necessity for highly crystalline graphite or VGCF was emphasized. Much of the literature shows improvement of electrical conductivity with intercalation compounds by a factor of ten or more [87]. In addition, some of the techniques involved are more suitable for scalability than the chemistry protocols of selective functionalization of CNT.

| Material | Conductivity | Comments |
|---|---|---|
| Pentafluorides | | |
| $AsF_5$/HOPG and VGCF | $1 \cdot 10^8$ S/m | Higher than metallic copper |
| Metal chlorides | | |
| $CuCl_2$/MPCF | $7.8 \cdot 10^6$ S/m | Creditable values, comparable with Cu |
| $FeCl_3$/VGCF | $1.4 \cdot 10^7$ S/m | |
| Fluorine | | |
| $F_2$/HOPG and various CF's | $2 \cdot 10^7$ S/m | Stable in air |
| Donor couple | | |
| K + Bi/HOPG | $2 \cdot 10^7$ S/m | Stable in air |
| Residue halogens | | |
| $Br_2$ or ICl/MPCF's | $1 \cdot 10^6$ S/m | Very stable under severe conditions |

Figure 61: "Highly conductive graphite intercalation compounds", Inagaki 1989 [87]

The introduction of foreign species to carbon nanotubes is more commonly described as *doping.* Doping in this sense can be broken down into three main categories [93]:

(a) Endohedral inclusion of the free space within the nanotube
(b) Replacement of carbon atoms of the nanotube structure with a dopant
(c) Exohedral incorporation of molecules between nanotubes within a bundle or agglomerate

The exohedral doping correlates closely to the intercalation of graphite, in particular when a charge transfer between dopant and nanotube leads to novel electrical properties [93,94].

For this initial study, $SbF_5$ was chosen as the intercalate species due to the high conductivities found in the literature, its ease of use *relative* to $AsF_5$ and that it has not been combined with carbon nanotubes previously.

**Experimental Method**

Single wall carbon nanotubes (SWNT) and $Sb_F$ were combined in a method based on one from Lalancette et al.[95] The SWNT were supplied by SouthWest NanoTechnologies Inc. (CG 100 grade). These SWNT are produced by a catalytic CVD process utilizing CO disproportionation at 700–950 °C in the presence of a Co-Mo catalyst [96]. 250 mg of as-produced SWNT were dried by heating under vacuum in a boiling flask for 72 hours at a temperature range of 90 – 110°C (Figure 62). The SWNT was transferred to a plastic glove bag for processing under an atmosphere of dry nitrogen. 0.084 mL of $SbF_5$ (Sigma Aldrich) was pipetted onto the SWNT inside a boiling flask to provide a 50% by weight concentration.

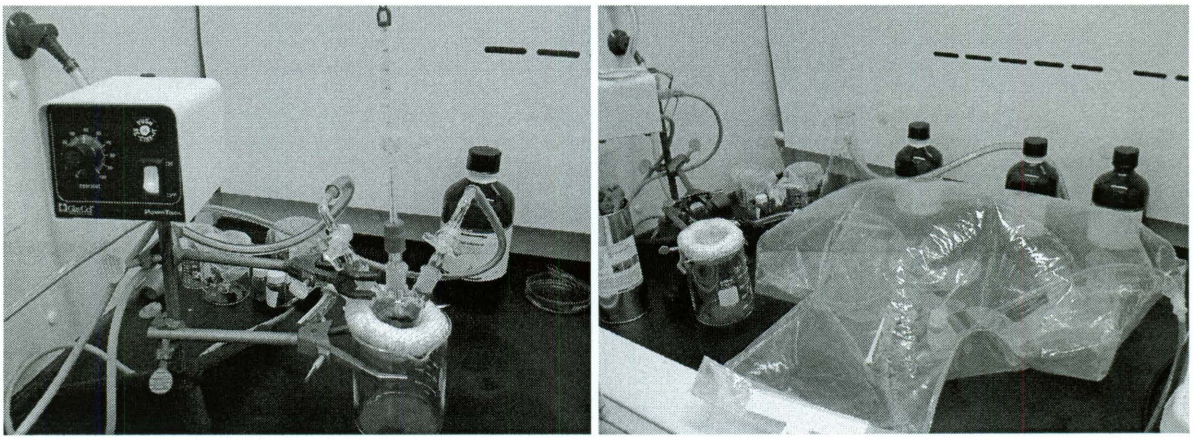

Figure 62: Vacuum heating flask and nitrogen-filled glove-bag

This preliminary experiment showed the necessity for dry inert conditions, as some residual moisture was clearly present in the glove bag, which reacted with the $SbF_5$ to produce hydrogen fluoride (HF) gas. These reactions and the products they presented produced the need to complete the experiment in an expedited fashion.

The resultant material was sealed in its flask, placed under vacuum and heated at 90-120°C for 72 hours. The initial application of vacuum, applied to the boiling flask while inside the glove bag, led to a deposition of black material on the inner surface of the vacuum line (Figure 63). The difficult conditions combined to reduce the expected yield of the experiment.

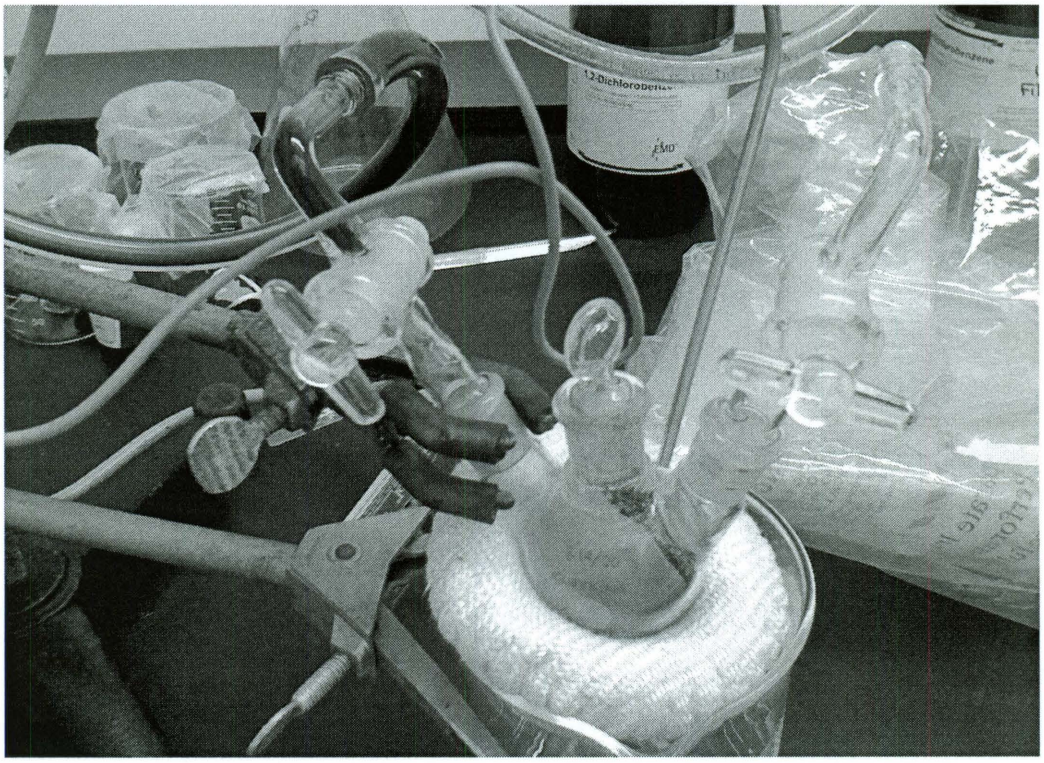

Figure 63: Resultant product and noted deposition inside vacuum line

The end product was a dry black powder, similar to the starting SWNT, which appeared stable under normal atmosphere and resistant to hydrolysis. The bulk of the material remained inside the boiling flask.

**Characterization and Results**

In order to measure electrical conductivity, the small amount of first-round material produced dictated the use of a simple two-point probe measurement. The material was placed inside a Teflon tube and a probe attached at each end. Two-point electrical probe measurements were obtained using a Commercial Electrical HDM350 Multimeter with the following results:

| **Nanotube** | **Resistance (Ω)** |
|---|---|
| Raw SWNT | 55.3 |
| SWNT SbF5 | 2.3 |

Table 10: Summary of 2-point resistance measurements

With additional samples, 4-point tests were prepared as described in earlier sections. In addition, a simple procedure of iodine doping was also explored [97].

| Nanotube | Dopant | Initial Resistivity (Ω•cm) | Post-Doping Resistivity (Ω•cm) |
|---|---|---|---|
| SWeNT CG100 | Iodine | 0.014 | 0.0027 |
| SWeNT CG100 | Iodine & $SbF_5$ | 0.014 | 0.0027 |
| SWeNT CG100 | $SbF_5$ | 0.014 | 0.0038 |
| HiPco SWNT | $SbF_5$ | 0.01 | 0.0003 |

Table 11: Summary of 4-point resistance measurements

The $SbF_5$–treated SWNT showed over an order of magnitude improvement in conductivity. This is in keeping the typical factor of ten improvement noted by Inagaki et al.'s review [87]. Given the difficult processing conditions, and the correlation of packing density of SWNT to electrical resistance, this result should be taken as a preliminary one with expected room for improvement.

The iodine samples also showed an impressive improvement, although there was no additive benefit from combining the two protocols. Both methods yielded stable doping, which had consistent resistivity results even 6 months after doping.

Scanning electron microscopy (SEM) and scanning transmission electron microscopy (STEM) was performed on both the main sample and the material found deposited inside the vacuum line (Hitachi S-5500). Simultaneous energy dispersive x-ray spectroscopy (EDS) was also carried out (Hitachi-Bruker).

Fourier transform infrared spectroscopy (FTIR) was performed on the original sample, with inconclusive results (Nicolet). XPS data was also collected and analyzed (PHI Quantera).

Two primary material subjects were studied using SEM and STEM: material recovered from inside the vacuum line and the main body of material produced. The specimens shared a number of key characteristics, while some differences were also observed. The material from the vacuum line contained two types of tube structure; one similar in size to the starting SWNT but with clear additions to the sidewall and a second tube type in the size range of 20-40nm (Figure 64).

EDS data confirmed the presence of carbon, antimony and fluorine with the vacuum line sample (Figure 65). One key difference noted when compared the bulk material produced, was that the larger tubes found were neither as rigid-looking, nor as straight as those found in the main sample.

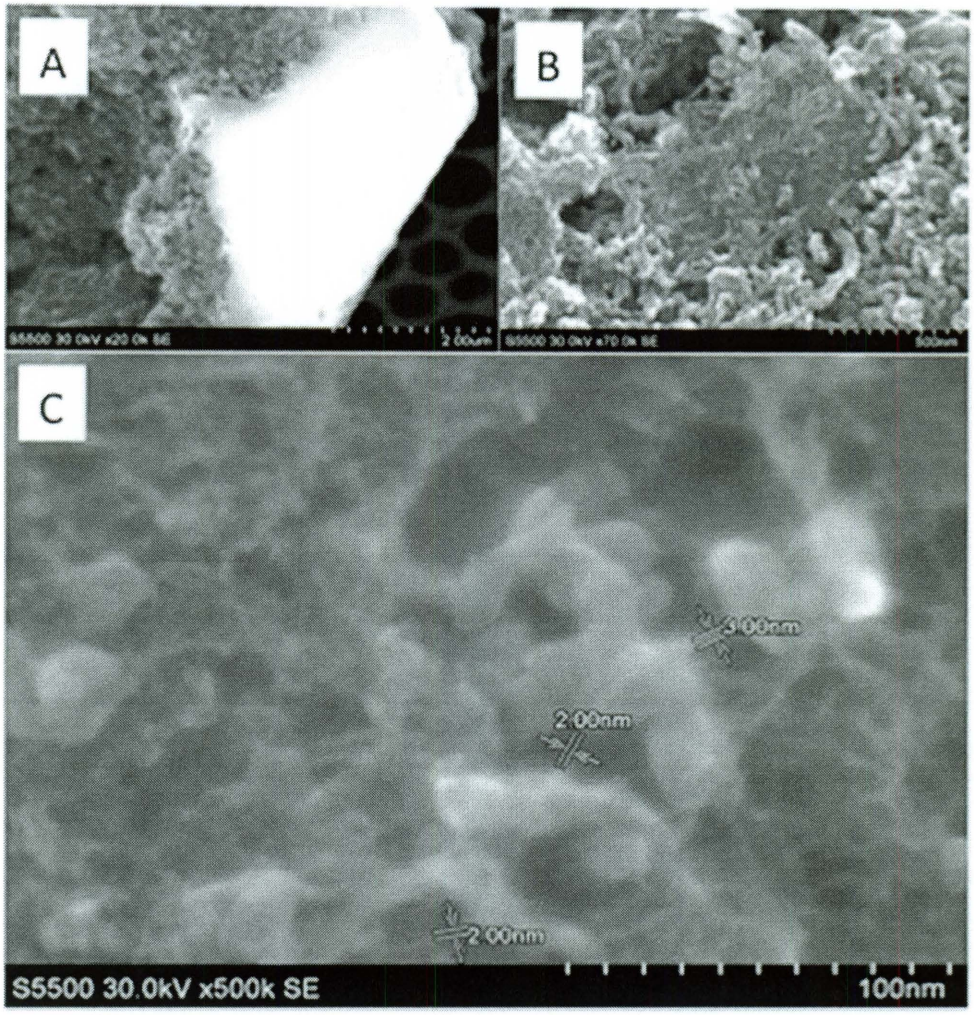


Figure 64: (A) Low resolution SEM of material inside vacuum line (B) two sizes of tube structure present, (B) High resolution SEM of smaller tube type

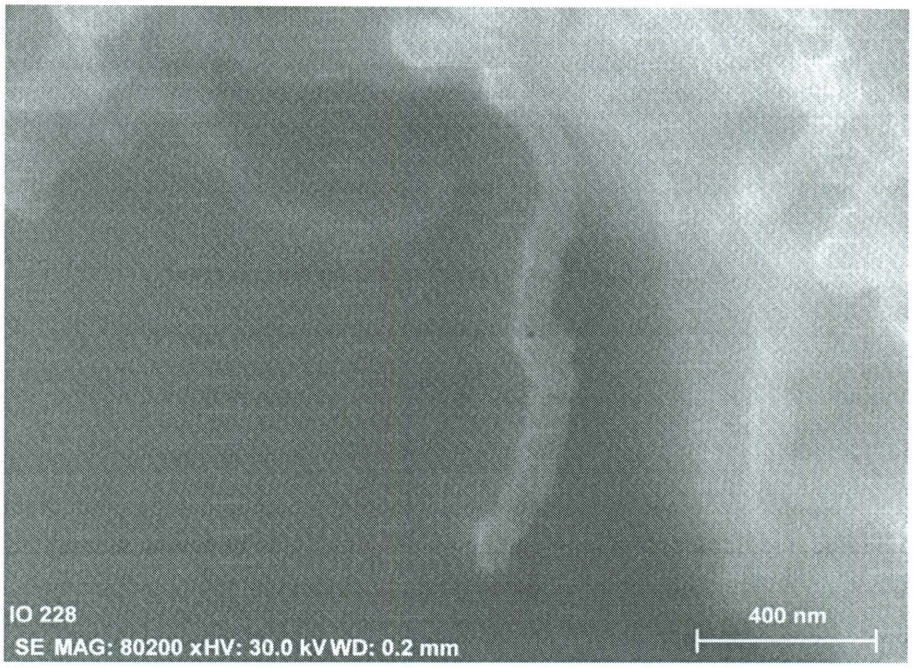


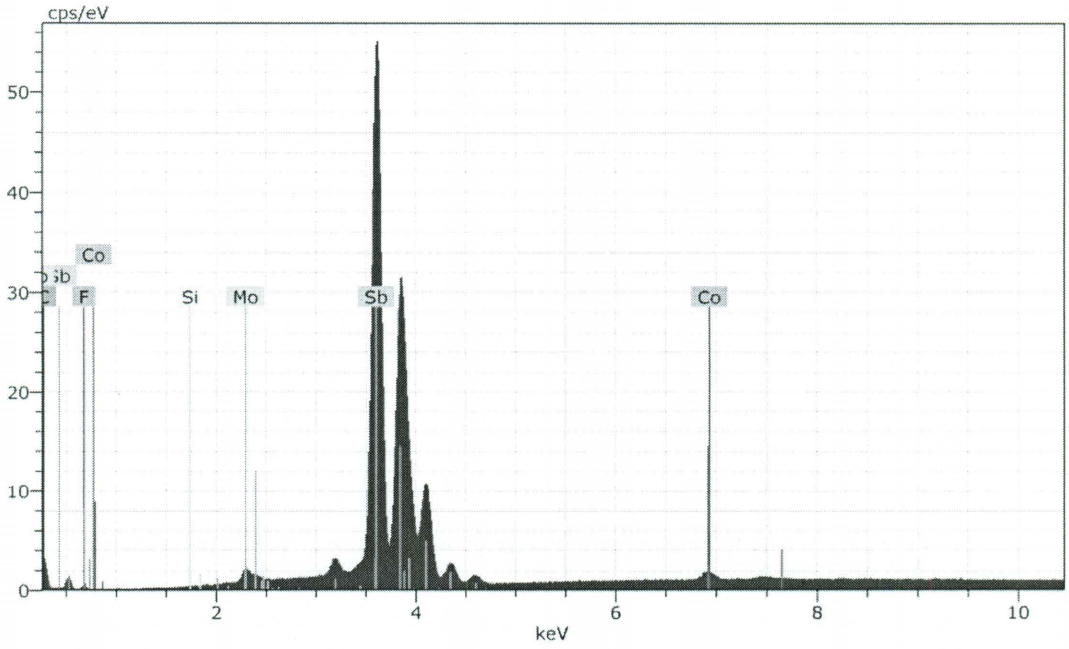


Figure 65: STEM and EDS analysis of larger tube structure

The main body of sample showed a similar mix of two tube types, but the microscopy consistently found very rigid and straight nanotubes in the 20-40nm range (Figure 66).

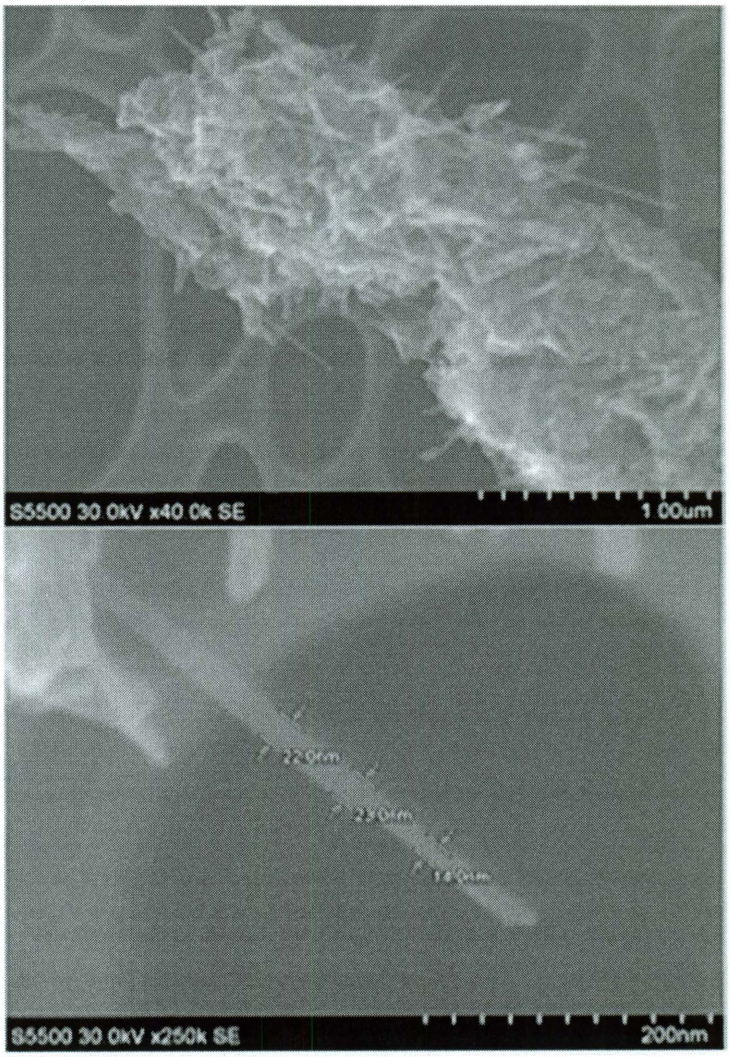


Figure 66: STEM imagery of material produced with high resolution images of large diameter tube structures

High-resolution STEM images of the smaller ~2nm nanotubes suggest these are modified or functionalized SWNT (Figure 67). EDS data shows the presence of C, Sb and F (Figure 68 and 69) on these smaller nanotubes.

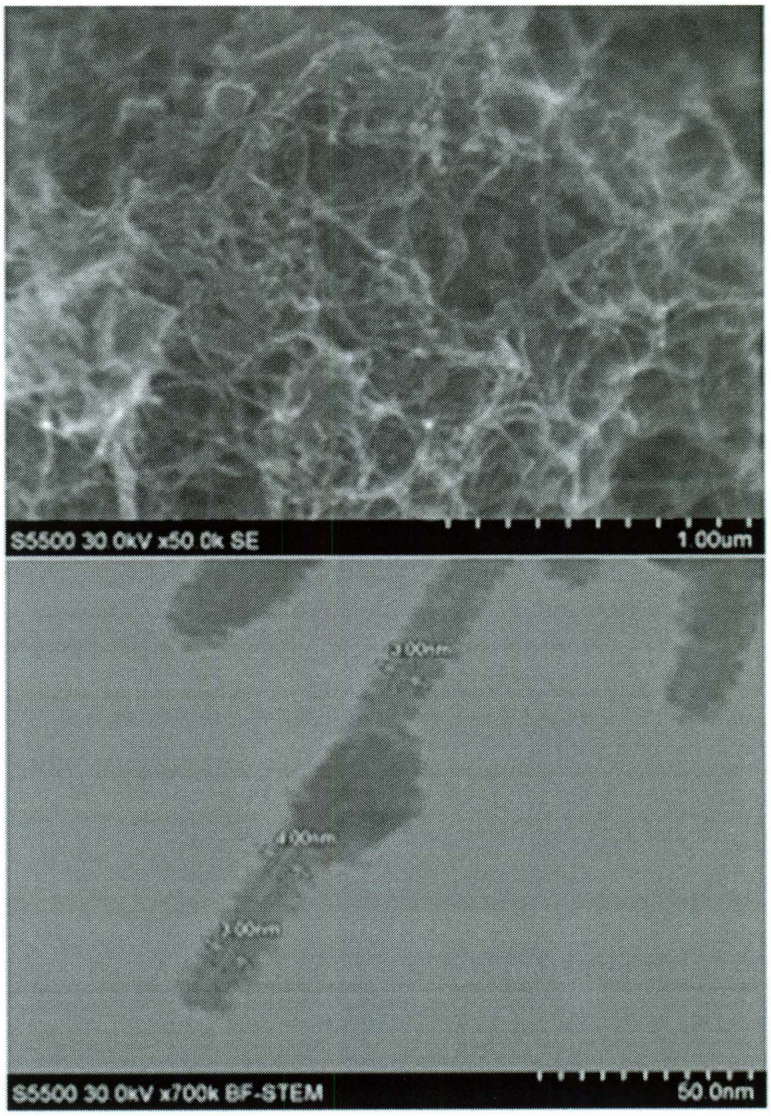


Figure 67: High resolution STEM of smaller tube structure

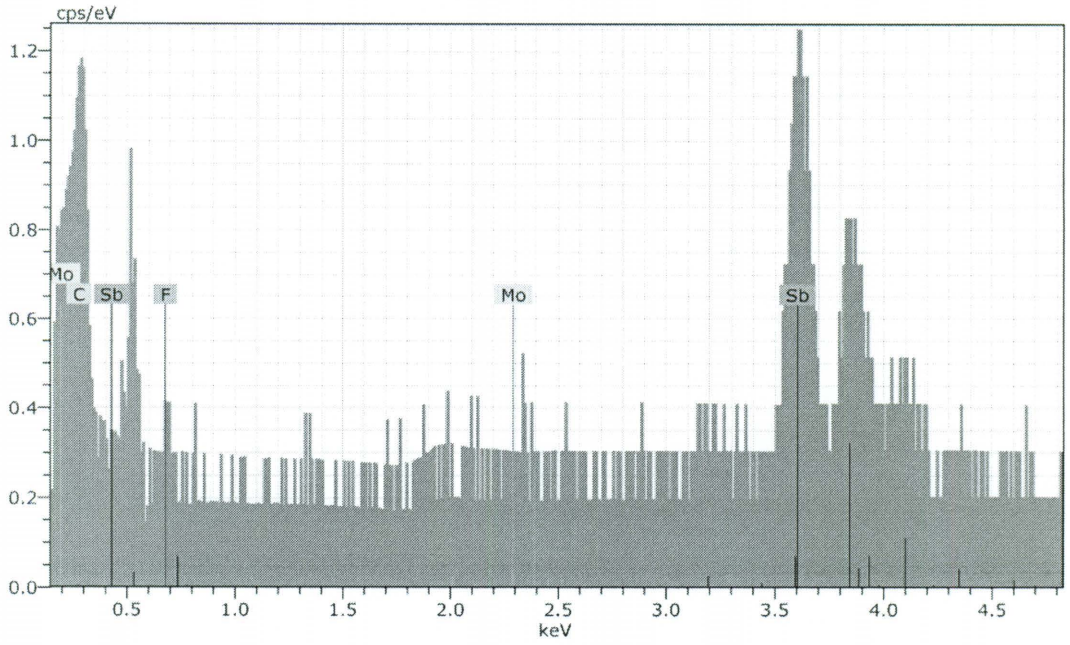


Figure 68: EDS spectra of small nanotube material

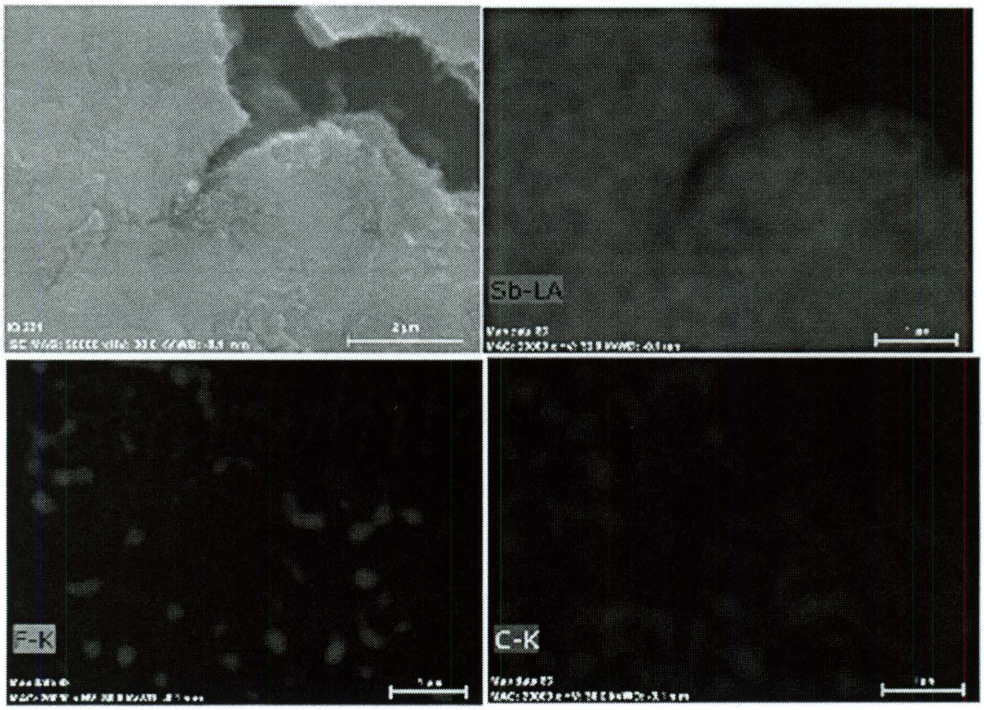


Figure 69: EDS and STEM area scan confirming the presence of C, Sb and F

Clearly, a complex morphology of material was formed at the nanoscale. TGA data confirmed that the CNT suffered damage, as the oxidation peak has been broadened and shifted. The production of large diameter, straight tubular structures is considered a factor here. A considerable amount of metallic species has been added by the process, >40% (Figures 70 & 71).

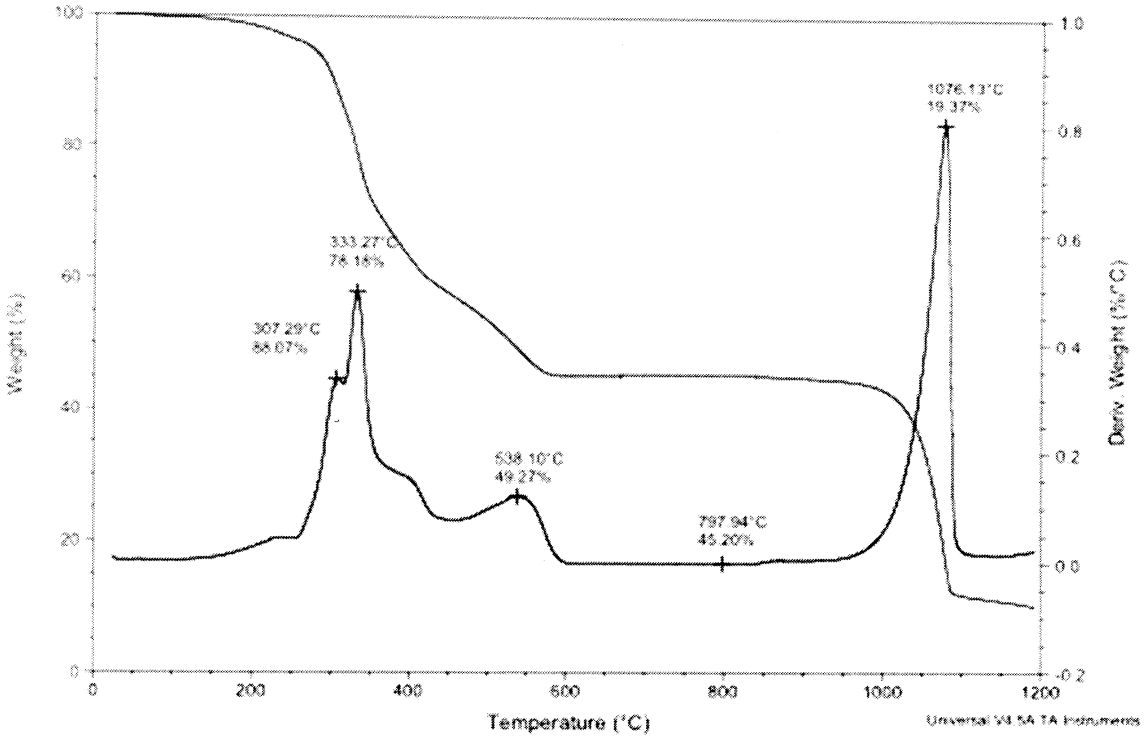


Figure 70: TGA data on CG100 SWNT doped with $SbF_5$

The XPS data did not provide a concrete answer to the species present. It appeared from the literature and NIST, that no XPS standard for $SbF_5$ currently exists. The data collected showed the presence of C, Sb and F. Analysis software suggested numerous forms of Sb present, including $KSbF_5$ and $KSbF_6$. The author and Rice

University Share Equipment Authority XPS expert took this as an attempt by the analysis software included in the XPS instrument to fit the data to as close a known standard.

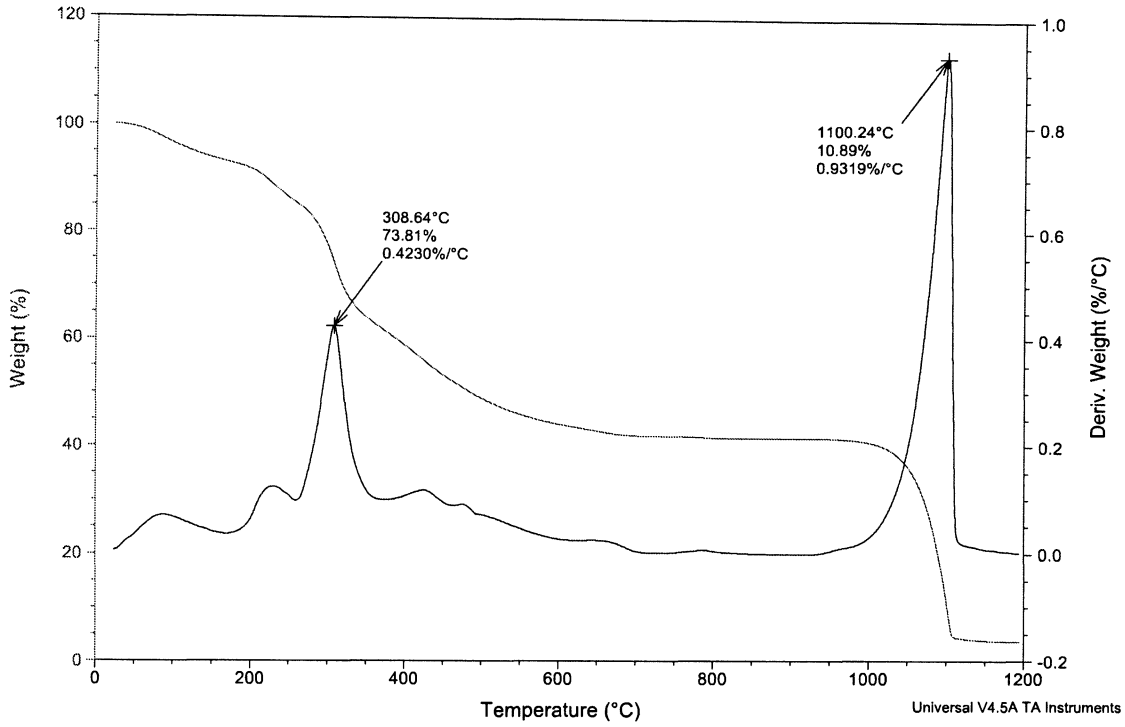


Figure 71: TGA data on HiPco SWNT doped with $SbF_5$

Both doped nanotube samples were explored as conductive fillers with MDPE. The samples were prepared as previously described and tested with a 4-point probe. Results were disappointing; resistivity had *increased* by 1-2 orders of magnitude. Given the CNT had suffered some modification and possible damage during the doping process, and considering the positive performance of the doped CNT tested with MDPE, the sonication process used during composite fabrication was

considered the main problem. Clearly, these doped materials are more suitable to used as-is, rather than be processed through vigorous processing procedures.

The most obvious improvement for future work will be to use a more robust nitrogen atmosphere glove box. The heated vacuum preparation of the SWNT was adequate, but using an actual vacuum furnace might also be beneficial.

Experimenting with additional types of CNT will also be useful. DWNT may provide a more robust nanotube surface as STEM and TEM analysis of the SWeNT CG 100 nanotubes show a rough surface morphology of carbon.

# CHAPTER 5: LIGHTWEIGHT AND LOW ENERGY NERVE GAS SENSOR

## 5.1 INTRODUCTION

Sensors based on carbon nanotubes (CNT) have been an area of interest since the material's discovery by Iijima in 1991 [25] , and an active area of research once CNT availability began to increase via the innovations of Smalley and others [24,26]. Their long aspect ratios of over 1000-to-1, varied electrical and thermal properties and a decade of research in manipulating nanotubes through functionalization chemistry make them an idea target material for sensor research. The scientific community has responded to this opportunity with a wealth of experiments using CNT to sense a wide range of analytes. Some of this work has yielded impressive results in an laboratory setting, such as parts per billion (ppb) sensitivity to chlorine [98] , ammonia [99] and nitrogen dioxide [100].

The author was given a broad requirement to apply the electrically conductive CNT MDPE composites towards a sensor application for the United States Army Research Laboratory (ARL). The application had to be novel, and suitable for use in micro air vehicles (MAV), whose operational environment and low energy use present some unique requirements. A thorough literature search was conducted, with special attention paid to use of CNT towards sensing analytes of potential suitability to this application.

A large body of work in the literature concentrates on hydrogen detection and the detection of water vapor. For relevance to applications of chemical detection, inclusion of these references has been kept to the minimum. Also of note is the sizable number of research studies that have been conducted in sensing of ammonia (NH3) and nitrous oxides (NOx). A summary of some of the most promising research in this field is provided in Appendix A.

## 5.2 PRIOR RESEARCH

As with all areas of active research, there are a number of pre-existing review articles of relevance to this study. Moore et al. have provided a good review of instrumentation for trace detection of explosives [101]. While this does not have direct relevance to nanotechnology, it benefits any research in the sensor area by providing information such as the vapor pressures of various common analytes of interest. Moore makes the useful distinction of breaking down electrochemical sensors in this field into two types, galvanic and electrolytic, a note often ignored by reviews of CNT sensors. A short review by Seto et al. gives a summary of the current sensing technology for nerve and chemical agents [102]. This work also includes testing of actual battlefield substances such as sarin, but also sensing of dimethyl methylphosphonate (DMMP) and other common chemicals that closely resemble such agents.

As this research will utilize composites of CNT and polymers, a useful reference is Lange et al. review on conductive polymer sensors [103]. This work includes a table of electrochemical and electrical results with analyte and polymer. Although of more relevance to biological sensing applications, Rajesh et al. have reviewed conductive polymers, in particular composite applications [104]. Included is a summary that highlights analyte, diameter/size, detection limit and voltage among other important data.

With regards to sensor reviews focusing on CNT-based technologies, there are a number of papers of note. Mahar et al. wrote a broad review of CNT sensors, summarizing many of the unique attributes of CNT materials and touched upon sensor applications ranging from temperature to strain [105]. They also highlighted research that showed changes in Raman spectroscopy data when single wall carbon nanotube (SWNT) are immersed in various liquids, including common organics [106]. In their review, Wang et al. provided a useful summary of specific data for interactions between single wall carbon nanotube (SWNT) and gases [107]. These included adsorption energy, charge transfer and tube-molecule distance.

Bondavalli concentrated on CNT field effect transistors (FET) in their review, a common technical approach taken in CNT sensors [108]. They present an informative table on source/drain current change after exposing two types of CNTFET functionalized with DNA sequences to various vapors, including DMMP. Also

focused on FET devices is a review by Yáñez-Sedeño [109]. This work investigated CNT-metallic nanoparticle electrodes. Rounding out these reviews is one by Jacobs et al. [110] which concentrated on CNT sensors for biomolecules, a broad review by Varghese et al. which included a useful explanation of sensor nomenclature and basics[111], and Sinha et al. which has a summary of gas sensors [112].

The most useful review work as reference for this research was by Kauffman et al. [113]. It came closest to summarizing the data of interest to the application, including tables that note analyte, method, detection limit, CNT material and references.

Appendix A summarizes the data from the literature most useful to the research while reflecting the most useful aspects of the aforementioned CNT sensor reviews.

Research by Boul et al. has previously developed CNT-based sensors for radiation sensing applications for NASA [64]. These consisted of networks of SWNT deposited on 32-channel/sensor pads (Figures 1 and 2). The SWNT were optimized via functionalization and were designed to register a change in resistivity upon impact from radiation. A change in resistivity will be the primary signal change for our current study.

## 5.3 ARMY MISSION APPLICABILITY – DIMETHYL METHYLPHOSPHONATE (DMMP)

DMMP was of particular interest to this study due to its suitability as a nerve agent simulant [102,114]. Use of color-changing paper is currently a commonly used method to test for nerve agents such as sarin [102,115]. The weaknesses of this method are that the agent must be applied directly to the paper in a liquid form, and that the material cannot distinguish between organic solvents, such as DMMP, and actual nerve agents. Instruments such as gas chromatograph-mass spectrometers, surface acoustic wavelength detectors and ion mobility spectrometers have been produced with a level of portability suitable for limited handheld application [102,116], but not miniaturized nor automated enough to warrant suitability to low power vehicle applications.

An optimized nanotube sensor could offer a solution for sensing a nerve agent simulant such as DMMP. Picking some of the most relevant research from the literature and focusing on the chemiresistive sensor approach, Figure 73 below illustrates chemical sensitivity to DMMP versus resistance change. One can note that an enormous resistance change is not produced in any of this previous research; these small-realized signal changes may make applicability of these technologies challenging.

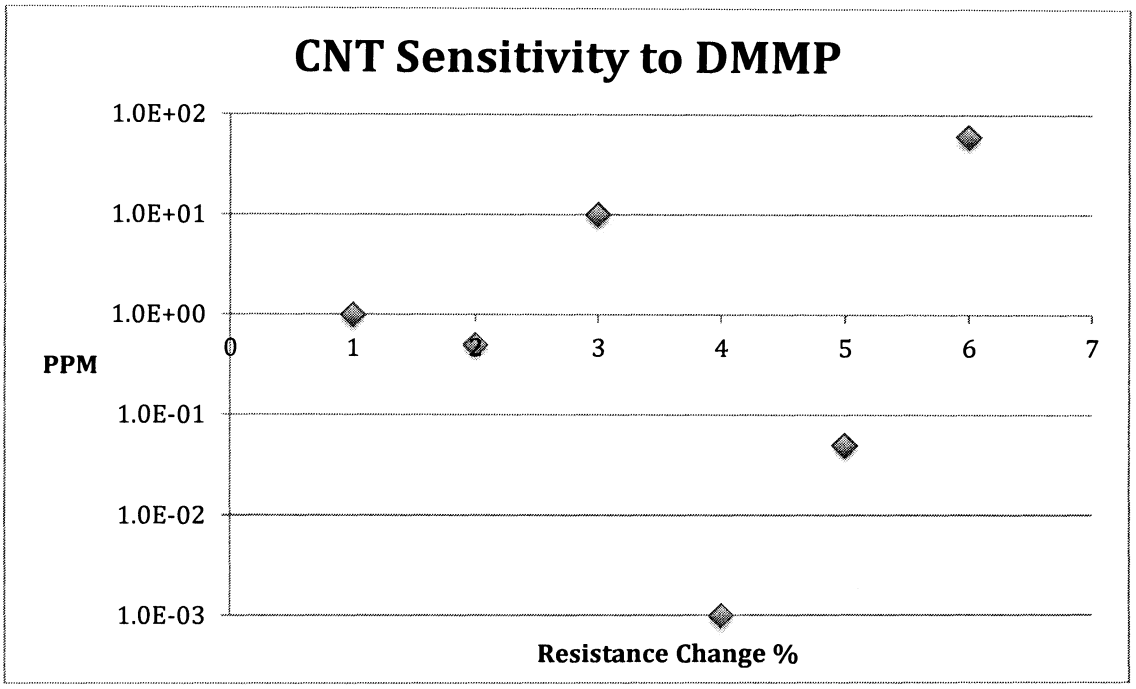


Figure 73. Summary of select research: sensitivity vs. relative resistance change of CNT-based DMMP sensors

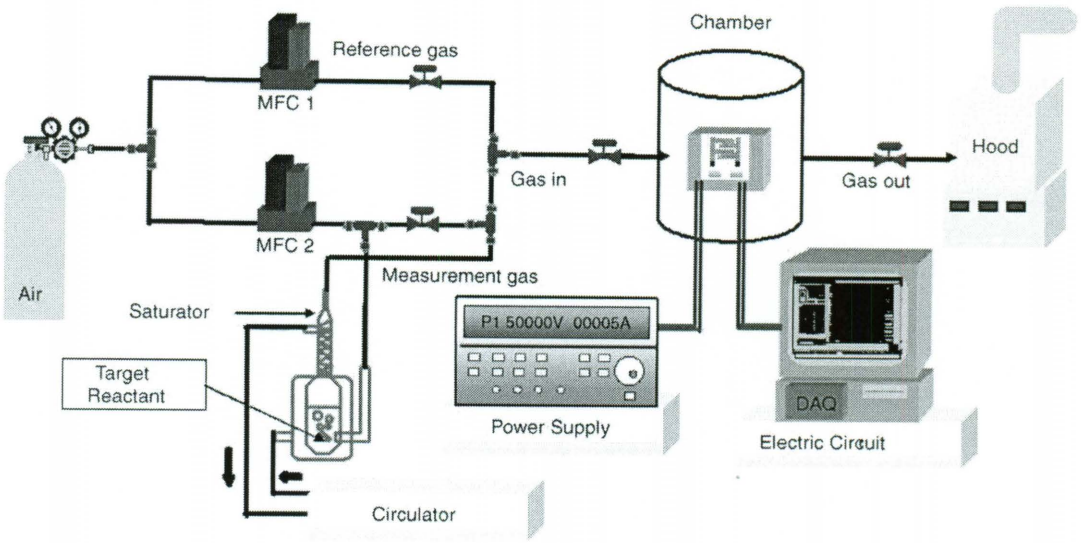


Figure 74: Suitable experimental setup [117]

Novak et al. used a permeation tube and mass flow controllers to deliver calibrated doses of DMMP [118]. They also improved the sensitivity of their sensor by applying a 100nm coating of an acidic strong hydrogen-bonding polycarbosilane, which acted as a chemical-selective polymer. In follow-on research, Snow and Novak improved the sensitivity further by changing to a capacitive rather than resistive response and achieved sensitivity in the parts per billion (ppb) level [119]. They also observed that DMMP absorbs onto SWNT, and is a strong electron donor, causing a transfer of negative charge which in turn changes transistor threshold voltage by -2V [118]. This work also showed that after an initial response of 10+ minutes, it took many hours for the sensor to fully recover as DMMP desorbs slowly from SWNT. An additional

positive charge can be applied to offset the negative resulting from DMMP adsorption and speed up recovery of the device.

Wang et al. also took a composite-style approach, using hexafluoroisopropanol substituted polythiophene (HFIP-PT) and poly(3-hexylthiphene) (P3HT) and SWNT spin coated films as chemiresistors [120]. They chose the HFIP group to polythiophene because of its H-binding with phosphate esters. These esters are common in chemical warfare agents including sarin gas and simulants such as DMMP. They showed sensitivity as low as 0.6ppm and responses as fast as 1-2 minutes.

Cattanach et al. produced network films of SWNT on substrates of polyethylene terephthalate (PET) [114]. This work is highly relevant from a composite standpoint to ours. They filter out interfering vapors such as hexane by using a 2-micron thick barrier film of chemical-selective polymer polyiobutylene (PIB) on the SWNT surface. Their experiment was at room temperature. A major advantage of their work is a large resistance swing of 75-100%, albeit at a response time measured in the 10's of minutes. Also, one should note that their experiments were conducted solely in the presence of DMMP, with no other gas present.

A variety of voltage levels were also found throughout the literature to "drive" such CNT sensors of DMMP. These range from 50mV [121], 0.1V [120] to 3V [118]. Such voltage levels should be taken into consideration when reflecting on the proposed application of such a sensor towards low-power applications. It was hoped that the

use of conductive nanotube fibers and composites in this study would reduce the overall power needs when compared to previous studies, while increasing the fidelity of signal change.

Observing relevant research in the literature, one can note a number of suitable experimental apparatus for gas sensing. The experimental setup as illustrated by Choi et al. represents what is probably the most optimal [117] (Figure 74). However, given the limited amount of time and resources available for this study, a less complex test setup was used. Instead, an approach similar to a simple one found in the literature was employed [122]. A glass vessel with a Teflon-taped plastic lid, was combined with the appropriate outlets for vacuum, wiring and syringe (to introduce the DMMP). Given the restrictions of having only one available multimeter, only one sample/sensor was tested at a given time.

With regards to the initial experiments conducted, a two-fold approach was initially proposed. Recently produced highly-conductive double wall carbon nanotube (DWNT) fibers were to be tested as chemiresistors for DMMP [97]. However, a scarcity of material and lack of mechanical robustness prevented their exploration towards this application. A follow-on experiment was proposed to modify these fibers with a polymer layer or functionalization to improve selectivity and sensitivity.

The second approach proposed, and eventually executed, was to use the conductive composites of polymer and CNT produced in earlier chapters of this thesis, as

chemiresistors of DMMP. An initial attempt was made to modify the porosity and available surface area of these composites to improve their suitability as a gas absorber by refluxing in boiling DCB. This step later proved unnecessary at the gas testing level used. DMMP was obtained from Sigma Aldrich. A colorless liquid, it has a boiling point of 181°C, a vapor pressure of 160 Pa at 25°C, vapor density of 4.2 and a liquid density of 1.15 g/mL [123] [124]. The flammable flash point is 69°C. Calculated and measured vapor pressure data in a temperature range from 263°K (-10°C) to 453.8°K (180.65°C) can be found in the literature [124] [125] (Figure 72).

**Table 3. Measured Vapor Pressures for DMMP, Calculated Values Based on Antoine Coefficients listed in Table 9, and Percent Difference**

| $T$ / K | $P$ / Pa | $P_{calcd}$ / Pa | difference[a] / % |
|---|---|---|---|
| 258.2 | 3.73 | 3.67 | 1.8 |
| 263.4 | 5.67 | 6.20 | - 8.6 |
| 273.2 | 15.2 | 15.2 | - 0.1 |
| 278.2 | 24.5 | 23.5 | 4.4 |
| 283.2 | 35.0 | 35.5 | - 1.4 |
| 285.0 | 41.7 | 41.0 | 1.7 |
| 288.2 | 52.8 | 52.8 | 0.1 |
| 293.2 | 78.5 | 77.2 | 1.8 |
| 326.4 | 653.3 | 677.3 | - 3.8 |
| 330.2 | 799.9 | 840.3 | - 4.8 |
| 332.4 | 933.3 | 949.5 | - 1.7 |
| 335.2 | 1067 | 1112 | - 4.1 |
| 337.6 | 1200 | 1265 | - 5.1 |
| 339.2 | 1387 | 1376 | 1.0 |
| 345.8 | 1973 | 1921 | 2.7 |
| 356.8 | 3346 | 3271 | 2.3 |
| 376.8 | 7999 | 7880 | 1.5 |
| 389.8 | 13 350 | 13 160 | 1.4 |
| 402.0 | 21 280 | 20 580 | 3.4 |
| 421.8 | 39 930 | 39 920 | 0.0 |
| 454.4 | 102 200 | 102 800 | - 0.6 |

[a] Percent difference was calculated as $100(P_{meas} - P_{calcd})/P_{calcd}$.

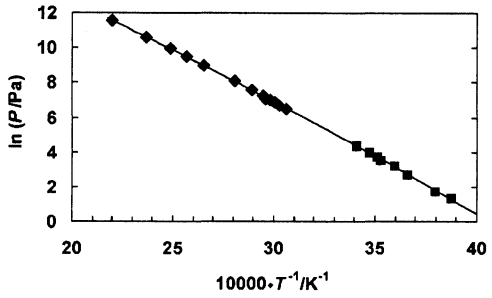


**Figure 3.** DMMP vapor pressure: [ , data generated by DSC methodology; 9, data generated by saturator methodology; s , Antoine correlation equation.

**Table 4. Calculated Vapor Pressure, Volatility, and Enthalpy of Vaporization for DMMP Based on Antoine Coefficients Listed in Table 9**

| $T$ / K | $P$ / Pa | volatility / mg·m$^{-3}$ | $\Delta_{vap}H$ / kJ·mol$^{-1}$ |
|---|---|---|---|
| 263.2 | 6.025 | 341.8 | 55.9 |
| 273.2 | 15.22 | 831.8 | 54.9 |
| 283.2 | 35.49 | 1871 | 54.0 |
| 293.2 | 77.15 | 3928 | 53.2 |
| 298.2 | 111.1 | 5562 | 52.8 |
| 303.2 | 157.7 | 7763 | 52.4 |
| 313.2 | 305.1 | 14 540 | 51.8 |
| 333.2 | 992.2 | 44 450 | 50.6 |
| 353.2 | 2760 | 116 600 | 49.5 |
| 373.2 | 6758 | 270 300 | 48.6 |
| 393.2 | 14 900 | 565 700 | 47.8 |
| 413.2 | 30 100 | 1 088 000 | 47.1 |
| 433.2 | 56 490 | 1 947 000 | 46.5 |
| 453.8 | 101 325 | 3 333 000 | 46.0 |

Figure 72: Measured and calculated vapor pressures for DMMP [124]

## 5.4 EXPERIMENT: COMPOSITE DMMP SENSOR

Early stage experiments were carried out using a sealed 2-liter glass vessel with air at ambient conditions. Small droplets of DMMP were placed at the bottom of the vessel to simulate various ppm conditions. The composites were placed on a four-point probe (Cascade C4S), sealed in the glass vessel and instrumented with a multimeter (Agilent 34410A). The vessel was then put on a hot plate to evaporate the analyte. Temperature near the sample and the hot plate were monitored using thermocouples.

High weight percentage composites of both SWNT (HiPco, Rice University) and MWNT (Mitsui) in medium density polyethylene (MDPE) were tested. The SWNT nanotubes were purified via a simple 1-pot method [50]. The MWNT were received in a highly pure state. Composite preparation was as described in Chapter 4. Percent loadings of 90% SWNT were utilized for these tests as they produce the lowest electrical resistivity (Chapter 4).

Data from these experiments show great promise. Figure 75 shows the results of 1000ppm DMMP exposure on the MWNT composites. Upon introduction of DMMP vapor into the air inside the vessel, the composites showed an increase in resistivity of almost 30% within minutes, and a recovery response time of 5-15 minutes. It should be noted that the atmosphere inside the vessel is static, an optimal testing regime would include active mixing of the analyte and controlled flow as previously

described. With that in consideration, these results here may actually be conservative.

The first of two possible sources of error was then considered for this experimental setup; radiative heating. Tests were performed that showed negligible effect from radiative heating on either the MWNT or SWNT samples, shown as "no DMMP" for both data sets. A resistance change 2% can be attributed to radiative heating for the MWNT samples and 1% for the SWNT samples.

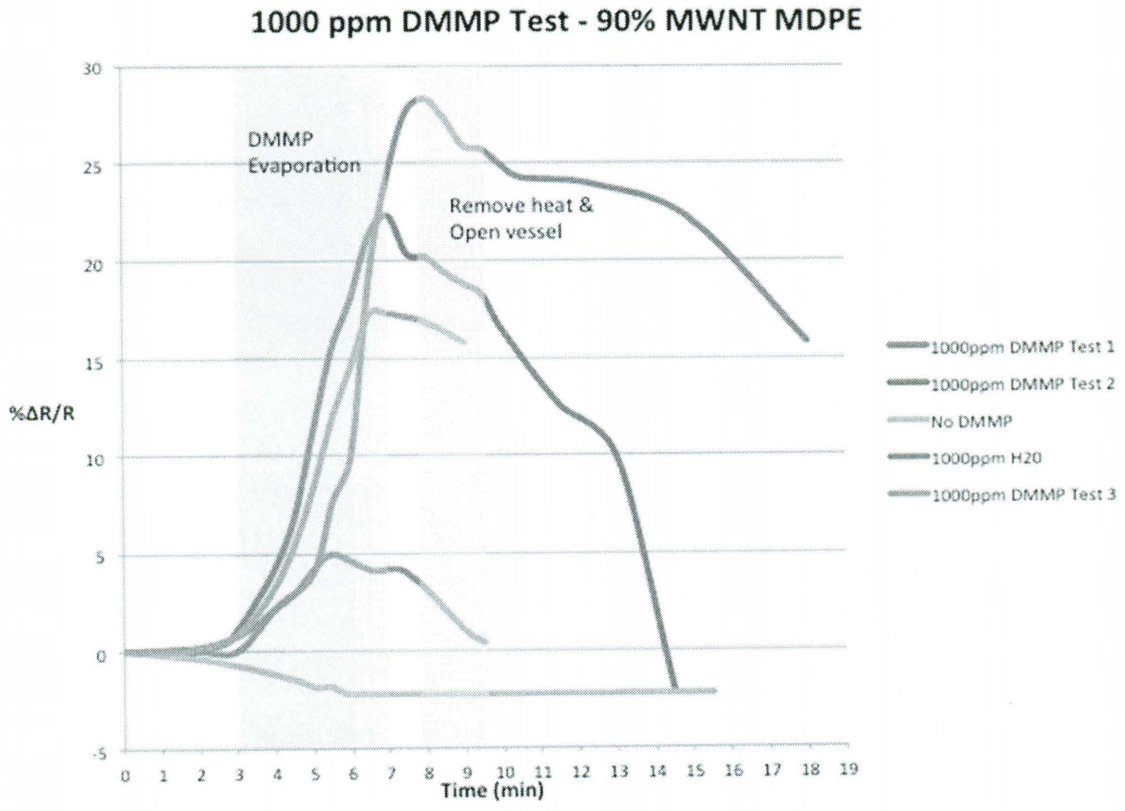


Figure 75: DMMP sensing tests with MWNT MDPE composites

The SWNT tests also showed interesting performance under the exposure to DMMP. 1000ppm testing had response times in minutes and a positive resistance change. The SWNT composite showed a higher sensitivity to both convective heating and water vapor than the MWNT. Figure 76 highlights this sensitivity. It should be noted that while opening the vessel and exposing the composites to fresh air contributed to signal recovery, the thermocouples showed that the heating effect on the samples and 4-point probe was slower to abate. This lead the author to believe that it is the presence of vapor that is causing the initial change in resistance, rather than any thermal effect.

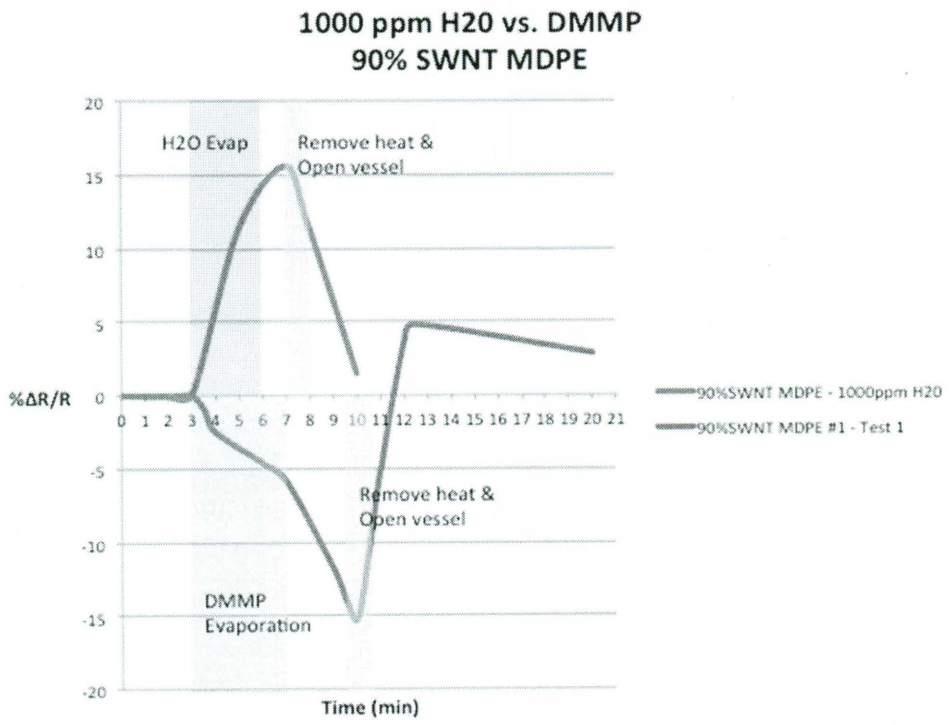


Figure 8: Water vs. DMMP.

Surface area and porosity analysis through BET was performed on the SWNT composites. Composites exposed to boiling dichlorobenzene, to increase porosity and surface area, showed no large surface area change. The surface area of these composites remains at 100-200$m^2g^{-1}$ and has no marked difference in DMMP sensitivity.

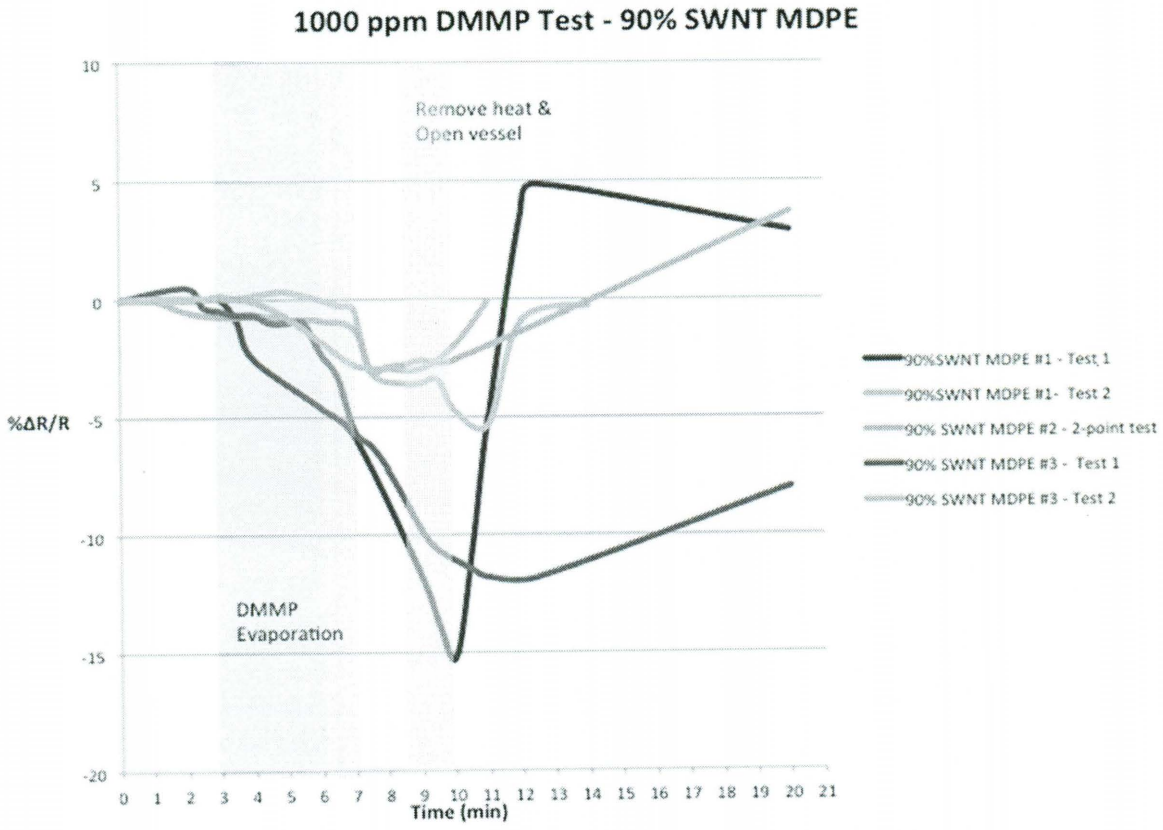


Figure 76: DMMP sensing tests with SWNT MDPE composites

Additional experiments were performed on the SWNT composites to explore the lower bounds of DMMP sensitivity. Given both the aforementioned simplicity and weaknesses of this initial experimental protocol, these data should be considered conservative. The 10 and 100ppm tests in Figure 77 show a positive change in resistivity. At these lower ppm, one can see that radiative and convective heating effects associated with this test, while ineffectual at 1000ppm, are now dominant and mask the sensing of the DMMP itself. Only at 500ppm does the DMMP sensing become dominant. Figure 78 explores this further by carrying out isolated water versus DMMP tests.

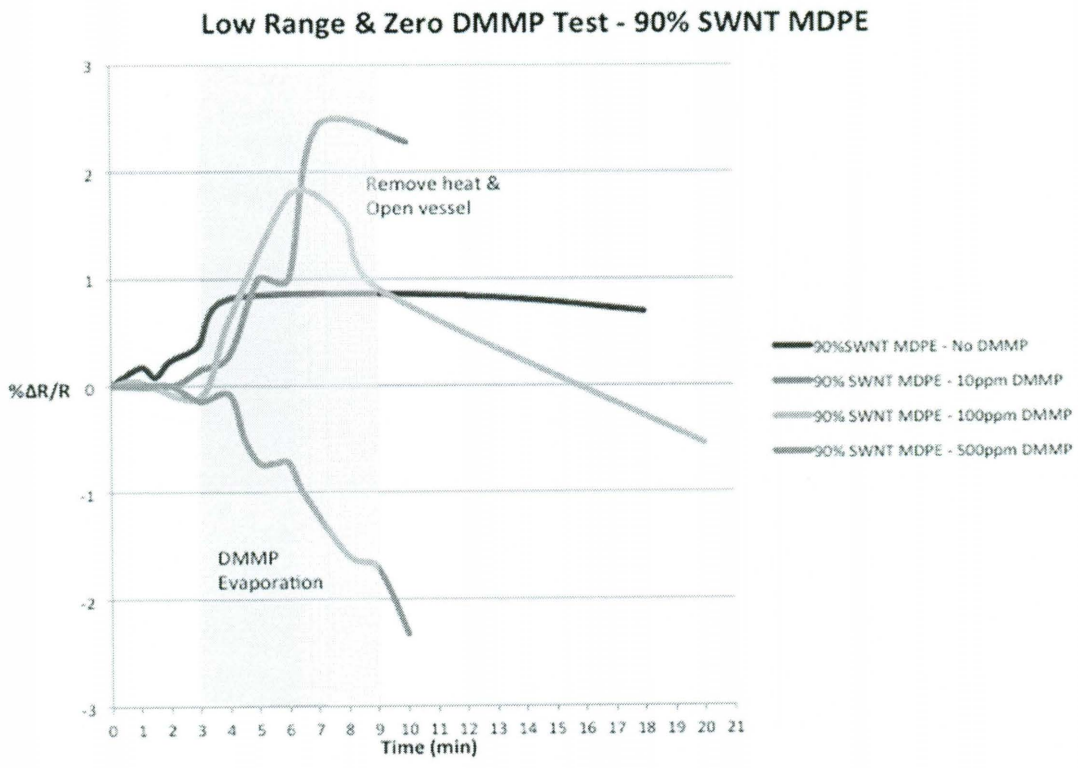


Figure 77: Low ppm exposure tests SWNT MDPE composite to DMMP

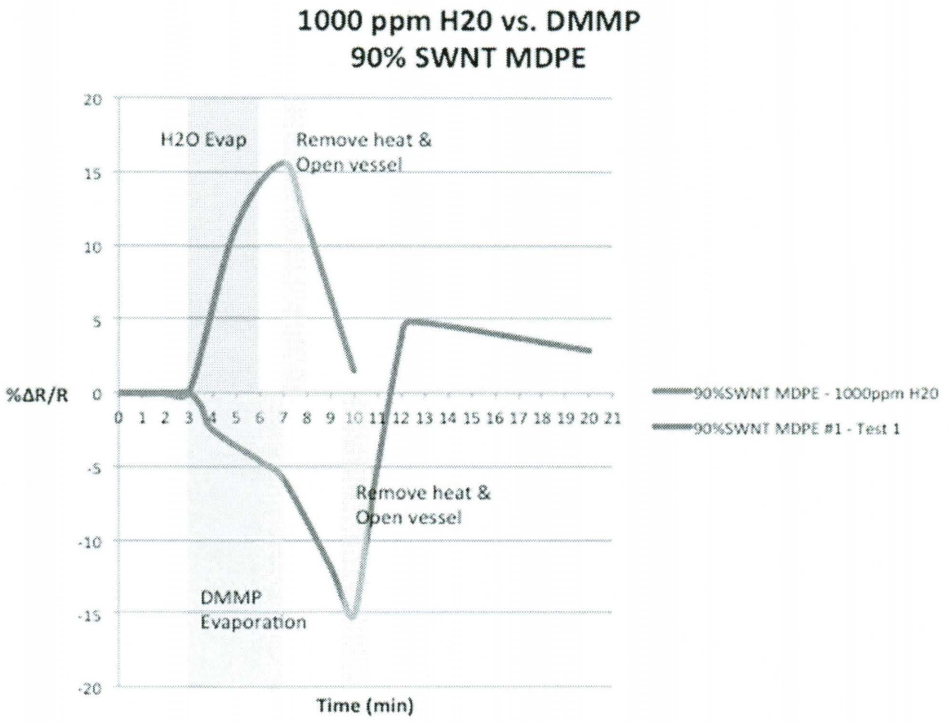


Figure 78: SWNT MDPE Composite sensitivity: Water vs. DMMP

## 5.5 DISCUSSION

The most interesting point that came from the data presented was not that the composites were sensitive to DMMP, but that the two different types of CNT changed resistivity with different sign.

It has been shown that when using CNT FETs comprised of different metals as electrodes, DMMP molecules influence the metal work function in a specific way despite metals such as Pd and Au having the same starting work function [126]. As mentioned, Snow et al. provided an experimental result showing a negative shift in voltage and an explanation of DMMP interaction with SWNT as a result of an electron transfer from DMMP to SWNT ("gas electron-donating behavior") [119]. What was also of note from this research was the question of whether the change was due to interaction between the DMMP and the SWNT-metal junctions or between the DMMP and the SWNT material itself. Given that the contact resistance between dissimilar SWNT (metallic and semiconducting) is higher than similar tube types [127,128], it has been proposed that the metal work function change at the contacts between the electrode metal and SWNT is dominant in influencing sensing [108,122]. Perhaps this begins to explain the performance of the SWNT versus the MWNT. In addition, there has been a previously observed correlation between sensor response and solvent polarity (ET30) for more common organic vapors that does not work for DIMP or DMMP [114]. Cattannach et al. proposed that DMMP could "preferentially

adsorb at sites whose microenvironment significantly affects electron transport through the SWNT film"[114].

Gohier et al. proposed in a study involving MWNT, that the response was dependent on the semiconducting behavior of the MWNT, and stated that the sign can be modified by n-doping using PEI as doping agent [98]. Aside from the effect of the semiconducting behavior, they demonstrated the crystallinity of the MWNTs plays a key role in the sensitivity of CNT-based sensors. While the ideas presented here do not provide a conclusive thesis on why the two CNT types performed in such different manner, the author proposes that the effects and attributes discussed are a starting point for further research

# CHAPTER 6: CONCLUSIONS & FUTURE DIRECTIONS

A real-world, engineering-scale challenge of producing a polymer composite, suitable as a replacement for copper in aerospace and energy exploration, was the central driver of this research. To that end, science on the nanoscale, which included material properties of polyethylene and examination of fundamental nanotube properties such as diameter and chirality of a suite of CNT types, was combined with materials engineering which studied, designed and optimized fabrication techniques to create low resistivity polyethylene and CNT composites.

The purity, chirality and diameters of a broad range of CNT types were evaluated. A purification process, relevant for industrial use, was matured and scaled-up. The resistivity of various CNT types was measured at both macro and micro scales. It was seen that the macro scale data in general matched the micro scale, despite the large differences in network size. It was shown that these resistivities on the whole reflected the chirality or metallic tube content of the CNT. It was shown that smaller diameters, in addition to surface coatings or damage to the tube sidewalls, have an adverse effect on conductivity, even if respectable amounts of metallic CNT are present.

A scalable and optimized composite fabrication method was developed. The presence of a sonopolymer, formed via sonication of solvent, was confirmed and

assisted in the dispersion of CNT in the polymer matrix. Crystallinity, CNT bundle size and composite morphology were observed. It was found that chirality or metallic CNT content was dominant. The initial idea that relatively high amounts of crystalline polymer, or at least many transitions between amorphous and crystalline zones, would aid in producing a low electrical resistivity composite was proven premature. Composites which flowed well under annealing and pressure treatments , which had relatively low amounts of crystallinity, were shown to be more useful.

Resistivities impressive for nanotube polymer nanocomposites in general, let alone nanotube polyethylene composites, were achieved with a lowest value in the $10^{-4}$ $\Omega \bullet cm$ (Figure 79). This result far outperforms data found for similar thermoplastic composites in the literature. Weight percent loadings of CNT in MDPE were achieved to a level not seen before in the literature. Annealing and pressure treatments were used to reduce bulk resistivities further. Additional optimization of annealing and pressure procedures warrant future research. Continued improvement in nanotube supply should be monitored and integrated into future research, in particular the production of higher metallic content CNT. The as-received conditions of the CNT used in this research were far from perfect. Additional purification and functionalization processes, also of a scalable nature, should be pursued. Selective functionalization was considered by the author early in the research, but not pursued as proven methods in the field have yields mostly in the microgram range. Although relationships suggested in the literature between both nanoscale and bulk aspects and resultant resistivity were explored and some

proven, such as crystallinity, bundle size and chirality, a clear dominant dependency on nanotube type and source was found.

The results in this thesis show *some* validity of the concept originally proposed for both the RPSEA and ATP programs. The supply of highly metallic nanotube stock was considered a dependency in these efforts, and considering the result showing polyethylene actually *reducing* the resistivity numbers of bulk CNT at high loadings in composites, using such metallic CNT with resistive polymers may offer surprising results. It is doubtful however, even with purely metallic CNT, that one could achieve the nanotube *densities* and *alignment* necessary in a composite with a polymer to produce the conductivities to match copper. The composites produced by this research have a unique mix of low resistivities and are malleable, flexible and formable. These materials have the potential to be of great use towards applications such as EMI/ESD shielding and abatement.

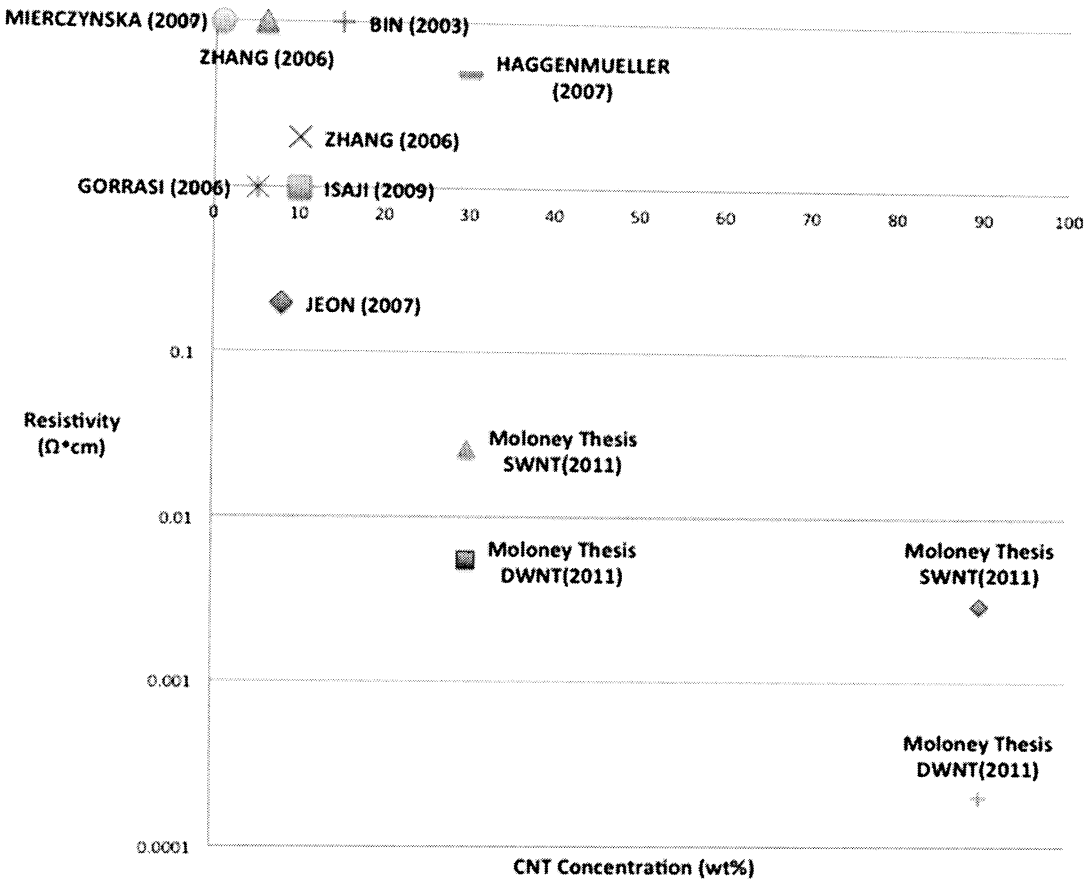


Figure 79: Low resistivity values of SWNT and DWNT composites compared with the best found in the literature

The author attempted some research in alignment, but availability of equipment to generate very strong AC fields (the most suitable for the task) that could be used in a chemical hood environment proved difficult. In early 2009, in collaboration with Dr. Ajayan, the author grew SWNT and DWNT in a CVD reactor to develop a second, alternative approach to CNT MDPE composites. Using fibers pulled or drawn from the produced material, it was thought that highly aligned nanotube cables could be produced. The resultant materials had relatively high resistivity, while availability of

the reactor was scarce. However, the concept was validated and proven with the use of DWNT from China by Dr. Yao Zhao of the Barrera Group [97].

In addition to annealing and pressure, a novel doping method was developed to decrease the resistivity of bulk CNT further using $SbF_5$. While its products proved unsuitable for use in solvent-blended composites, it reduced the resistivity of purified HiPco SWNT by over an order of magnitude to $10^{-3}$ Ω•cm.

The most obvious improvement for future work in this doping method would be the availability of a more robust nitrogen atmosphere glove box. The heated vacuum preparation of the SWNT was adequate, but using an actual vacuum furnace would be beneficial. Experimenting with additional types of CNT will also be useful. DWNT may provide a more robust nanotube surface as STEM and TEM analysis of the SWeNT CG 100 nanotubes show a rough surface morphology of carbon.

Future doping work may include exposure to moist air for further exploration of resistance to hydrolysis. Lalancette et al. also investigated the suitability of their graphite $SbF_5$ as an agent for the exchange of halogens with organic chlorides with a view to producing a stable and useful fluorinating agent [95]. This is perhaps a worthy target application for the SWNT $SbF_5$. With regards to characterization, perhaps further XPS work is warranted, in conjunction with a standards authority such as NIST, in order to produce a reliable standard for $SbF_5$.

As its purpose was to reduce the resistivity of CNT polymer composites, the use of microwave processing produced only a tangential success in this thesis. It showed however great promise, especially with thermoset and extruded composites. There remains a dearth of research on how microwaves interact with CNT. Size and antenna effects were noted in this research, and warrant further attention. High intensity thermal effects in the immediate vicinity of the CNT due to microwaves may have combinatorial effects with additional species introduced into the composite such as metals. Use of microwave heating techniques were put forward for patent consideration as central to repair mechanisms for complex carbon fiber composite structures, in addition to large civil structures such as bridges and roadways.

A novel composite gas sensor for sensing a nerve gas simulant was presented. This research has been put forward for additional funding. This early stage work created a possible binary composite approach to sensing, using two variants of CNT composites that could easily be integrated as a wing material for a micro air vehicle. It warrants an improved test setup, and the author has proposed one based on a gas permutation tube system. Modification of either the polymer layer and/or functionalization should be explored as a means to improve selectivity and sensitivity. Further research and optimization of pore size would also be valuable.

# BIBLIOGRAPHY


1 NanoridgeMaterialsInc. Final Report; Ultra-High Conductivity Umbilicals: A Paradigm Change in Conductors Using Carbon Nanotubes. (2010).

2 Ma, J., Tang, J., Zhang, H., Shinya, N. & Qin, L. C. Ultrathin Carbon Nanotube Fibrils of High Electrochemical Capacitance. *Acs Nano* **3**, 3679-3683 (2009).

3 Jorio, A., Dresselhaus, G. & Dresselhaus, M. S. *Carbon nanotubes: advanced topics in the synthesis, structure, properties and applications*. Vol. 111 (Springer Verlag, 2008).

4 NIST. NanoCable Project. (2011).

5 Sigma-Aldrich. *Polyethylene Medium Density - Sigma-Aldrich.com*, <http://www.sigmaaldrich.com/catalog/ProductDetail.do?lang=en&N4=332119%7CALDRICH&N5=SEARCH_CONCAT_PNO%7CBRAND_KEY&F=SPEC> (2011).

6 Barrera, E. NanoCable Project. *National Institute of Standards and Technology (NIST), Advanced Technology Program (ATP)* (2007).

7 Peacock, A. J. *Handbook of polyethylene: structures, properties, and applications*. Vol. 57 (CRC, 2000).

8 Yahagi, K. Dielectric properties and morphology in polyethylene. *Electrical Insulation, IEEE Transactions on*, 241-250 (1980).

9 Tanaka, Y., Ohnuma, N., Katsunami, K. & Ohki, Y. Effects of crystallinity and electron mean-free-path on dielectric strength of low-density polyethylene. *Electrical Insulation, IEEE Transactions on* **26**, 258-265 (1991).

10 Kitchin, D. & Pratt, O. Treeing in Polyethylene as a Prelude to Breakdown. *Power Apparatus and Systems, Part III. Transactions of the American Institute of Electrical Engineers* **77**, 180-185 (1958).

11 Mackenzie, B., Singh, N. & Lever, R. Influence of Inorganic Fillers on the Voltage Endurance of Solid Dielectric Power Cables. *Power Apparatus and Systems, IEEE Transactions on*, 1169-1173 (1973).

12 Fothergill, J. C. 1-10 (IEEE).

13 Frechette, M. & Reed, C. 458-465 (IEEE).

14 Stauffer, D. & Aharony, A. *Introduction to percolation theory*. (CRC, 1994).

15 Kirkpatrick, S. Percolation and Conduction. *Reviews of Modern Physics* **45**, 574 (1973).

16 Ambrosetti, G. *et al.* Solution of the tunneling-percolation problem in the nanocomposite regime. *Phys Rev B* **81**, 155434 (2010).

17 Li, C. Dominant role of tunneling resistance in the electrical conductivity of carbon nanotube?based composites. *Appl. Phys. Lett.* **91**, 223114 (2007).

18 Vionnet-Menot, S., Grimaldi, C., Maeder, T., Str√ § ssler, S. & Ryser, P. Tunneling-percolation origin of nonuniversality:,ÄÉTheory and experiments. *Phys Rev B* **71**, 064201 (2005).

19 Bauhofer, W. & Kovacs, J. Z. A review and analysis of electrical percolation in carbon nanotube polymer composites. *Compos Sci Technol* **69**, 1486-1498, doi:Doi 10.1016/J.Compscitech.2008.06.018 (2009).

20 Balberg, I. Tunnelling and percolation in lattices and the continuum. *Journal of Physics D: Applied Physics* **42**, 064003 (2009).

21 Higginbotham, A. L. *et al.* Carbon nanotube composite curing through absorption of microwave radiation. *Compos Sci Technol* **68**, 3087-3092, doi:10.1016/j.compscitech.2008.07.004 (2008).

22 Moloney, P. *et al.* Advanced life support for space exploration: Air revitalization using amine coated single wall carbon nanotubes. *Mater. Res. Soc. Symp. Proc.* **851** (2005).

23 AREPALLI, S. *et al.* 389.

24 Nikolaev, P. *et al.* Gas-phase catalytic growth of single-walled carbon nanotubes from carbon monoxide. *Chem Phys Lett* **313**, 91-97 (1999).

25 Iijima, S. Helical Microtubules of Graphitic Carbon. *Nature* **354**, 56-58 (1991).

26 Guo, T., Nikolaev, P., Thess, A., Colbert, D. & Smalley, R. Catalytic growth of single-walled manotubes by laser vaporization. *Chem Phys Lett* **243**, 49-54 (1995).

27 Stadermann, M. *et al.* Nanoscale study of conduction through carbon nanotube networks. *Phys. Rev. B* **69**, 201402, doi:10.1103/PhysRevB.69.201402 (2004).

28 Li, C., Thostenson, E. T. & Chou, T.-W. Dominant role of tunneling resistance in the electrical conductivity of carbon nanotube-based composites. *Appl. Phys. Lett.* **91**, 223114, doi:10.1063/1.2819690 (2007).

29 Nirmalraj, P. N., Lyons, P. E., De, S., Coleman, J. N. & Boland, J. J. Electrical connectivity in single-walled carbon nanotube networks. *Nano Lett* **9**, 3890-3895 (2009).

30 White, C. & Todorov, T. Carbon nanotubes as long ballistic conductors. *Nature* **393**, 240-242 (1998).

31 Wei, B., Vajtai, R. & Ajayan, P. Reliability and current carrying capacity of carbon nanotubes. *Appl Phys Lett* **79**, 1172 (2001).

32 Kebes. *Wikipedia* (2011).

33 Skakalova, V., Dettlaff-Weglikowska, U. & Roth, S. Electrical and mechanical properties of nanocomposites of single wall carbon nanotubes with PMMA. *Synthetic Metals* **152**, 349-352, doi:10.1016/j.synthmet.2005.07.291 (2005).

34 Blanchet, G., Fincher, C. & Gao, F. Polyaniline nanotube composites: A high-resolution printable conductor. *Appl. Phys. Lett.* **82**, 1290-1292, doi:10.1063/1.1553991 (2003).

35 Koerner, H. *et al.* Deformation-morphology correlations in electrically conductive carbon nanotube--thermoplastic polyurethane nanocomposites. *Polymer* **46**, 4405-4420 (2005).

36 Bin, Y., Kitanaka, M., Zhu, D. & Matsuo, M. Development of highly oriented polyethylene filled with aligned carbon nanotubes by gelation/crystallization from solutions. *Macromolecules* **36**, 6213-6219 (2003).

37 Xi, Y., Yamanaka, A., Bin, Y. & Matsuo, M. Electrical properties of segreated ultrahigh molecular weight polyethylene/multiwalled carbon nanotube composites. *J Appl Polym Sci* **105**, 2868-2876, doi:10.1002/app.26282 (2007).

38 Zhao, D., Lei, Q., Qin, C. & Bai, X. Melt process and performance of multi-walled carbon nanotubes reinforced LDPE composites. *Pigment & resin technology* **35**, 341-345 (2006).

39 Haggenmueller, R., Fischer, J. E. & Winey, K. I. Single Wall Carbon Nanotube/Polyethylene Nanocomposites: Nucleating and Templating Polyethylene Crystallites. *Macromolecules* **39**, 2964-2971, doi:10.1021/ma0527698 (2006).

40 Haggenmueller, R., Guthy, C., Lukes, J. R., Fischer, J. E. & Winey, K. I. Single wall carbon nanotube/polyethylene nanocomposites: Thermal and electrical conductivity. *Macromolecules* **40**, 2417-2421, doi:10.1021/ma0615046 (2007).

41 Jeon, K. *et al.* Low electrical conductivity threshold and crystalline morphology of single-walled carbon nanotubes-high density polyethylene nanocomposites characterized by SEM, Raman spectroscopy and AFM. *Polymer* **48**, 4751-4764 (2007).

42 McNally, T. *et al.* Polyethylene multiwalled carbon nanotube composites. *Polymer* **46**, 8222-8232 (2005).

43 Lisunova, M., Mamunya, Y. P., Lebovka, N. & Melezhyk, A. Percolation behaviour of ultrahigh molecular weight polyethylene/multi-walled carbon nanotubes composites. *European Polymer Journal* **43**, 949-958 (2007).

44 Gorrasi, G. *et al.* Incorporation of carbon nanotubes into polyethylene by high energy ball milling: Morphology and physical properties. *Journal of Polymer Science Part B: Polymer Physics* **45**, 597-606 (2007).

45 Mierczynska, A., Mayne L'Hermite, M., Boiteux, G. & Jeszka, J. Electrical and mechanical properties of carbon nanotube/ultrahigh molecular weight polyethylene composites prepared by a filler prelocalization method. *Journal of Applied Polymer Science* **105**, 158-168 (2007).

46 Zhang, Q., Lippits, D. R. & Rastogi, S. Dispersion and rheological aspects of SWNTs in ultrahigh molecular weight polyethylene. *Macromolecules* **39**, 658-666 (2006).

47 Arepalli, S. *et al.* Protocol for the characterization of single-wall carbon nanotube material quality. *Carbon* **42**, 1783-1791 (2004).

48 Chiang, I. *et al.* Purification and characterization of single-wall carbon nanotubes (SWNTs) obtained from the gas-phase decomposition of CO (HiPco process). *The Journal of Physical Chemistry B* **105**, 8297-8301 (2001).

49 Nikolaev, P. *et al.* Soft-bake purification of single-walled carbon nanotubes produced by pulsed laser vaporization. *The Journal of Physical Chemistry C* **111**, 17678-17683 (2007).

50 Wang, Y. H., Shan, H. W., Hauge, R. H., Pasquali, M. & Smalley, R. E. A highly selective, one-pot purification method for single-walled carbon nanotubes. *J Phys Chem B* **111**, 1249-1252, doi:10.1021/jp068229+ (2007).

51 Miyata, Y., Maniwa, Y. & Kataura, H. Selective oxidation of semiconducting single-wall carbon nanotubes by hydrogen peroxide. *The Journal of Physical Chemistry B* **110**, 25-29 (2006).

52 Shaffer, M., Fan, X. & Windle, A. Dispersion and packing of carbon nanotubes. *Carbon* **36**, 1603-1612 (1998).

53 Whitby, R. L. D., Fukuda, T., Maekawa, T., James, S. L. & Mikhalovsky, S. V. Geometric control and tuneable pore size distribution of buckypaper and buckydiscs. *Carbon* **46**, 949-956 (2008).

54 Dresselhaus, M., Dresselhaus, G., Jorio, A., Souza, A. & Saito, R. Raman spectroscopy on isolated single wall carbon nanotubes. *Carbon* **40**, 2043-2061 (2002).

55 Rao, A., Eklund, P., Bandow, S., Thess, A. & Smalley, R. Evidence for charge transfer in doped carbon nanotube bundles from Raman scattering. *Nature* **388**, 257-259 (1997).

56 Strano, M. S. *et al.* Assignment of (n, m) Raman and optical features of metallic single-walled carbon nanotubes. *Nano Lett* **3**, 1091-1096 (2003).

57 O'connell, M. J. *et al.* Band gap fluorescence from individual single-walled carbon nanotubes. *Science* **297**, 593 (2002).

58 Bachilo, S. M. *et al.* Structure-assigned optical spectra of single-walled carbon nanotubes. *Science* **298**, 2361 (2002).

59 Rocha, J. D. R., Bachilo, S. M., Ghosh, S., Arepalli, S. & Weisman, R. B. Efficient Spectrofluorimetric Analysis of Single-Walled Carbon Nanotube Samples. *Analytical chemistry* (2011).

60 Naumov, A. V. *et al.* Quantifying the semiconducting fraction in single-walled carbon nanotube samples through comparative atomic force and photoluminescence microscopies. *Nano Lett* **9**, 3203-3208 (2009).

61 FourPointProbes. Four Point Probe Equations. (2011).

62 Valdes, L. Resistivity measurements on germanium for transistors. *Proceedings of the IRE* **42**, 420-427 (1954).

63 Li, J. *et al.* Carbon Nanotube Sensors for Gas and Organic Vapor Detection. *Nano Lett* **3**, 929-933, doi:10.1021/nl034220x (2003).

64 Boul, P. J. *et al.* Single Wall Carbon Nanotube Response to Proton Radiation. *The Journal of Physical Chemistry C* **113**, 14467-14473 (2009).

65 EBBESEN, T. *et al.* Electrical conductivity of individual carbon nanotubes. *Nature* **382**, 54-56 (1996).

66 Bahr, J. L., Mickelson, E. T., Bronikowski, M. J., Smalley, R. E. & Tour, J. M. Dissolution of small diameter single-wall carbon nanotubes in organic solvents? *Chem. Commun.*, 193-194 (2001).

67 Du, F., Fischer, J. E. & Winey, K. I. A coagulation method to prepare single-walled carbon nanotube/pmma composites and their modulus, electrical conductivity, and thermal stability. (2003).

68 Chakravarthi, D. K. *Carbon Nanotubes Filled Polymer Composites: A Comprehensive Study on Improving Dispersion, Network Formation and Electrical Conductivity*, RICE UNIVERSITY, (2010).

69 Perkins, J. P. Sonochemistry: the use of ultrasound in chemistry : an interdivisional symposium *Royal Society of Chemistry annual chemical congress* (1986).

70 Shelimov, K. B., Esenaliev, R. O., Rinzler, A. G., Huffman, C. B. & Smalley, R. E. Purification of single-wall carbon nanotubes by ultrasonically assisted filtration. *Chem Phys Lett* **282**, 429-434 (1998).

71 Hecht, D., Hu, L. & Gruner, G. Conductivity scaling with bundle length and diameter in single walled carbon nanotube networks. *Appl. Phys. Lett.* **89**, 133112, doi:10.1063/1.2356999 (2006).

72 Hennrich, F. *et al.* The mechanism of cavitation-induced scission of single-walled carbon nanotubes. *The Journal of Physical Chemistry B* **111**, 1932-1937 (2007).

73 Lucas, A. *et al.* Kinetics of nanotube and microfiber scission under sonication. *The Journal of Physical Chemistry C* **113**, 20599-20605 (2009).

74 Trankner, T., Hedenqvist, M. & Gedde, U. Molecular and lamellar structure of an extrusion-grade medium density polyethylene for gas distribution. *Polymer Engineering & Science* **34**, 1581-1588 (1994).

75 Sano, H., Usami, T. & Nakagawa, H. Lamellar morphologies of melt-crystallized polyethylene, isotactic polypropylene and ethylene-propylene copolymers by the RuO4 staining technique. *Polymer* **27**, 1497-1504 (1986).

76 Conde Brana, M., Sainz, J., Terselius, B. & Gedde, U. Morphology of binary blends of linear and branched polyethylene: transmission electron microscopy. *Polymer* **30**, 410-415 (1989).

77 Lobo, H. & Bonilla, J. V. *Handbook of plastics analysis*. Vol. 68 (Crc Press, 2003).

78 Forrest, M. J. *Analysis of plastics*. Vol. 13 (Smart Pubns, 2002).

79 Moloney, P. *et al.* PEM fuel cell electrodes using Single Wall Carbon Nanotubes. *Mater. Res. Soc. Symp. Proc.* **885** (2005).

80 Dykstra, M. J. & Reuss, L. E. *Biological electron microscopy: theory, techniques, and troubleshooting*. (Plenum Pub Corp, 2003).

81 Stuart, B. Polymer crystallinity studied using Raman spectroscopy. *Vibrational spectroscopy* **10**, 79-87 (1996).

82 Strobl, G. & Hagedorn, W. Raman spectroscopic method for determining the crystallinity of polyethylene. *Journal of Polymer Science: Polymer Physics Edition* **16**, 1181-1193 (1978).

83 Carroll, D., Czerw, R. & Webster, S. Polymer-nanotube composites for transparent, conducting thin films. *Synthetic Metals* **155**, 694-697, doi:10.1016/j.synthmet.2005.08.031 (2005).

84 Jeon, K. *et al.* Low electrical conductivity threshold and crystalline morphology of single-walled carbon nanotubes – high density polyethylene nanocomposites characterized by SEM, Raman spectroscopy and AFM. *Polymer* **48**, 4751-4764, doi:10.1016/j.polymer.2007.05.078 (2007).

85 Imholt, T. *et al.* Nanotubes in microwave fields: Light emission, intense heat, outgassing, and reconstruction. *Chem Mater* **15**, 3969-3970, doi:10.1021/cm034530g (2003).

86 Roberts, J. *et al.* Electromagnetic wave properties of polymer blends of single wall carbon nanotubes using a resonant microwave cavity as a probe. *Journal of Applied Physics* **95**, 4352-4356, doi:10.1063/1.1651339 (2004).

87 Inagaki, M. Applications of Graphite-Intercalation Compounds. *Journal of Materials Research* **4**, 1560-1568 (1989).

88 Vogel, F. L. Electrical-Conductivity of Graphite Intercalated with Superacid Fluorides - Experiments with Antimony Pentafluoride. *Journal of Materials Science* **12**, 982-986 (1977).

89 Vogel, F. L. Graphite Intercalation Compounds .5. Electrical-Conductivity of Graphite Intercalated with Sbf-5. *Bulletin of the American Physical Society* **21**, 262-262 (1976).

90 Vogel, F. L., Foley, G. M. T., Zeller, C., Falardeau, E. R. & Gan, J. High Electrical-Conductivity in Graphite Intercalated with Acid Fluorides. *Materials Science and Engineering* **31**, 261-265 (1977).

91 Matsubara, H., Yamaguchi, Y., Shioya, J. & Murakami, S. Preparation and Properties of Graphite Grown in Vapor-Phase. *Synthetic Metals* **18**, 503-507 (1987).

92 Shioya, J., Matsubara, H. & Murakami, S. Properties of Asf5-Intercalated Vapor-Grown Graphite. *Synthetic Metals* **14**, 113-123 (1986).

93 Enoki, T., Suzuki, M. & Endo, M. *Graphite intercalation compounds and applications.* (Oxford University Press, 2003).

94 Fischer, J. E. Chemical Doping of Single-Wall Carbon Nanotubes. *Accounts of Chemical Research* **35**, 1079-1086, doi:10.1021/ar0101638 (2002).

95 Lalancet.Jm & Lafontai.J. Intercalation of Antimony Pentafluoride in Lattice of Graphite. *Journal of the Chemical Society-Chemical Communications*, 815-815 (1973).

96 Kitiyanan, B., Alvarez, W. E., Harwell, J. H. & Resasco, D. E. Controlled production of single-wall carbon nanotubes by catalytic decomposition of CO on bimetallic Co-Mo catalysts. *Chemical Physics Letters* **317**, 497-503 (2000).

97 Zhao, Y., Wei, J., Vajtai, R., Ajayan, P. M. & Barrera, E. V. Iodine doped carbon nanotube cables exceeding specific electrical conductivity of metals. *Sci. Rep.* **1** (2011).

98 Gohier, A. *et al.* Optimized network of multi-walled carbon nanotubes for chemical sensing. *Nanotechnology* **22**, - (2011).

99 Zhang, T., Mubeen, S., Yoo, B., Myung, N. V. & Deshusses, M. A. A gas nanosensor unaffected by humidity. *Nanotechnology* **20**, - (2009).

100 Young, P., Lu, Y., Terrill, R. & Li, J. High-Sensitivity NO2 Detection with Carbon Nanotube-Gold Nanoparticle Composite Films. *Journal of nanoscience and nanotechnology* **5**, 1509-1513 (2005).

101 Moore, D. Instrumentation for trace detection of high explosives. *Review of Scientific Instruments* **75**, 2499 (2004).

102 Seto, Y. *et al.* Sensing technology for chemical-warfare agents and its evaluation using authentic agents. *Sensors and Actuators B: Chemical* **108**, 193-197, doi:10.1016/j.snb.2004.12.084 (2005).

103 Lange, U., Roznyatovskaya, N. V., Hao, Q. & Mirsky, V. M. in *Artificial Receptors for Chemical Sensors* 361-390 (Wiley-VCH Verlag GmbH & Co. KGaA, 2010).

104 Rajesh, Ahuja, T. & Kumar, D. Recent progress in the development of nano-structured conducting polymers/nanocomposites for sensor applications. *Sensors and Actuators B: Chemical* **136**, 275-286, doi:10.1016/j.snb.2008.09.014 (2009).

105 Mahar, B., Laslau, C., Yip, R. & Sun, Y. Development of carbon nanotube-based sensors - A review. *Ieee Sens J* **7**, 266-284, doi:Doi 10.1109/Jsen.2006.886863 (2007).

106 Wood, J. R. & Wagner, H. D. Single-wall carbon nanotubes as molecular pressure sensors. *Appl Phys Lett* **76**, 2883 (2000).

107 Wang, Y. & Yeow, T. A review of carbon nanotubes-based gas sensors. *Journal of Sensors* **2009** (2009).

108 Bondavalli, P. Carbon nanotubes based transistors composed of single-walled carbon nanotubes mats as gas sensors: A review. *Cr Phys* **11**, 389-396, doi:Doi 10.1016/J.Crhy.2010.06.002 (2010).

109 Yáñez-Sedeño, P., PingarrÛn, J. M., Riu, J. & Rius, F. X. Electrochemical sensing based on carbon nanotubes. *TrAC Trends in Analytical Chemistry* (2010).

110 RJacobs, C. B., Peairs, M. J. & Venton, B. J. Review: Carbon nanotube based electrochemical sensors for biomolecules. *Anal Chim Acta* **662**, 105-127, doi:10.1016/j.aca.2010.01.009 (2010).

111 Varghese, S. H. *et al.* Sensors Based On Carbon Nanotubes and Their Applications: A Review. *Curr Nanosci* **6**, 331-346 (2010).

112 Sinha, N., Ma, J. & Yeow, J. T. W. Carbon nanotube-based sensors. *Journal of nanoscience and nanotechnology* **6**, 573-590 (2006).

113 Kauffman, D. R. & Star, A. Carbon nanotube gas and vapor sensors. *Angew Chem Int Edit* **47**, 6550-6570, doi:Doi 10.1002/Anie.200704488 (2008).

114 Cattanach, K. & et al. Flexible carbon nanotube sensors for nerve agent simulants. *Nanotechnology* **17**, 4123 (2006).

115 Dwyer, A., Eldridge, J. & Kernan, M. *Jane's Chem-Bio Handbook.* (Janes Information Group, 2003).

116 Harris, C. M. Seeing SAW potential. *Analytical chemistry* **75**, 355A (2003).

117 Choi, N.-J. *et al.* Classification of chemical warfare agents using thick film gas sensor array. *Sensors and Actuators B: Chemical* **108**, 298-304, doi:10.1016/j.snb.2004.11.022 (2005).

118 Novak, J. *et al.* Nerve agent detection using networks of single-walled carbon nanotubes. *Appl Phys Lett* **83**, 4026-4028 (2003).

119 Snow, E., Perkins, F., Houser, E., Badescu, S. & Reinecke, T. Chemical detection with a single-walled carbon nanotube capacitor. *Science* **307**, 1942 (2005).

120 Wang, F., Gu, H. & Swager, T. M. Carbon Nanotube/Polythiophene Chemiresistive Sensors for Chemical Warfare Agents. *J Am Chem Soc* **130**, 5392-5393, doi:10.1021/ja710795k (2008).

121 Wang, Y. *et al.* Single-walled carbon nanotube/cobalt phthalocyanine derivative hybrid material: preparation, characterization and its gas sensing properties. *J. Mater. Chem.* (2011).
122 Parikh, K. *et al.* Flexible vapour sensors using single walled carbon nanotubes. *Sensors and Actuators B: Chemical* **113**, 55-63, doi:10.1016/j.snb.2005.02.021 (2006).
123 Aldrich, S. (2011).
124 Butrow, A. B., Buchanan, J. H. & Tevault, D. E. Vapor Pressure of Organophosphorus Nerve Agent Simulant Compounds. *Journal of Chemical & Engineering Data* **54**, 1876-1883 (2009).
125 Fan, C. L. & Wang, L. S. Vapor Pressure of Dimethyl Phosphite and Dimethyl Methylphosphonate. *Journal of Chemical & Engineering Data* **55**, 479-481 (2009).
126 Bondavalli, P., Legagneux, P. & Pribat, D. Carbon nanotubes based transistors as gas sensors: State of the art and critical review. *Sensor Actuat B-Chem* **140**, 304-318 (2009).
127 Gao, B., Chen, Y. F., Fuhrer, M. S., Glattli, D. C. & Bachtold, A. Four-Point Resistance of Individual Single-Wall Carbon Nanotubes. *Physical review letters* **95**, 196802 (2005).
128 McEuen, P. L. *et al.* in *Device Research Conference, 2001.* 107-110.
129 Robinson, J. A., Snow, E. S., BaÃåadescu, û. C., Reinecke, T. L. & Perkins, F. K. Role of Defects in Single-Walled Carbon Nanotube Chemical Sensors. *Nano Lett* **6**, 1747-1751, doi:10.1021/nl0612289 (2006).
130 Anand, A. *et al.* Select gas absorption in carbon nanotubes loading a resonant cavity to sense airborne toxin gases. *Nucl Instrum Meth B* **241**, 511-516, doi:Doi 10.1016/J.Nimb.2005.07.062 (2005).
131 Chung, J., Lee, K. H., Lee, J., Troya, D. & Schatz, G. C. Multi-walled carbon nanotubes experiencing electrical breakdown as gas sensors. *Nanotechnology* **15**, 1596 (2004).
132 Someya, T., Small, J., Kim, P., Nuckolls, C. & Yardley, J. T. Alcohol vapor sensors based on single-walled carbon nanotube field effect transistors. *Nano Lett* **3**, 877-881 (2003).
133 Kim, S. CNT sensors for detecting gases with low adsorption energy by ionization. *Sensors* **6**, 503-513 (2006).
134 Leghrib, R. *et al.* Room-temperature, selective detection of benzene at trace levels using plasma-treated metal-decorated multiwalled carbon nanotubes. *Carbon* **48**, 3477-3484, doi:10.1016/j.carbon.2010.05.045 (2010).
135 Cho, S. M., Kim, Y. J., Kim, Y. S., Yang, Y. & Ha, S. C. 701-704 vol. 702 (IEEE).
136 Mabrook, M. F., Pearson, C., Jombert, A. S., Zeze, D. A. & Petty, M. C. The morphology, electrical conductivity and vapour sensing ability of inkjet-printed thin films of single-wall carbon nanotubes. *Carbon* **47**, 752-757, doi:10.1016/j.carbon.2008.11.009 (2009).
137 Yang, C.-M., Kanoh, H., Kaneko, K., Yudasaka, M. & Iijima, S. Adsorption Behaviors of HiPco Single-Walled Carbon Nanotube Aggregates for Alcohol Vapors. *The Journal of Physical Chemistry B* **106**, 8994-8999, doi:10.1021/jp025767n (2002).

138 Santhanam, K. S. V., Sangoi, R. & Fuller, L. A chemical sensor for chloromethanes using a nanocomposite of multiwalled carbon nanotubes with poly(3-methylthiophene). *Sensors and Actuators B: Chemical* **106**, 766-771, doi:10.1016/j.snb.2004.09.034 (2005).

139 He, J. B., Chen, C. L. & Liu, J. H. Study of multi-wall carbon nanotubes self-assembled electrode and its application to the determination of carbon monoxide. *Sensors and Actuators B: Chemical* **99**, 1-5 (2004).

140 Wanna, Y. *et al.* The effect of carbon nanotube dispersion on CO gas sensing characteristics of polyaniline gas sensor. *Journal of nanoscience and nanotechnology* **6**, 3893-3896 (2006).

141 Santhosh, P., Manesh, K. M., Gopalan, A. & Lee, K.-P. Novel amperometric carbon monoxide sensor based on multi-wall carbon nanotubes grafted with polydiphenylamine--Fabrication and performance. *Sensors and Actuators B: Chemical* **125**, 92-99, doi:10.1016/j.snb.2007.01.044 (2007).

142 Wongwiriyapan, W. *et al.* Highly sensitive detection of carbon monoxide at room temperature using platinum-decorated single-walled carbon nanotubes. *Applied Physics Express* **1**, 14004 (2008).

143 Kauffman, D. R. *et al.* Understanding the Sensor Response of Metal-Decorated Carbon Nanotubes. *Nano Lett* **10**, 958-963 (2010).

144 Kuzmych, O., Allen, B. L. & Star, A. Carbon nanotube sensors for exhaled breath components. *Nanotechnology* **18**, 375502 (2007).

145 Ong, K. & Grimes, C. A Carbon Nanotube-based Sensor for CO2 Monitoring. *Sensors* **1**, 193-205 (2001).

146 Star, A., Han, T. R., Joshi, V., Gabriel, J. C. P. & Grüner, G. Nanoelectronic Carbon Dioxide Sensors. *Adv Mater* **16**, 2049-2052, doi:10.1002/adma.200400322 (2004).

147 Zribi, A., Knobloch, A. & Rao, R. CO detection using carbon nanotube networks and micromachined resonant transducers. *Appl Phys Lett* **86**, 203112 (2005).

148 Philip, B., Abraham, J. K., Chandrasekhar, A. & Varadan, V. K. Carbon nanotube/PMMA composite thin films for gas-sensing applications. *Smart Materials and Structures* **12**, 935 (2003).

149 Jose, K. A. & et al. A compact wireless gas sensor using a¬†carbon nanotube/PMMA thin film chemiresistor. *Smart Materials and Structures* **13**, 1045 (2004).

150 Wang, Y. *et al.* Flexible gas sensors with assembled carbon nanotube thin films for DMMP vapor detection. *Sensors and Actuators B: Chemical* (2010).

151 Hopkins, A. R. & Lewis, N. S. Detection and Classification Characteristics of Arrays of Carbon Black/Organic Polymer Composite Chemiresistive Vapor Detectors for the Nerve Agent Simulants Dimethylmethylphosphonate and Diisopropylmethylphosponate. *Analytical chemistry* **73**, 884-892, doi:10.1021/ac0008439 (2001).

152 Ali, S. R. *et al.* A nonoxidative sensor based on a self-doped polyaniline/carbon nanotube composite for sensitive and selective detection of the neurotransmitter dopamine. *Analytical chemistry* **79**, 2583-2587 (2007).

153 Delalande, M. *et al.* Chemical functionalization of electrodes for detection of gaseous nerve agents with carbon nanotube field-effect transistors. *Chem. Commun.* (2011).
154 Yujin, C. & et al. The enhanced ethanol sensing properties of multi-walled carbon nanotubes / SnO 2 core/shell nanostructures. *Nanotechnology* **17**, 3012 (2006).
155 Krishna Kumar, M., Leela Mohana Reddy, A. & Ramaprabhu, S. Exfoliated single-walled carbon nanotube-based hydrogen sensor. *Sensors and Actuators B: Chemical* **130**, 653-660 (2008).
156 Zilli, D., Bonelli, P. R. & Cukierman, A. L. Room temperature hydrogen gas sensor nanocomposite based on Pd-decorated multi-walled carbon nanotubes thin films. *Sensors and Actuators B: Chemical* **157**, 169-176, doi:10.1016/j.snb.2011.03.045 (2011).
157 Liu, C. *et al.* Hydrogen storage in single-walled carbon nanotubes at room temperature. *Science* **286**, 1127 (1999).
158 Gong, J., Sun, J. & Chen, Q. Micromachined sol-gel carbon nanotube/SnO2 nanocomposite hydrogen sensor. *Sensors and Actuators B: Chemical* **130**, 829-835 (2008).
159 Kong, J., Chapline, M. G. & Dai, H. Functionalized Carbon Nanotubes for Molecular Hydrogen Sensors. *Adv Mater* **13**, 1384-1386, doi:10.1002/1521-4095(200109)13:18<1384::aid-adma1384>3.0.co;2-8 (2001).
160 Sayago, I. *et al.* Hydrogen sensors based on carbon nanotubes thin films. *Synthetic metals* **148**, 15-19 (2005).
161 Sayago, I. *et al.* Novel selective sensors based on carbon nanotube films for hydrogen detection. *Sensors and Actuators B: Chemical* **122**, 75-80, doi:10.1016/j.snb.2006.05.005 (2007).
162 Srivastava, S. *et al.* Characterization of gas sensing behavior of multi walled carbon nanotube polyaniline composite films. *International Journal of Hydrogen Energy* **34**, 8444-8450, doi:10.1016/j.ijhydene.2009.08.017 (2009).
163 Wong, Y., Kang, W., Davidson, J., Wisitsora-At, A. & Soh, K. A novel microelectronic gas sensor utilizing carbon nanotubes for hydrogen gas detection. *Sensors and Actuators B: Chemical* **93**, 327-332 (2003).
164 Sippel-Oakley, J. *et al.* Carbon nanotube films for room temperature hydrogen sensing. *Nanotechnology* **16**, 2218 (2005).
165 Ahn, K. S., Kim, J. H., Lee, K. N., Kim, C. O. & Hong, J. P. Multi-wall carbon nanotubes as a high-efficiency gas sensor. *Journal of the Korean Physical Society* **45**, 158-161 (2004).
166 Star, A., Joshi, V., Skarupo, S., Thomas, D. & Gabriel, J. C. P. Gas sensor array based on metal-decorated carbon nanotubes. *The Journal of Physical Chemistry B* **110**, 21014-21020 (2006).
167 Staii, C. & Johnson, A. T. DNA-decorated carbon nanotubes for chemical sensing. *Nano Lett* **5**, 1774-1778, doi:Doi 10.1021/Nl051261f (2005).
168 Bekyarova, E. *et al.* Chemically Engineered Single Walled Carbon Nanotube Materials for the Electronic Detection of Hydrogen Chloride. *Adv Mater* **22**, 848-852 (2010).

169 Zahab, A. *et al.* Water-vapor effect on the electrical conductivity of a single-walled carbon nanotube mat. *Phys Rev B* **62**, 10000 (2000).
170 Kim, W. *et al.* Hysteresis caused by water molecules in carbon nanotube field-effect transistors. *Nano Lett* **3**, 193-198 (2003).
171 Star, A., Han, T.-R., Joshi, V. & Stetter, J. R. Sensing with Nafion Coated Carbon Nanotube Field-Effect Transistors. *Electroanalysis* **16**, 108-112, doi:10.1002/elan.200302925 (2004).
172 Chen, H.-W., Wu, R.-J., Chan, K.-H., Sun, Y.-L. & Su, P.-G. The application of CNT/Nafion composite material to low humidity sensing measurement. *Sensors and Actuators B: Chemical* **104**, 80-84, doi:10.1016/j.snb.2004.04.105 (2005).
173 Na, P. S. *et al.* Investigation of the humidity effect on the electrical properties of single-walled carbon nanotube transistors. *Appl Phys Lett* **87**, 093101 (2005).
174 Su, P.-G. & Huang, S.-C. Electrical and humidity sensing properties of carbon nanotubes-SiO2-poly(2-acrylamido-2-methylpropane sulfonate) composite material. *Sensors and Actuators B: Chemical* **113**, 142-149, doi:10.1016/j.snb.2005.02.040 (2006).
175 Yu, H. *et al.* Layer-by-Layer assembly and humidity sensitive behavior of poly(ethyleneimine)/multiwall carbon nanotube composite films. *Sensors and Actuators B: Chemical* **119**, 512-515, doi:10.1016/j.snb.2005.12.048 (2006).
176 Jiang, W. F., Xiao, S. H., Feng, C. Y., Li, H. Y. & Li, X. J. Resistive humidity sensitivity of arrayed multi-wall carbon nanotube nests grown on arrayed nanoporous silicon pillars. *Sensors and Actuators B: Chemical* **125**, 651-655, doi:10.1016/j.snb.2007.03.015 (2007).
177 Su, P.-G. & Wang, C.-S. In situ synthesized composite thin films of MWCNTs/PMMA doped with KOH as a resistive humidity sensor. *Sensors and Actuators B: Chemical* **124**, 303-308, doi:10.1016/j.snb.2006.12.034 (2007).
178 Tang, Q. Y., Chan, Y. C. & Zhang, K. Fast response resistive humidity sensitivity of polyimide/multiwall carbon nanotube composite films. *Sensors and Actuators, B: Chemical* **152**, 99-106 (2011).
179 Wang, J. & Musameh, M. Carbon Nanotube/Teflon Composite Electrochemical Sensors and Biosensors. *Analytical chemistry* **75**, 2075-2079, doi:10.1021/ac030007+ (2003).
180 Izadi, N., Rashidi, A. M., Golzardi, S., Talaei, Z. & Mahjoub, A. R. Hydrogen Sulfide sensing properties of Multi walled carbon nanotubes. *Ceramics International* **In Press, Accepted Manuscript**, doi:10.1016/j.ceramint.2011.06.038 (2011).
181 Fam, D. W. H. *et al.* Selective sensing of hydrogen sulphide using silver nanoparticle decorated carbon nanotubes. *Sensors and Actuators, B: Chemical* **138**, 189-192 (2009).
182 Valentini, L. *et al.* Sensors for inorganic vapor detection based on carbon nanotubes and poly(o-anisidine) nanocomposite material. *Chem Phys Lett* **383**, 617-622, doi:10.1016/j.cplett.2003.11.091 (2004).

183 Li, J., Lu, Y. J. & Meyyappan, M. Nano chemical sensors with polymer-coated carbon nanotubes. *Ieee Sens J* **6**, 1047-1051, doi:Doi 10.1109/Jsen.2006.881018 (2006).
184 Wang, R., Zhang, D., Zhang, Y. & Liu, C. Boron-Doped Carbon Nanotubes Serving as a Novel Chemical Sensor for Formaldehyde. *The Journal of Physical Chemistry B* **110**, 18267-18271, doi:10.1021/jp061766+ (2006).
185 Khani, H., Rofouei, M. K., Arab, P., Gupta, V. K. & Vafaei, Z. Multi-walled carbon nanotubes-ionic liquid-carbon paste electrode as a super selectivity sensor: Application to potentiometric monitoring of mercury ion(II). *Journal of Hazardous Materials* **183**, 402-409, doi:10.1016/j.jhazmat.2010.07.039 (2010).
186 Lee, M. *et al.* 100 nm scale low-noise sensors based on aligned carbon nanotube networks: overcoming the fundamental limitation of network-based sensors. *Nanotechnology* **21**, 055504 (2010).
187 Liu, Y.-L. *et al.* Gas sensing properties of tin dioxide coated onto multi-walled carbon nanotubes. *Thin Solid Films* **497**, 355-360, doi:10.1016/j.tsf.2005.11.018 (2006).
188 Bartlett, P. N., Archer, P. & Ling-Chung, S. K. Conducting polymer gas sensors part I: fabrication and characterization. *Sensors and Actuators* **19**, 125-140 (1989).
189 Chen, C. L. *et al.* DNA-decorated carbon-nanotube-based chemical sensors on complementary metal oxide semiconductor circuitry. *Nanotechnology* **21**, - (2010).
190 Valentini, L., Armentano, I., Lozzi, L., Santucci, S. & Kenny, J. M. Interaction of methane with carbon nanotube thin films: role of defects and oxygen adsorption. *Mat Sci Eng C-Bio S* **24**, 527-533, doi:Doi 10.1016/J.Msec.2004.01.003 (2004).
191 Arab, M., Picaud, F., Devel, M., Ramseyer, C. & Girardet, C. Molecular selectivity due to adsorption properties in nanotubes. *Phys Rev B* **69**, -, doi:Artn 165401
Doi 10.1103/Physrevb.69.165401 (2004).
192 Tooski, S. Functionalized single wall carbon nanotube sensor in a perturbed microwave resonant cavity based toxin/pollutant gas pressure sensor. *Journal of Applied Physics* **107**, 034315-034315-034319 (2010).
193 Bradley, K., Cumings, J., Star, A., Gabriel, J.-C. P. & Gr√°ner, G. Influence of Mobile Ions on Nanotube Based FET Devices. *Nano Lett* **3**, 639-641, doi:10.1021/nl025941j (2003).
194 Loh, Y. S. *et al.* Sensing mechanism of metal decorated single walled carbon nanotube field effect transistor sensors. *physica status solidi (b)* **246**, 2824-2827 (2009).
195 Huang, C., Huang, B., Jang, Y., Tsai, M. & Yeh, C. Three-terminal CNTs gas sensor for N2 detection. *Diam Relat Mater* **14**, 1872-1875 (2005).
196 Sumanasekera, G., Adu, C., Fang, S. & Eklund, P. Effects of gas adsorption and collisions on electrical transport in single-walled carbon nanotubes. *Physical review letters* **85**, 1096-1099 (2000).

197 Varghese, O. *et al.* Gas sensing characteristics of multi-wall carbon nanotubes. *Sensors and Actuators B: Chemical* **81**, 32-41 (2001).
198 Chopra, S., Pham, A., Gaillard, J., Parker, A. & Rao, A. Carbon-nanotube-based resonant-circuit sensor for ammonia. *Appl Phys Lett* **80**, 4632 (2002).
199 Bradley, K. *et al.* Charge Transfer from Ammonia Physisorbed on Nanotubes. *Physical review letters* **91**, 218301 (2003).
200 Bradley, K., Gabriel, J. C. P. & Gr¸ner, G. Flexible nanotube electronics. *Nano Lett* **3**, 1353-1355 (2003).
201 Modi, A., Koratkar, N., Lass, E., Wei, B. & Ajayan, P. M. Miniaturized gas ionization sensors using carbon nanotubes. *Nature* **424**, 171-174 (2003).
202 Suehiro, J., Zhou, G. & Hara, M. Fabrication of a carbon nanotube-based gas sensor using dielectrophoresis and its application for ammonia detection by impedance spectroscopy. *Journal of Physics D: Applied Physics* **36**, L109 (2003).
203 Bekyarova, E. *et al.* Chemically Functionalized Single-Walled Carbon Nanotubes as Ammonia Sensors,Ä†. *The Journal of Physical Chemistry B* **108**, 19717-19720, doi:10.1021/jp0471857 (2004).
204 Jang, Y. T., Moon, S. I., Ahn, J. H., Lee, Y. H. & Ju, B. K. A simple approach in fabricating chemical sensor using laterally grown multi-walled carbon nanotubes. *Sensors and Actuators B: Chemical* **99**, 118-122 (2004).
205 Lu, Y. J. *et al.* Room temperature methane detection using palladium loaded single-walled carbon nanotube sensors. *Chem Phys Lett* **391**, 344-348, doi:Doi 10.1016/J.Cplett.2004.05.029 (2004).
206 Wang, S., Zhang, Q., Yang, D., Sellin, P. & Zhong, G. Multi-walled carbon nanotube-based gas sensors for NH3 detection. *Diam Relat Mater* **13**, 1327-1332 (2004).
207 Feng, X. *et al.* Sensitivity of Ammonia Interaction with Single-Walled Carbon Nanotube Bundles to the Presence of Defect Sites and Functionalities. *J Am Chem Soc* **127**, 10533-10538, doi:10.1021/ja042998u (2005).
208 Li, Y. H. *et al.* Mechanical and NH3 sensing properties of long multi-walled carbon nanotube ropes. *Carbon* **44**, 1821-1825, doi:Doi 10.1016/J.Carbon.2005.12.032 (2006).
209 Nguyen, H. Q. & Huh, J. S. Behavior of single-walled carbon nanotube-based gas sensors at various temperatures of treatment and operation. *Sensors and Actuators B: Chemical* **117**, 426-430 (2006).
210 Quang, N. H., Van Trinh, M., Lee, B.-H. & Huh, J.-S. Effect of NH3 gas on the electrical properties of single-walled carbon nanotube bundles. *Sensors and Actuators B: Chemical* **113**, 341-346, doi:10.1016/j.snb.2005.03.089 (2006).
211 Zhang, T., Nix, M. B., Yoo, B.-Y., Deshusses, M. A. & Myung, N. V. Electrochemically Functionalized Single-Walled Carbon Nanotube Gas Sensor. *Electroanalysis* **18**, 1153-1158, doi:10.1002/elan.200603527 (2006).
212 Duc Hoa, N., Van Quy, N., Suk Cho, Y. & Kim, D. Nanocomposite of SWNTs and SnO2 fabricated by soldering process for ammonia gas sensor application. *physica status solidi (a)* **204**, 1820-1824, doi:10.1002/pssa.200675318 (2007).

213 Van Hieu, N., Thuy, L. T. B. & Chien, N. D. Highly sensitive thin film NH3 gas sensor operating at room temperature based on SnO2/MWCNTs composite. *Sensors and Actuators B: Chemical* **129**, 888-895 (2008).
214 He, L. F., Jia, Y., Meng, F. L., Li, M. Q. & Liu, J. H. Gas sensors for ammonia detection based on polyaniline-coated multi-wall carbon nanotubes. *Mater Sci Eng B-Adv* **163**, 76-81, doi:Doi 10.1016/J.Mseb.2009.05.009 (2009).
215 Lim, J. H. *et al.* Electrical and Sensing Properties of Single Walled Carbon Nanotubes Network: Effect of Alignment and Selective Breakdown. *Electroanalysis* **22**, 99-105 (2010).
216 Mangu, R. *et al.* Ammonia sensing properties of multiwalled carbon nanotubes embedded in porous alumina templates. *Materials Science and Engineering: B* **174**, 2-8 (2010).
217 Peng, N., Zhang, Q., Chow, C. L., Tan, O. K. & Marzari, N. Sensing mechanisms for carbon nanotube based NH3 gas detection. *Nano Lett* **9**, 1626-1630 (2009).
218 Villalpando-P·ez, F. *et al.* Fabrication of vapor and gas sensors using films of aligned CNx nanotubes. *Chem Phys Lett* **386**, 137-143, doi:10.1016/j.cplett.2004.01.052 (2004).
219 Chopra, S., McGuire, K., Gothard, N., Rao, A. M. & Pham, A. Selective gas detection using a carbon nanotube sensor. *Appl Phys Lett* **83**, 2280-2282, doi:Doi 10.1063/1.1610251 (2003).
220 Bittencourt, C. *et al.* WO3 films modified with functionalised multi-wall carbon nanotubes: Morphological, compositional and gas response studies. *Sensors and Actuators B: Chemical* **115**, 33-41, doi:10.1016/j.snb.2005.07.067 (2006).
221 Jones, F., Talin, A., Léonard, F., Dentinger, P. & Clift, W. Effect of electrode material on transport and chemical sensing characteristics of metal/carbon nanotube contacts. *Journal of Electronic Materials* **35**, 1641-1646, doi:10.1007/s11664-006-0211-0 (2006).
222 Li, Y., Wang, H.-c. & Yang, M.-j. n-Type gas sensing characteristics of chemically modified multi-walled carbon nanotubes and PMMA composite. *Sensors and Actuators B: Chemical* **121**, 496-500, doi:10.1016/j.snb.2006.04.074 (2007).
223 Ma, X. *et al.* Preparation of Nano-Structured Polyaniline Composite Film via "Carbon Nanotubes Seeding" Approach and its Gas-Response Studies. *Macromolecular Materials and Engineering* **291**, 75-82, doi:10.1002/mame.200500296 (2006).
224 Zhang, T. *et al.* Poly(m-aminobenzene sulfonic acid) functionalized single-walled carbon nanotubes based gas sensor. *Nanotechnology* **18**, -, doi:Artn 165504
Doi 10.1088/0957-4484/18/16/165504 (2007).
225 Mangu, R., Rajaputra, S. & Singh, V. P. MWCNTñpolymer composites as highly sensitive and selective room temperature gas sensors. *Nanotechnology* **22**, 215502 (2011).
226 Terranova, M. L. *et al.* Carbon nanotubes for gas detection: materials preparation and device assembly. *J Phys-Condens Mat* **19**, -, doi:Artn 225004

Doi 10.1088/0953-8984/19/22/225004 (2007).
227 Ong, K. G., Zeng, K. & Grimes, C. A. A wireless, passive carbon nanotube-based gas sensor. *Sensors Journal, IEEE* **2**, 82-88 (2002).
228 Tabib-Azar, M. & Xie, Y. Sensitive NH3OH and HCl gas sensors using self-aligned and self-welded multiwalled carbon nanotubes. *Sensors Journal, IEEE* **7**, 1435-1439 (2007).
229 Maklin, J. *et al.* Nitric oxide gas sensors with functionalized carbon nanotubes. *physica status solidi (b)* **244**, 4298-4302 (2007).
230 Li, K., Wang, W. & Cao, D. Metal (Pd, Pt)-Decorated Carbon Nanotubes for CO and NO Sensing. *Sensors and Actuators B: Chemical* **In Press, Accepted Manuscript**, doi:10.1016/j.snb.2011.06.068 (2011).
231 Hoa, N. D., Van Quy, N., Cho, Y. & Kim, D. Porous single-wall carbon nanotube films formed by in Situ arc-discharge deposition for gas sensors application. *Sensors and Actuators B: Chemical* **135**, 656-663, doi:10.1016/j.snb.2008.10.041 (2009).
232 Cantalini, C. *et al.* Sensitivity to NO2 and cross-sensitivity analysis to NH3, ethanol and humidity of carbon nanotubes thin film prepared by PECVD. *Sensors and Actuators B: Chemical* **95**, 195-202, doi:10.1016/s0925-4005(03)00418-0 (2003).
233 Valentini, L. *et al.* Sensors for sub-ppm NO gas detection based on carbon nanotube thin films. *Appl Phys Lett* **82**, 961 (2003).
234 An, K. H., Jeong, S. Y., Hwang, H. R. & Lee, Y. H. Enhanced Sensitivity of a Gas Sensor Incorporating Single Walled Carbon NanotubeñPolypyrrole Nanocomposites. *Adv Mater* **16**, 1005-1009 (2004).
235 Cantalini, C. *et al.* Carbon nanotubes as new materials for gas sensing applications. *Journal of the European Ceramic Society* **24**, 1405-1408 (2004).
236 Valentini, L. *et al.* Highly sensitive and selective sensors based on carbon nanotubes thin films for molecular detection. *Diam Relat Mater* **13**, 1301-1305 (2004).
237 Mercuri, F., Sgamellotti, A., Valentini, L., Armentano, I. & Kenny, J. M. Vacancy-Induced Chemisorption of NO2 on Carbon Nanotubes:,Äâ A Combined Theoretical and Experimental Study. *The Journal of Physical Chemistry B* **109**, 13175-13179, doi:10.1021/jp0507290 (2005).
238 Larciprete, R., Lizzit, S., Petaccia, L. & Goldoni, A. NO2 decomposition on Rh clusters supported on single-walled carbon nanotubes. *Appl Phys Lett* **88**, -, doi:Artn 243111
Doi 10.1063/1.2211190 (2006).
239 Suehiro, J. *et al.* Schottky-type response of carbon nanotube NO2 gas sensor fabricated onto aluminum electrodes by dielectrophoresis. *Sensor Actuat B-Chem* **114**, 943-949, doi:Doi 10.1016/J.Snb.2005.08.043 (2006).
240 Wongwiriyapan, W. *et al.* Influence of the growth morphology of single-walled carbon nanotubes on gas sensing performance. *Nanotechnology* **17**, 4424 (2006).
241 Zhang, J., Boyd, A., Tselev, A., Paranjape, M. & Barbara, P. Mechanism of NO2 detection in carbon nanotube field effect transistor chemical sensors. *Appl Phys Lett* **88**, -, doi:Artn 123112

Doi 10.1063/1.2187510 (2006).
242 Larciprete, R., Petaccia, L., Lizzit, S. & Goldoni, A. The Role of Metal Contact in the Sensitivity of Single-Walled Carbon Nanotubes to NO2. *The Journal of Physical Chemistry C* **111**, 12169-12174, doi:10.1021/jp067673+ (2007).
243 Bal·zsi, C., Sedl·ckov·, K., Llobet, E. & Ionescu, R. Novel hexagonal WO3 nanopowder with metal decorated carbon nanotubes as NO2 gas sensor. *Sensors and Actuators B: Chemical* **133**, 151-155, doi:10.1016/j.snb.2008.02.006 (2008).
244 Lee, K., Lee, J. W., Dong, K. Y. & Ju, B. K. Gas sensing properties of single-wall carbon nanotubes dispersed with dimethylformamide. *Sensors and Actuators B: Chemical* **135**, 214-218 (2008).
245 Moon, S. I. L. *et al.* Bias-heating recovery of MWCNT gas sensor. *Materials letters* **62**, 2422-2425 (2008).
246 Leghrib, R., Felten, A., Pireaux, J. J. & Llobet, E. Gas sensors based on doped-CNT/SnO2 composites for NO2 detection at room temperature. *Thin Solid Films* **In Press, Corrected Proof**, doi:10.1016/j.tsf.2011.04.186 (2011).
247 Wei, B. Y. *et al.* A novel SnO2 gas sensor doped with carbon nanotubes operating at room temperature. *Sensors and Actuators B: Chemical* **101**, 81-89 (2004).
248 Liang, Y. X., Chen, Y. J. & Wang, J. H. Low-resistance gas sensors fabricated from multiwalled carbon nanotubes coated with a thin tin oxide layer. *Appl Phys Lett* **85**, 666-668 (2004).
249 Santucci, S. *et al.* NO2 and CO gas adsorption on carbon nanotubes: Experiment and theory. *J Chem Phys* **119**, 10904-10910, doi:Doi 10.1063/1.1619948 (2003).
250 Lu, Y., Partridge, C., Meyyappan, M. & Li, J. A carbon nanotube sensor array for sensitive gas discrimination using principal component analysis. *J Electroanal Chem* **593**, 105-110, doi:10.1016/j.jelechem.2006.03.056 (2006).
251 Kong, J. *et al.* Nanotube molecular wires as chemical sensors. *Science* **287**, 622 (2000).
252 Qi, P. *et al.* Toward large arrays of multiplex functionalized carbon nanotube sensors for highly sensitive and selective molecular detection. *Nano Lett* **3**, 347-351 (2003).
253 Li, J., Lu, Y. J., Ye, Q., Delzeit, L. & Meyyappan, M. A gas sensor array using carbon nanotubes and microfabrication technology. *Electrochem Solid St* **8**, H100-H102 (2005).
254 Jung, H. Y., Jung, S. M., Kim, J. & Suh, J. S. Chemical sensors for sensing gas adsorbed on the inner surface of carbon nanotube channels. *Appl Phys Lett* **90** (2007).
255 Penza, M. *et al.* Effect of growth catalysts on gas sensitivity in carbon nanotube film based chemiresistive sensors. *Appl Phys Lett* **90** (2007).
256 Penza, M. *et al.* Enhancement of sensitivity in gas chemiresistors based on carbon nanotube surface functionalized with noble metal (Au, Pt) nanoclusters. *Appl Phys Lett* **90**, 173123 (2007).

257 Penza, M. *et al.* Pt-and Pd-nanoclusters functionalized carbon nanotubes networked films for sub-ppm gas sensors. *Sensors and Actuators B: Chemical* **135**, 289-297 (2008).

258 Goldoni, A., Larciprete, R., Petaccia, L. & Lizzit, S. Single-Wall Carbon Nanotube Interaction with Gases:‚Äâ Sample Contaminants and Environmental Monitoring. *J Am Chem Soc* **125**, 11329-11333, doi:10.1021/ja034898e (2003).

259 Goldoni, A. *et al.* Spectroscopic characterization of contaminants and interaction with gases in single-walled carbon nanotubes. *Carbon* **42**, 2099-2112, doi:Doi 10.1016/J.Carbon.2004.04.011 (2004).

260 Ueda, T. *et al.* Development of carbon nanotube-based gas sensors for NOx gas detection working at low temperature. *Physica E: Low-dimensional Systems and Nanostructures* **40**, 2272-2277 (2008).

261 Ueda, T. *et al.* Effect of laser irradiation on carbon nanotube films for NOx gas sensor. *Surface and Coatings Technology* **202**, 5325-5328 (2008).

262 Ueda, T. *et al.* Fabrication and characterization of carbon nanotube based high sensitive gas sensors operable at room temperature. *Diam Relat Mater* **17**, 1586-1589 (2008).

263 Collins, P. G., Bradley, K., Ishigami, M. & Zettl, A. Extreme oxygen sensitivity of electronic properties of carbon nanotubes. *Science* **287**, 1801 (2000).

264 Wadhawan, A., Stallcup, R., Stephens, K., Perez, J. & Akwani, I. Effects of O2, Ar, and H2 gases on the field-emission properties of single-walled and multiwalled carbon nanotubes. *Appl Phys Lett* **79**, 1867-1869 (2001).

265 Watts, P. C. P. *et al.* The importance of oxygen-containing defects on carbon nanotubes for the detection of polar and non-polar vapours through hydrogen bond formation. *Nanotechnology* **18**, 175701 (2007).

266 Valentini, L. *et al.* Effects of oxygen annealing on cross sensitivity of carbon nanotubes thin films for gas sensing applications. *Sensors and Actuators B: Chemical* **100**, 33-40, doi:10.1016/j.snb.2003.12.017 (2004).

267 Ghaddab, B. *et al.* Detection of O3 and NH3 using hybrid tin dioxide/carbon nanotubes sensors: Influence of materials and processing on sensor's sensitivity. *Sensors and Actuators B: Chemical* **In Press, Corrected Proof**, doi:10.1016/j.snb.2011.01.044.

268 Zhao, Y. L., Hu, L., Stoddart, J. F. & Gr¸ner, G. Pyrenecyclodextrin Decorated Single Walled Carbon Nanotube Field Effect Transistors as Chemical Sensors. *Adv Mater* **20**, 1910-1915 (2008).

269 Picozzi, S., Santucci, S., Lozzi, L., Valentini, L. & Delley, B. Ozone adsorption on carbon nanotubes: The role of Stone-Wales defects. *J Chem Phys* **120**, 7147-7152, doi:Doi 10.1063/1.1669381 (2004).

270 Choi, J. & Kim, J. Batch-processed carbon nanotube wall as pressure and flow sensor. *Nanotechnology* **21**, 105502 (2010).

271 Suehiro, J., Zhou, G. & Hara, M. Detection of partial discharge in SF6 gas using a carbon nanotube-based gas sensor. *Sensors and Actuators B: Chemical* **105**, 164-169, doi:10.1016/j.snb.2004.05.050 (2005).

272 Kang, H., Lim, S., Park, N., Chun, K. Y. & Baik, S. Improving the sensitivity of carbon nanotube sensors by benzene functionalization. *Sensors and Actuators B: Chemical* **147**, 316-321 (2010).
273 Chaudhury, P. K., Dubey, P., Saxena, M. & Sarkar, S. Multiwalled Carbon Nanotube-Polystyrene Composite Modified Pt Electrode as an Electrochemical Gas Sensor. *Adv Sci Lett* **4**, 558-560, doi:Doi 10.1166/Asl.2011.1220 (2011).
274 Lee, C., Baik, S., Zhang, J., Masel, R. & Strano, M. Charge transfer from metallic single-walled carbon nanotube sensor arrays. *J Phys Chem B* **110**, 11055-11061, doi:10.1021/jp056425v (2006).
275 Auvray, S. *et al.* Chemical optimization of self-assembled carbon nanotube transistors. *Nano Lett* **5**, 451-455 (2005).
276 Wei, C., Dai, L., Roy, A. & Tolle, T. B. Multifunctional Chemical Vapor Sensors of Aligned Carbon Nanotube and Polymer Composites. *J Am Chem Soc* **128**, 1412-1413, doi:10.1021/ja0570335 (2006).
277 Parikh, K. *et al.* Flexible vapour sensors using single walled carbon nanotubes. *Sensor Actuat B-Chem* **113**, 55-63, doi:Doi 10.1016/J.Snb.2005.02.021 (2006).
278 Consales, M. *et al.* Carbon nanotubes coated acoustic and optical VOCs sensors: Towards the tailoring of the sensing performances. *Ieee T Nanotechnol* **6**, 601-612, doi:Doi 10.1109/Tnano.2007.907843 (2007).
279 Doleman, B. J. & Lewis, N. S. Comparison of odor detection thresholds and odor discriminablities of a conducting polymer composite electronic nose versus mammalian olfaction. *Sensors and Actuators B: Chemical* **72**, 41-50, doi:10.1016/s0925-4005(00)00635-3 (2001).
280 Hosseini, S. H. & Entezami, A. A. Chemical and electrochemical synthesis of conducting graft copolymer of vinyl acetate with pyrrole and studies of its gas and vapor sensing. *Journal of Applied Polymer Science* **90**, 40-48, doi:10.1002/app.12483 (2003).
281 Penza, M., Antolini, F. & Antisari, M. V. Carbon nanotubes as SAW chemical sensors materials. *Sensors and Actuators B: Chemical* **100**, 47-59 (2004).
282 Penza, M., Tagliente, M. A., Aversa, P. & Cassano, G. Organic-vapor detection using carbon-nanotubes nanocomposite microacoustic sensors. *Chem Phys Lett* **409**, 349-354, doi:Doi 10.1016/J.Cplett.2005.05.005 (2005).
283 Snow, E. S., Perkins, F. K. & Robinson, J. A. Chemical vapor detection using single-walled carbon nanotubes. *Chemical Society Reviews* **35**, 790-798 (2006).
284 Picaud, F. *et al.* Gas-induced variation in the dielectric properties of carbon nanotube bundles for selective sensing. *Journal of Applied Physics* **97**, 114316 (2005).

# APPENDIX A – SPECTROFLUORIMETRIC ANALYSIS DATA FOR CHIRALITY AND DIAMETER MEASUREMENT OF SWNT

NASA JSC LASER ABLATION SWNT, BATCH JSC 390 AQW

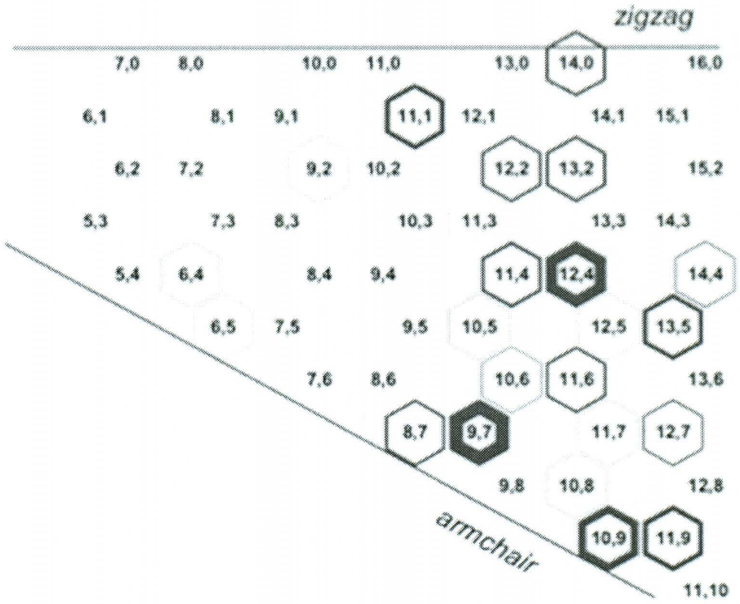


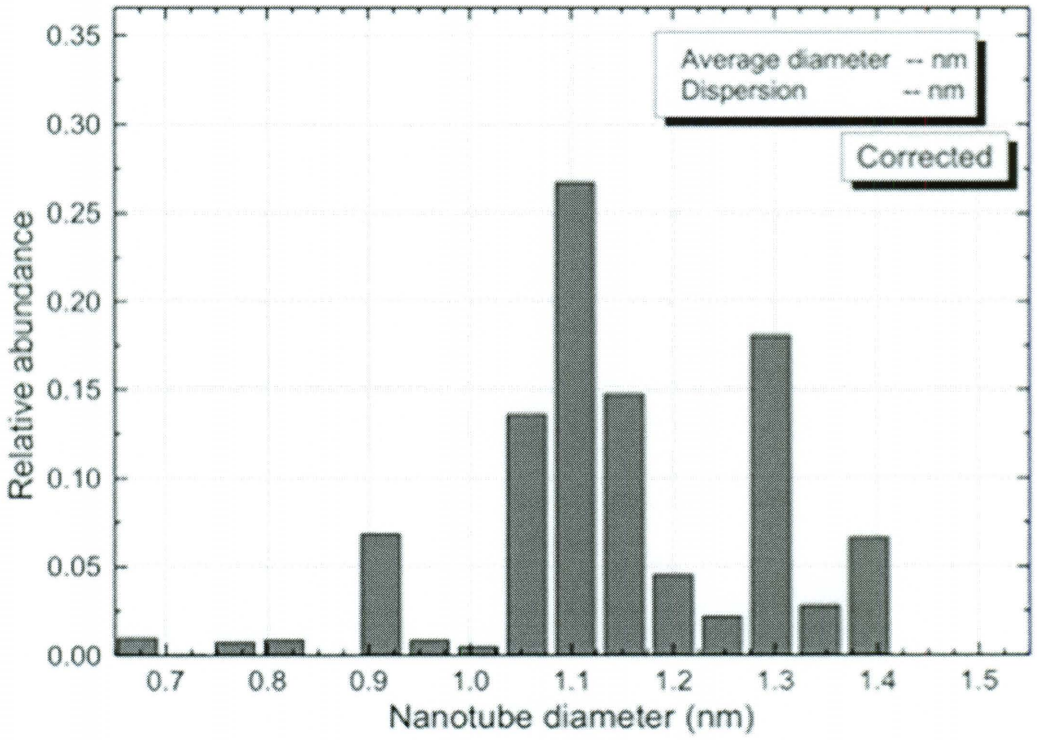

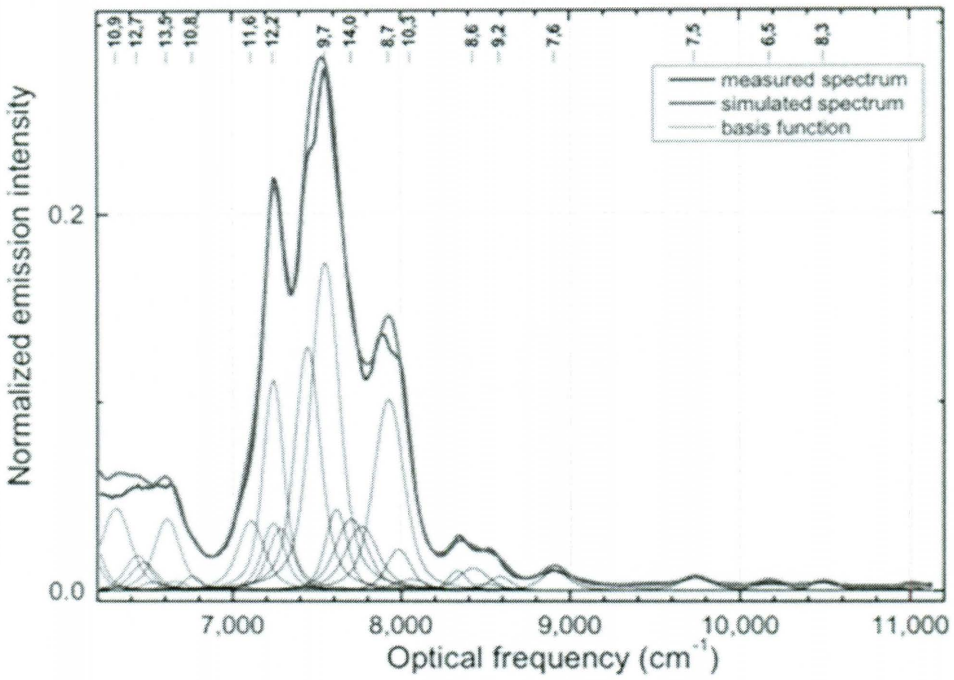
10.9
12.7
13.5
10.8
11.6
12.2
9.7
14.0
8.7
10.3
8.6
9.2
7.6
7.5
6.5
8.3
measured spectrum
simulated spectrum
basis function
Normalized emission intensity
0.2
0.0
7,000
8,000
9,000
10,000
11,000
Optical frequency (cm-1)

SWENT INC. COMOCAT SWNT, BATCH CG-100

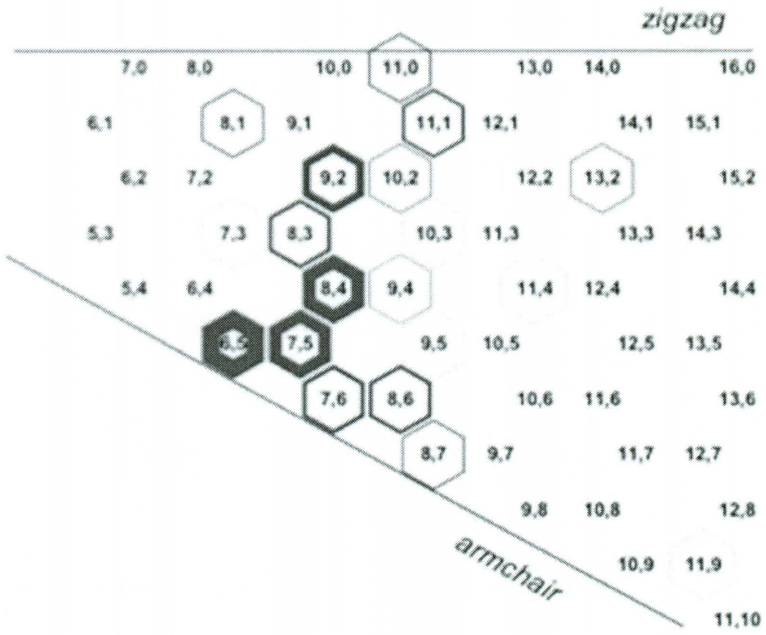

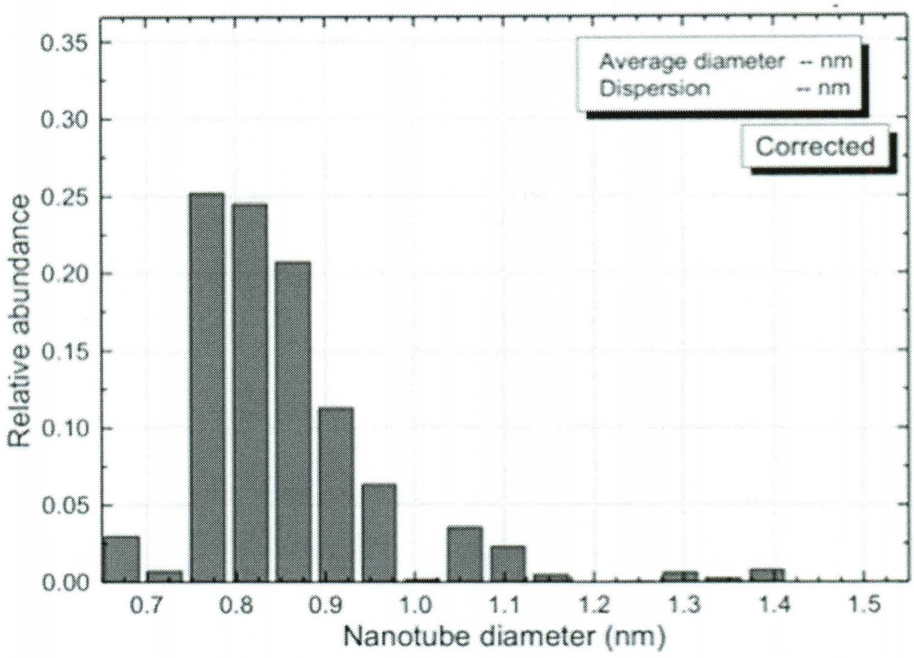
Average diameter -- nm
Dispersion -- nm
Corrected
Relative abundance
0.35
0.30
0.25
0.20
0.15
0.10
0.05
0.00
0.7
0.8
0.9
1.0
1.1
1.2
1.3
1.4
1.5
Nanotube diameter (nm)

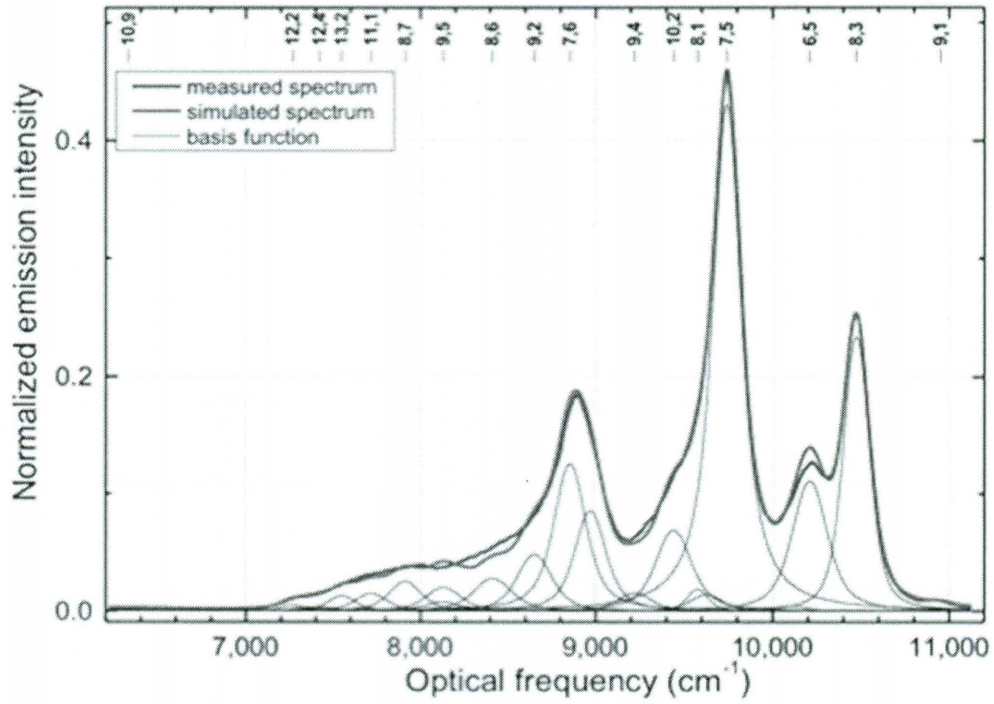
10,9
12,2
12,4
13,2
11,1
8,7
9,5
8,6
9,2
7,6
9,4
10,2
8,1
7,5
6,5
8,3
9,1
measured spectrum
simulated spectrum
basis function
Normalized emission intensity
0.4
0.2
0.0
7,000
8,000
9,000
10,000
11,000
Optical frequency (cm-1)

SWENT INC. COMOCAT SWNT, BATCH CG-200 LOT 400

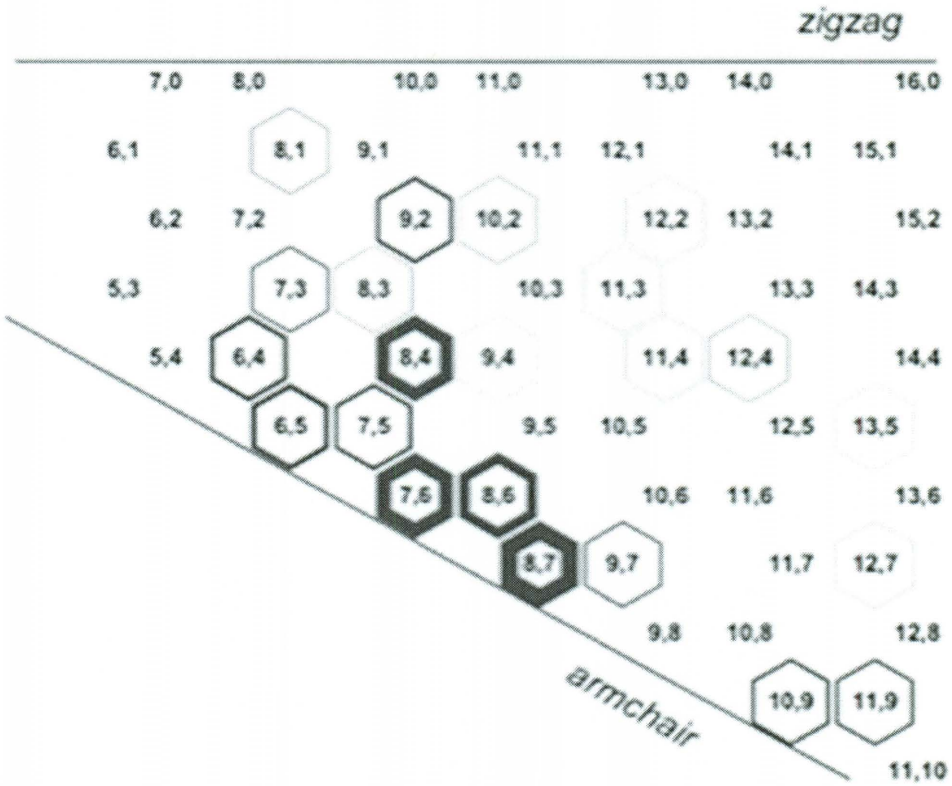

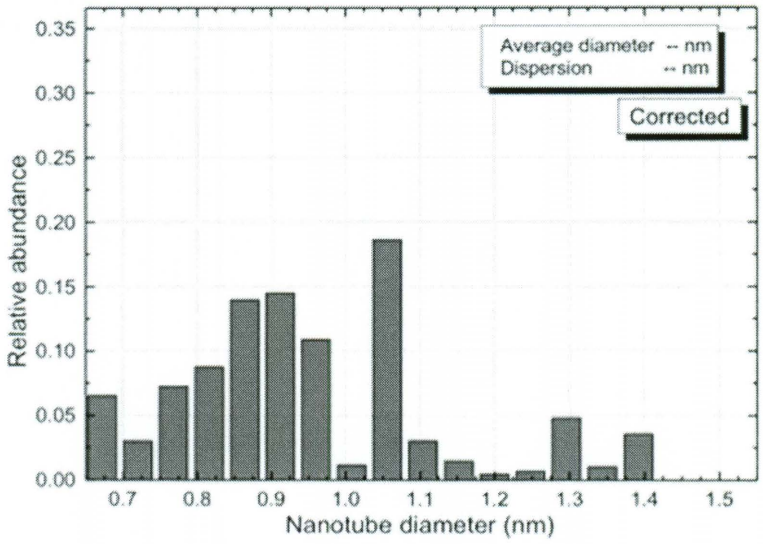
Average diameter -- nm
Dispersion -- nm
Corrected
Relative abundance
0.35
0.30
0.25
0.20
0.15
0.10
0.05
0.00
0.7
0.8
0.9
1.0
1.1
1.2
1.3
1.4
1.5
Nanotube diameter (nm)

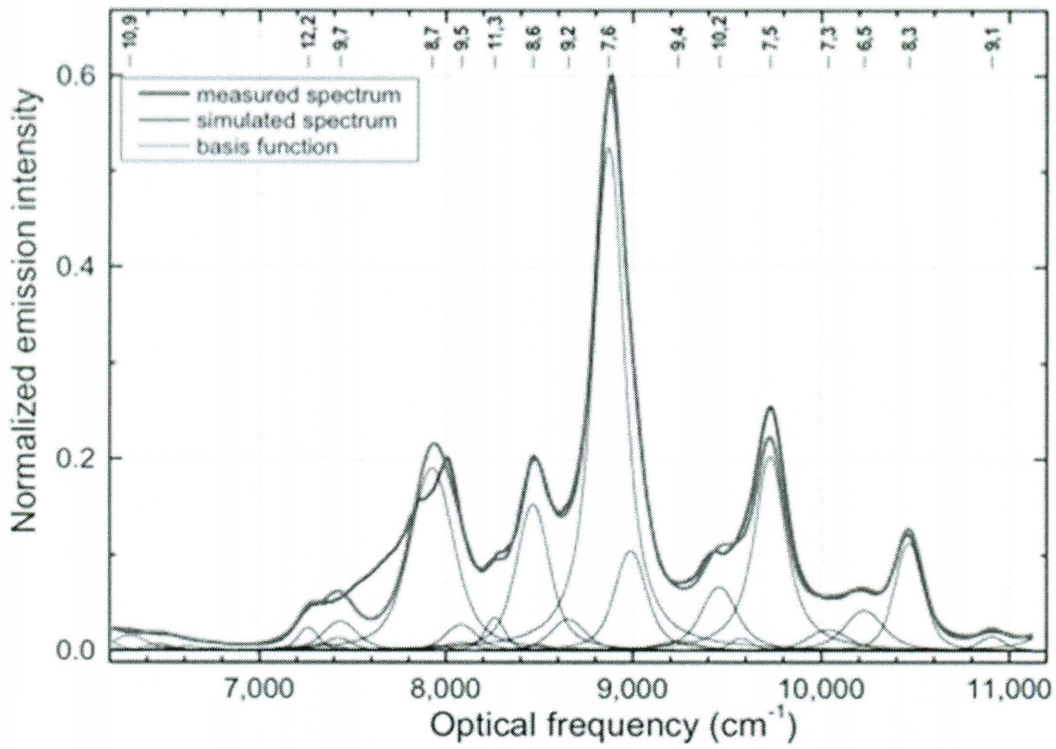
(10,9)
(12,2)
(9,7)
(8,7)
(9,5)
(11,3)
(8,6)
(9,2)
(7,6)
(9,4)
(10,2)
(7,5)
(7,3)
(6,5)
(8,3)
(9,1)
measured spectrum
simulated spectrum
basis function
Normalized emission intensity
0.6
0.4
0.2
0.0
7,000
8,000
9,000
10,000
11,000
Optical frequency (cm-1)

SWENT INC. COMOCAT SWNT, BATCH CG-200 LOT 700

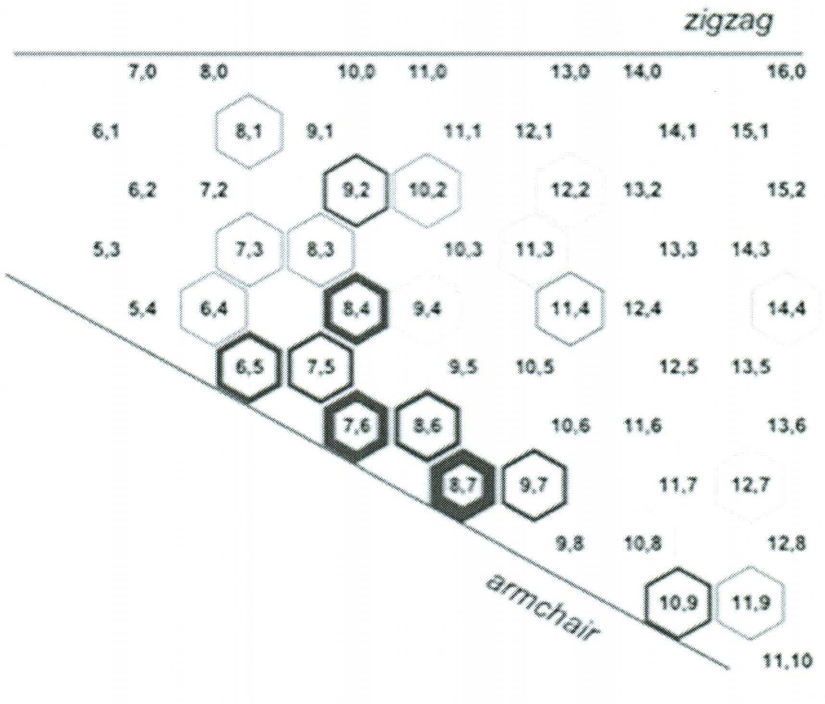

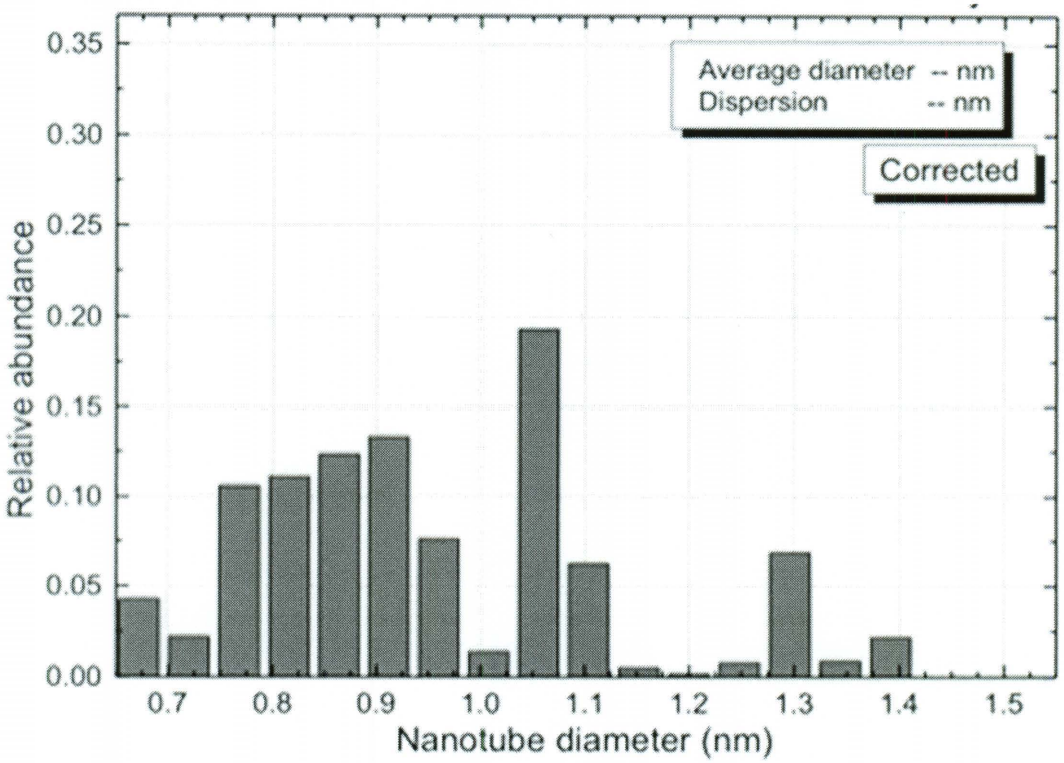
Average diameter -- nm
Dispersion -- nm
Corrected
Relative abundance
0.35
0.30
0.25
0.20
0.15
0.10
0.05
0.00
0.7
0.8
0.9
1.0
1.1
1.2
1.3
1.4
1.5
Nanotube diameter (nm)

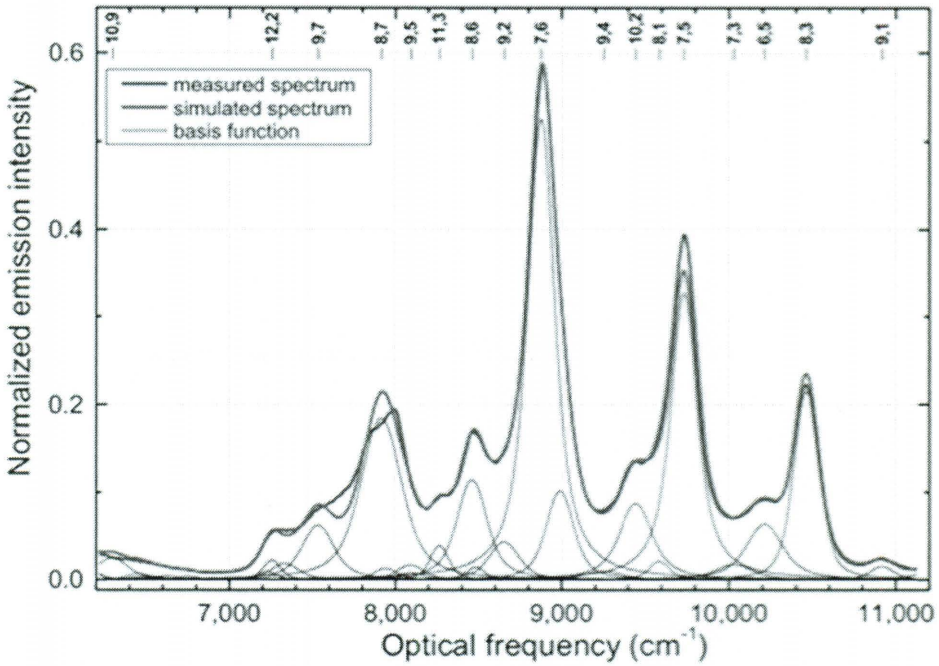
10,9
12,2
9,7
8,7
9,5
11,3
8,6
9,2
7,6
9,4
10,2
8,1
7,5
7,3
6,5
8,3
9,1
measured spectrum
simulated spectrum
basis function
Normalized emission intensity
0.6
0.4
0.2
0.0
7,000
8,000
9,000
10,000
11,000
Optical frequency (cm-1)

RICE UNIVERSITY HIPCO SWNT

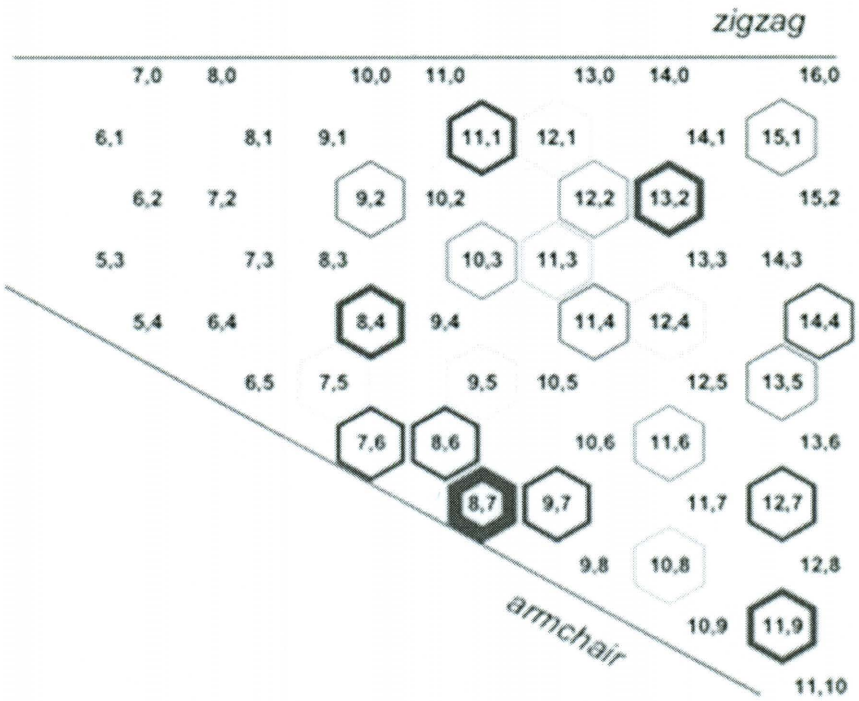

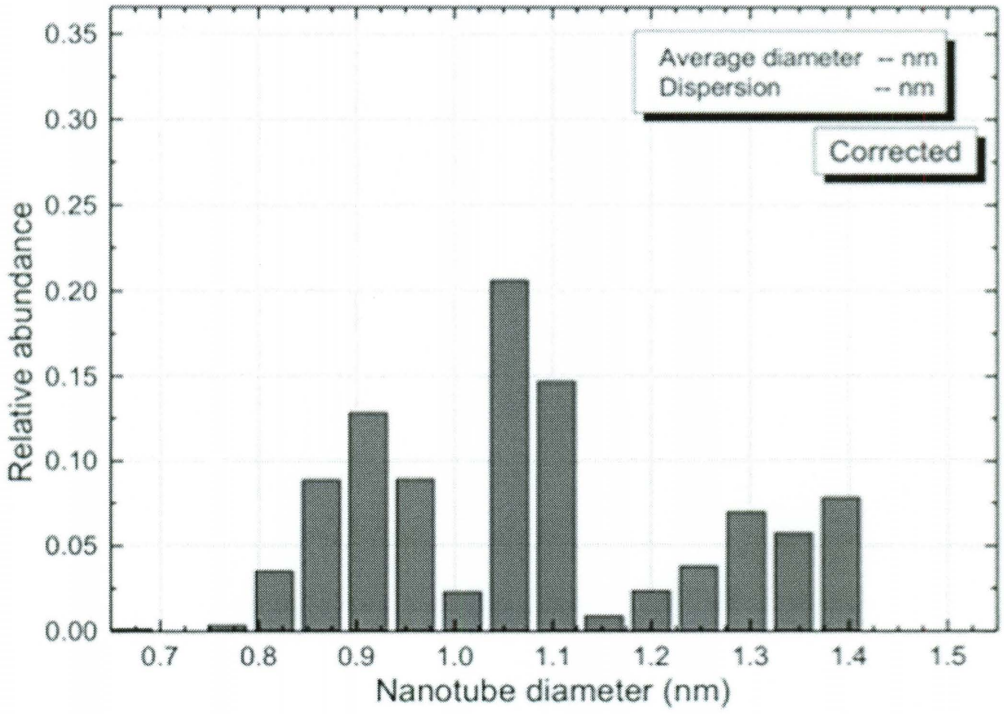
Average diameter -- nm
Dispersion -- nm
Corrected
Relative abundance
Nanotube diameter (nm)
0.00
0.05
0.10
0.15
0.20
0.25
0.30
0.35
0.7
0.8
0.9
1.0
1.1
1.2
1.3
1.4
1.5

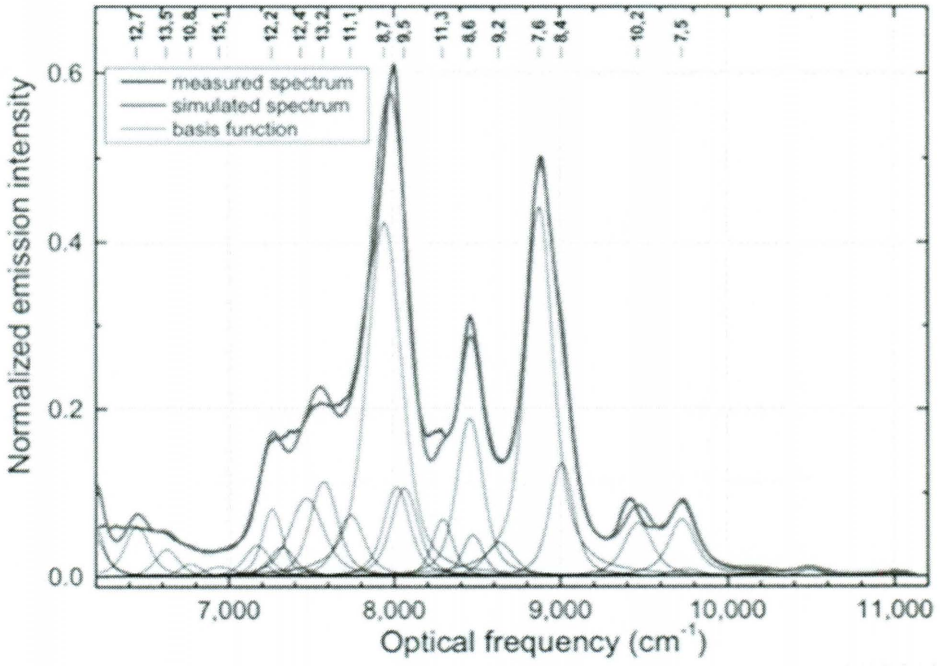
12,7
13,5
10,8
15,1
12,2
12,4
13,2
11,1
8,7
9,5
11,3
8,6
9,2
7,6
8,4
10,2
7,5
measured spectrum
simulated spectrum
basis function
Normalized emission intensity
Optical frequency (cm-1)
0.0
0.2
0.4
0.6
7,000
8,000
9,000
10,000
11,000

# APPENDIX B – SUMMARY TABLE OF CNT GAS SENSOR RESEARCH.

(Arranged alphabetically with respect to analyte targeted by sensor)

| Year | Author | Analyte | CNT Type | Functionalized /Matrix | Enviro | Method | Detection Limit | Ref. |
|---|---|---|---|---|---|---|---|---|
| 2006 | Robinson | Acetone, MeOH | SWNT | Oxidation | Gas | Resistance, Capacitance | -- | 129 |
| 2005 | Anand | Air | SWNT | -- | Gas | Resonant Cavity | -- | 130 |
| 2004 | Chung | Air, oxygen | MWNT | -- | Gas | Voltage | -- | 131 |
| 2003 | Someya | Alcohols | SWNT | -- | Gas | Current | -- | 132 |
| 2006 | Kim | Ar | MWNT | -- | Gas | Voltage | -- | 133 |
| 2010 | Leghrib | Benzene | MWNT | Rh, Pt, Au, Pd, Ni | Gas | Resistance | 50ppb | 134 |
| 2004 | Cho | Benzene, ethanol | SWNT | Ethyl cellulose | Gas | Resistance | 1000ppm | 135 |
| 2009 | Mabrook | C2H5OH | SWNT | Polyelectrolyte inkjet | Gas | Current | 300ppm | 136 |
| 2002 | Yang | CH3OH, C2H5OH | SWNT | -- | Gas | Absorbance | -- | 137 |
| 2005 | Santhanam | Chloromethane | MWNT | poly(3-methylthiophene) | Gas | Resistance | 5ppm | 138 |
| 2011 | Gohier | Cl2 | MWNT | PEI | Gas | Resistance | 27ppb | 98 |
| 2004 | He | CO | MWNT | HClO4 | Gas | Cyclic volt | -- | 139 |
| 2006 | Wanna | CO | MWNT | PANI | Gas | Resistance | 150ppm | 140 |
| 2007 | Santhosh | CO | MWNT | PDPA | Gas, Liquid | Voltage | 0.01ppm | 141 |

| | | | | | | | | |
|---|---|---|---|---|---|---|---|---|
| 2008 | Wongwiriyapan | CO | SWNT | Pt | Gas | Resistance | 1ppm | 142 |
| 2010 | Kauffman | CO | SWNT | Au | Gas | Modeling Paper | | 143 |
| 2007 | Kuzmych | CO, CO2, O2 | SWNT | PEI | Gas | Resistance | 5ppb | 144 |
| 2001 | Ong | CO2 | MWNT | SiO2 | Gas | Permittivity | -- | 145 |
| 2004 | Star | CO2 | SWNT | PEI, Starch | Gas | Current | -- | 146 |
| 2005 | Zribi | CO2 | SWNT | -- | Gas | Vibrational Resonance | -- | 147 |
| 2003 | Philip | Dichloromethane, acetone, chloroform | SWNT | Oxidation, PMMA | Gas | Resistance | -- | 148 |
| 2004 | Jose | Dichloromethane, acetone, chloroform | MWNT | PMMA | Gas | Resistance | -- | 149 |
| 2010 | Wang | DMMP | SWNT | PEI | Gas | Resistance | 1ppm | 150 |
| 2011 | Wang | DMMP | SWNT | CoPc | Gas | Resistance | 0.5ppm | 121 |
| 2001 | Hopkins | DMMP, DIMP | -- | Carbon Black/Polymer | Gas | Resistance | -- | 151 |
| 2006 | Cattanach | DMMP, DIMP | SWNT | PET, PIB | Gas | Resistance | 299ppm | 114 |
| 2005 | Choi | DMMP, DPGME, DCM | -- | Al2O3, In2O3, Pt, Pd, ZnO, ZrO2 | Gas | Resistance | 0.5 ppm | 117 |
| 2003 | Novak | DMMP, Hexanes, Xylenes, H2O | SWNT | -- | Gas | Resistance | -- | 118 |

| | | | | | | | | |
|---|---|---|---|---|---|---|---|---|
| 2008 | Wang | DMMP, VOC | SWNT | HFIP-PT, P3HT | Gas | Voltage, Resistance | 0.05ppm | 120 |
| 2007 | Ali | Dopamine | SWNT | PABA | Liquid | Cyclic volt, diff pulse volt | 40pM, 1nM | 152 |
| 2011 | Delalande | DPCP | SWNT | Au | Gas | Voltage | 1ppm | 153 |
| 2006 | Yujin | Ethanol | MWNT | SnO2 | Gas | Resistance | 50ppm | 154 |
| 2008 | Krishna | H2 | SWNT | Pd | Gas | Resistance | -- | 155 |
| 2011 | Zilli | H2 | MWNT | Pd | Gas | Resistance | 70ppm | 156 |
| 1999 | Liu | H2 | SWNT | | | | | 157 |
| 2008 | Gong | H2 | SWNT | SnO2 | Gas | Resistance | -- | 158 |
| 2001 | Kong | H2 | SWNT | Pd | Gas | Resistance | 40ppm | 159 |
| 2005 | Sayago | H2 | SWNT | Pd | Gas | Resistance | -- | 160 |
| 2007 | Sayago | H2 | SWNT | Pd | Gas | Resistance | -- | 161 |
| 2009 | Srivastava | H2 | MWNT | PANI | Gas | Resistance | -- | 162 |
| 2003 | Wong | H2 | MWNT | Pd | Gas | Voltage | -- | 163 |
| 2005 | Sippel-Oakley | H2 | SWNT | Pd | Gas | Resistance | 10ppm | 164 |
| 2004 | Ahn | H2, NH3 | MWNT Forest | -- | Gas | D.C. | 8 ppm | 165 |
| 2006 | Star | H2, CH4, CO, H2S | SWNT | Pd, Pt, Rh, Au | Gas | Voltage | 5 ppm | 166 |
| 2005 | Staii | H20, acid, MeOH DMMP etc. | SWNT | DNA | Gas | Current | 25 ppm | 167 |
| 2010 | Bekyarova | H2Cl | SWNT | | | | | 168 |
| 2000 | Zahab | H2O | SWNT | | Gas | Resistance | -- | 169 |
| 2003 | Kim | H2O | SWNT | PMMA | Gas | Voltage | -- | 170 |
| 2004 | Star | H2O | SWNT | Nafion | Gas | Current | -- | 171 |
| 2005 | Chen | H2O | SWNT | Nafion | Gas | Quartz microbalance | 15.76 | 172 |
| 2005 | Na | H2O | SWNT | -- | Gas | Voltage | -- | 173 |

| | | | | | | | | |
|---|---|---|---|---|---|---|---|---|
| 2006 | Su | H2O | SWNT | PAMPS-SiO2 | Gas | Impedance | -- | 174 |
| 2006 | Yu | H2O | MWNT | PEI | Gas | Resistance | -- | 175 |
| 2007 | Jiang | H2O | MWNT | | Liquid | Resistance | -- | 176 |
| 2007 | Su | H2O | MWNT | PMMA, KOH | Gas | Impedance | -- | 177 |
| 2011 | Tang | H2O | MWNT | PI | Gas | Resistance | -- | 178 |
| | | H2O2, | | | | Voltage, | | |
| 2003 | Wang | NADH | SWNT | Teflon | Liquid | Resistance | -- | 179 |
| | | | | Carboxyl, amide, | | | | |
| 2011 | Izadi | H2S | MWNT | Mo, Pt | Gas | Resistance | -- | 180 |
| | | H2S, CO, | | | | | | |
| 2009 | Fam | NO | SWNT | Ag | Gas | Current | 2ppm | 181 |
| 2004 | Valentini | HCl | MWNT | POAS | Gas | Resistance | 100ppm | 182 |
| 2006 | Li | HCl, Cl2 | SWNT | CSPE, HPC | Gas | Resistance | 2ppm | 183 |
| | | | | Boron modeling | | | | |
| 2006 | Zhang | HCN | SWNT | paper | Gas | -- | -- | 184 |
| 2006 | Wang | HCOH | SWNT | Modeling paper | | -- | -- | 184 |
| 2010 | Khani | Hg(II) | MWNT | BMIM.BF4 | Liquid | Voltage | 0.5ppb | 185 |
| 2010 | Lee | Hg2+ | SWNT | -- | Liquid | Resistance | -- | 186 |
| | | LPG, | | | | | | |
| 2006 | Liu | C2H5OH | MWNT | SnO2 | Gas | Voltage | 10ppm | 187 |
| | | | | Gold Mylar | | | | |
| 1989 | Bartlett | MeOH | -- | Layers | Gas | Resistance | -- | 188 |
| 2010 | Chen | MeOH, IPA | SWNT | DNA | Gas | Resistance | -- | 189 |
| 2004 | Valentini | Methane | MWNT | | Gas | Resistance | | 190 |
| | | Modeled | | | | | | |
| 2004 | Arab | Various | SWNT | -- | Gas | -- | -- | 191 |
| | | Modeled | | | | | | |
| 2010 | Tooski. | Various | -- | -- | -- | -- | -- | 192 |
| 2003 | Bradley | -- | CNT | NaPSS polymer | Gas | Voltage | -- | 193 |
| 2009 | Loh | -- | SWNT | Ni | Gas | Voltage | -- | 194 |

| | | | | | | | | |
|---|---|---|---|---|---|---|---|---|
| 2005 | Huang | N2 | MWNT | -- | Gas | Resistance | -- | 195 |
| 2000 | Sumanase kera | N2, He | SWNT | -- | Gas | Resistance | -- | 196 |
| 2001 | Varghese | NH3 | MWNT | SiO2 | Gas | Impedance | -- | 197 |
| 2002 | Chopra | NH3 | SWNT | Epoxy conductive | Gas | Microwave Resonance | 100ppm | 198 |
| 2003 | Bradley | NH3 | SWNT | | Liquid/Gas | Voltage | -- | 199 |
| 2003 | Bradley | NH3 | SWNT | PEI | Gas | Voltage | -- | 200 |
| 2003 | Modi | NH3 | MWNT | -- | Gas | Voltage | -- | 201 |
| 2003 | Suehiro | NH3 | MWNT | | Gas | Resistance | 10ppm | 202 |
| 2004 | Bekyarova | NH3 | SWNT | PABS | Gas | Resistance | 5 ppm | 203 |
| 2004 | Jang | NH3 | MWNT | | Gas | Resistance | -- | 204 |
| 2004 | Lu | NH3 | SWNT | Pd | Gas | Resistance | 6ppm | 205 |
| 2004 | Wang | NH3 | MWNT | -- | Gas | Resistance | >10ppm | 206 |
| 2005 | Feng | NH3 | SWNT | HNO3 | Gas | Absorbance | -- | 207 |
| 2006 | Li | NH3 | MWNT SWNT | -- | Gas | Resistance | 50ppm | 208 |
| 2006 | Nguyen | NH3 | MWNT | -- | Gas | Resistance | 5ppm | 209 |
| 2006 | Quang | NH3 | SWNT | | Gas | Resistance | 5ppm | 210 |
| 2006 | Zhang | NH3 | SWNT | PANI | Gas | Resistance | 50ppb | 211 |
| 2007 | Duc Hoa | NH3 | SWNT | SnO2 | Gas | Resistance | 10ppm | 212 |
| 2008 | Van Hieu | NH3 | MWNT | SnO2 | Gas | Resistance | >100ppm | 213 |
| 2009 | He | NH3 | MWNT | PANI | Gas | Resistance | <12ppm | 214 |
| 2009 | Zhang | NH3 | SWNT | PANI(CSA) | Gas | Resistance | 10ppb | 99 |
| 2010 | Lim | NH3 | SWNT | -- | Gas | Resistance | 1ppm | 215 |
| 2010 | Mangu | NH3 | MWNT | alumina | Gas | Resistance | -- | 216 |
| 2009 | Peng . | NH3 | SWNT | SiO2 | Gas | Resistance | <100ppm | 217 |
| 2004 | Villalpando -Perez | NH3, acetone, OH | -- | Modeling paper | -- | -- | -- | 218 |
| 2003 | Chopra | NH3, CO, Ar, N2, O2 | SWNT | Epoxy conductive | Gas | Dielectric | 100ppm | 219 |

| | | | | | | | | |
|---|---|---|---|---|---|---|---|---|
| 2006 | Bittencourt | NH3, CO, NO2 | MWNT | WO3 | Gas | Resistance | 100 ppm, 10ppm, 500ppb | 220 |
| 2006 | Jones | NH3, EtOH, H2O | SWNT | DNA, ACDEP | Gas | Voltage | -- | 221 |
| 2007 | Li | NH3, MeOH | MWNT | (NH2OH)(HCL), PMMA | Gas | Voltage | -- | 222 |
| 2006 | Ma | NH3, N(CH3)3, Et3N | MWNT | PANI | Gas | Current | -- | 223 |
| 2007 | Zhang | NH3, NO2 | SWNT | PABS | Gas | Resistance | 100ppb, 20ppb | 224 |
| 2011 | Mangu | NH3, NO2 | MWNT | PEDOT:PSS, PANI | Gas | Resistance | 100ppm | 225 |
| 2010 | Lim . | NH3, NO2, H2S | SWNT | PANI | Gas | Resistance | 50, 500 and 500ppb | 215 |
| 2007 | Terranova | NH3, NOx | SWNT | -- | Gas | Resistance | 75ppm | 226 |
| 2002 | Ong | NH3, O2, CO2 | MWNT | SiO2 | Gas | Permittivity | -- | 227 |
| 2007 | Tabib-Azar | NH3Oh, HCl | MWNT SWNT | -- | Gas | voltage | -- | 228 |
| 2007 | Maklin | NO | MWNT | carboxyl | Gas | Resistance | 100ppm | 229 |
| 2011 | Li | NO CO | SWNT | Pd, PT | Gas | Modeling Paper | | 230 |
| 2009 | Hoa | NO, NH3 | SWNT | -- | Gas | Resistance | 2ppm | 231 |
| 2003 | Cantalini | NO2 | MWNT | -- | Gas | Resistance | 10 ppb | 232 |
| 2003 | Valentini | NO2 | MWNT | -- | Gas | Resistance | <10ppb | 233 |
| 2004 | An | NO2 | SWNT | Ppy | Gas | Resistance | 5 ppm (extrapolated) | 234 |
| 2004 | Cantalini | NO2 | MWNT | -- | Gas | Resistance | 10 ppb | 235 |

| | | | | | | | | |
|---|---|---|---|---|---|---|---|---|
| 2004 | Valentini | NO2 | MWNT | -- | Gas | Resistance | 10ppb | 236 |
| 2005 | Mercuri | NO2 | SWNT | -- | Gas | Photoemission | -- | 237 |
| 2005 | Young | NO2 | SWNT | MPCs | Gas | Current | 4.6ppb | 100 |
| 2006 | Larciprete | NO2 | SWNT | Rh | Gas | Photoemission | -- | 238 |
| 2006 | Suehiro | NO2 | MWNT | Al , Cr | Gas | Resistance | 0.5 ppm | 239 |
| 2006 | Wongwiriy apan | NO2 | SWNT | -- | Gas | Resistance | 200ppb | 240 |
| 2006 | Zhang | NO2 | SWNT | PMMA, SU-8 | Gas | Resistance | 20ppm | 241 |
| 2007 | Larciprete | NO2 | SWNT | Rh | Gas | Photoemission | -- | 242 |
| 2008 | Bal·zsi | NO2 | MWNT | hex-WO3, Ag Au | Gas | Resistance | 100 ppb | 243 |
| 2008 | Lee | NO2 | SWNT | -- | Gas | Resistance | 3ppm | 244 |
| 2008 | Moon | NO2 | MWNT | Binder | Gas | Voltage | 50ppm | 245 |
| 2011 | Leghrib | NO2 | MWNT | B, N, SnO2, | Gas | Resistance | 100ppb | 246 |
| 2004 | Wei | NO2 | SWNT | SnO2 | Gas | Resistance | 200ppm | 247 |
| 2004 | Liang | NO2, | MWNT | SnO2 | Gas | Resistance | 2ppm | 248 |
| 2003 | Santucci | NO2, CO | MWNT | -- | Gas | Resistance | 10ppb | 249 |
| 2003 | Cantalini | NO2, CO, NH3, EtOH, C6H6, H20 | MWNT | -- | Gas | Resistance | 10 ppb (NO2) | 232 |
| 2004 | Valentini | NO2, CO, NH3, H2O, C2H5OH | MWNT | -- | Gas | Resistance | 10ppb | 236 |
| 2006 | Lu | NO2, HCN, HCl, Cl-2, acetone, benzene | SWNT | Metal, polymer coatings | Gas | Resistance | Various ppm | 250 |
| 2000 | Kong | NO2, NH3 | SWNT | Semiconducting Tubes | Gas | Resistance | 200ppm | 251 |
| 2003 | Qi | NO2, NH3 | SWNT | Nafion, PEI | Gas | Resistance | <1ppb | 252 |

| | | | | | | | | |
|---|---|---|---|---|---|---|---|---|
| 2005 | Li | NO2, NH3 | SWNT | -- | Gas | Resistance | | 253 |
| 2007 | Jung | NO2, NH3 | MWNT | -- | Gas | Resistance | 100 ppb | 254 |
| 2007 | Penza | NO2, NH3 | MWNT | -- | Gas | Resistance | 10ppm | 255 |
| 2007 | Penza | NO2, NH3 | MWNT | Au, Pt | Gas | Resistance | 5ppm, 100ppb | 256 |
| 2008 | Penza | NO2, NH3, H2S | MWNT | Pt, Pd | Gas | Resistance | <1ppm | 257 |
| 2003 | Li | NO2, nitrotoluene | SWNT | -- | Gas | Resistance | <44ppb | 63 |
| 2003 | Goldoni | NO2, SO2, NH3 | SWNT | -- | Gas | Photoemission | <10ppb | 258 |
| 2004 | Goldoni | NO2, SO2, NO | SWNT | -- | Gas | Photoemission | <10ppb | 259 |
| 2008 | Ueda | NOx | MWNT | -- | Gas | Resistance | 2ppm | 260 |
| 2008 | Ueda | NOx | MWNT | laser | Gas | Resistance | -- | 261 |
| 2008 | Ueda | NOx | SWNT, MWNT | -- | Gas | Resistance | 5ppm | 262 |
| 2000 | Collins | O2 | SWNT | -- | Gas | Voltage | -- | 263 |
| 2001 | Wadhawan | O2, Ar, H2 | SWNT | -- | Gas | Voltage | -- | 264 |
| 2007 | Watts | O2, H2O, | MWNT | -- | Gas | Resistance | -- | 265 |
| 2004 | Valentini | O2, H2O, NH3, NO2 | MWNT | -- | Gas | Resistance | 100 ppb | 266 |
| 2011 | Ghaddab | O3, NH3 | SWNT | SNO2 | Gas | Resistance | 20ppb, 1ppm | 267 |
| 2008 | Zhao | Organic | SWNT | Pyrenecyclodextrin | Liquid | Resistance | -- | 268 |
| 2004 | Picozzi | Ozone | SWNT | modeling paper | | -- | | 269 |
| 2010 | Choi et al. | Pressure, Flow | MWNT | -- | Gas | Resistance | -- | 270 |

| | | | | | | | | |
|---|---|---|---|---|---|---|---|---|
| 2005 | Suehiro | SF6 | MWNT | -- | Gas | Resistance/Partial Discharge | -- | 271 |
| 2010 | Kang | SF6 | SWNT | Benzene | Gas | Resistance | -- | 272 |
| 2011 | Chaudhury | SO2, H2S | MWNT | PS | Gas | cyclic volt | -- | 273 |
| 2006 | Lee | SOCl2, DMMP | SWNT | DNA | Gas | Resistance | 50ppm | 274 |
| 2005 | Auvray | TEA(aminoc ylane) | SWNT | -- | Gas | Voltage | 20 ppb | 275 |
| 2006 | Wei | THF, ethanol, cyclohexane | MWNT | PVAc, PI | Gas | Resistance | -- | 276 |
| 2006 | Parikh | Toluene, acetone, hexane, water | MWNT | PET | Gas | Resistance | -- | 277 |
| 2007 | Consales | Toluene, xylene | SWNT | -- | Gas | Optical, Acoustic | 120ppb | 278 |
| 2001 | Doleman | VOC | -- | Polymers | Gas | -- | 1ppm | 279 |
| 2003 | Hosseini | VOC | -- | PVAc-graft-PPy | Gas | cyclic volt | 200ppm | 280 |
| 2004 | Penza | VOC | SWNT, MWNT | -- | Gas | Acoustic | 2ppm | 281 |
| 2005 | Penza | VOC | SWNT | CdA | Gas | Acoustic | <1ppm | 282 |
| 2005 | Snow | VOC, DMMP | SWNT | Pd | Gas | Capacitance | 60ppm | 119 |
| 2006 | Snow | VOC, DMMP | SWNT | -- | -- | Capacitance, Resistance | -- | 283 |
| 2005 | Picaud | VOCs, other gases | SWNT | -- | -- | Resonant Cavity | ppb | 284 |